

**Computational modelling of normal
function and pathology in neural
systems: new tools, techniques and
results in cortex and basal ganglia**

A thesis submitted to The University of Sheffield for the degree of Doctor of
Philosophy

Alexander Blenkinsop

Department of Automatic Control and Systems Engineering

Department of Psychology

December 2013

Abstract

Oscillations between various populations of neurons are common and well documented. However, there are oscillations that can emerge within networks of neurons that are pathological and highly detrimental to the normal functioning of the brain. This thesis is concerned with modelling the transition from healthy network states to the pathological oscillatory states in two different brain disorders; epilepsy and Parkinson's disease (PD). To study these transitions, existing computational methods for modelling large systems of interacting populations of neurons are used and new tools are developed.

The first half of this thesis explores the evidence for the dynamic evolution of focal epilepsy using bifurcation analysis of a neural mass model, and relating these bifurcations to specific features of clinical data recordings in the time-domain. These findings are used to map out the evolution of seizures based on features of segments of the clinically recorded electroencephalograms. The similarity of seizure evolution within patients is tested. Statistically significant similarities were found between the evolutions of seizures from the same patient.

In the latter half of the thesis a way of creating firing rate models is described, in which the value of the membrane time constant is dependent on the activity of afferent populations. This method is applied to modelling the basal ganglia (BG). The hypothesis that the BG are responsible for selection in

the primate brain is tested and confirmed. The model is then used to investigate the development of PD. It was found that the loss of dopaminergic innervation caused a failure of selection capability but did not directly give rise to the beta oscillations ubiquitous in PD. Network connection strength changes that are seen in PD cause the model to regain selection functionality but lead to a beta frequency resting state oscillation, as is the case in real PD.

Acknowledgments

I would like to thank the following people for their support, guidance and comments:

John Terry

Sean Anderson

Kevin Gurney

Anthony Leader

James Hensman

Chris and Jenny Blenkinsop

Nina Petchey

Contents

Abstract	i
Acknowledgments	iii
Contents	iv
List of Tables	x
Nomenclature	xi
Chapter 1: Introduction	1
1.1: BACKGROUND	1
1.2: AIMS AND THESIS OVERVIEW	1
1.3: CONTRIBUTIONS ARISING FROM THE THESIS	4
Chapter 2: Literature Review	7
2.1: OVERVIEW OF EPILEPSY	7
2.2: OVERVIEW OF PARKINSON'S DISEASE	11
2.3: COMPUTATIONAL MODELS OF NEURAL STRUCTURES	14
2.3.1: <i>Modelling of epilepsy</i>	15
2.3.2: <i>Modelling of the basal ganglia and Parkinson's disease</i>	16
2.4: MODELS OF MASS ACTION IN THE BRAIN	20
2.4.1: <i>Mass action models in general</i>	20
2.5: PARAMETER ESTIMATION FOR NEURAL MODELS	29
2.6: ANALYSIS OF DYNAMICS WITH NEURAL MODELS	33
2.6.1: <i>Bifurcation analysis</i>	33
2.7: SUMMARY	39
Chapter 3: The dynamic evolution of focal onset epilepsy	41

3.1: INTRODUCTION	41
3.2: MATERIALS AND METHODS	46
3.2.1: Intracranial EEG recordings	46
3.2.2: A neural mass model for intracranial EEG recordings	48
3.2.3: A generative neural mass model of hippocampal cortical tissue.....	50
3.2.4: Bifurcation theory and numerical continuation.....	56
3.2.5: Relating model solutions to clinical data	61
3.3: RESULTS AND STATISTICAL ANALYSES.....	67
3.3.1: Bifurcation analysis: Part I.....	68
3.3.2: Bifurcation analysis: Part II.....	77
3.3.3: Consistency of seizure evolution in clinical recordings	83
3.4: DISCUSSION.....	90
3.5: SUMMARY.....	93

Chapter 4: Bayesian estimation of connection strengths between neural populations using SMC-ABC..... 95

4.1: INTRODUCTION	95
4.2: DESCRIPTION OF THE METHOD.....	97
4.2.1: Introduction to likelihood free Bayesian inference	97
4.2.2: SMC-ABC method.....	99
4.2.3: SMC-ABC Algorithm	102
4.2.4: Validating the use of SMC-ABC.....	104
4.3: DISCUSSION.....	109
4.4: SUMMARY.....	113

Chapter 5: A novel firing rate model of the basal ganglia 115

5.1: INTRODUCTION	115
5.2: MATERIALS AND METHODS	119
5.2.1: Model architecture	119

5.2.2: <i>Initial attempts to model the basal ganglia using a first order model</i>	122
5.2.3: <i>Second order firing rate model of the basal ganglia</i>	131
5.2.4: <i>Second order model with variable time constants</i>	135
5.2.5: <i>Model summary</i>	145
5.3: RESULTS.....	148
5.3.1: <i>Parameter estimation using ABC gives an accurate description of BG dynamics</i>	148
5.3.2: <i>Parameter distributions</i>	151
5.3.3: <i>The identified model accurately predicts an independent validation data set of BG dynamics</i>	153
5.4: DISCUSSION	158
5.5: SUMMARY	159
Chapter 6: Computational analysis of basal ganglia function	161
6.1: INTRODUCTION.....	161
6.2: FUNCTION AND PATHOLOGIES OF THE BASAL GANGLIA	162
6.3: EMERGENCE OF ACTION SELECTION IN THE MODEL OF BASAL GANGLIA	163
6.3.1: <i>Selection tests</i>	167
6.3.2: <i>Selection properties</i>	168
6.4: CONSEQUENCES OF NETWORK CHANGES IN PARKINSON’S DISEASE	173
6.5: TARGETED GPe GABA ANTAGONISTS AS A POSSIBLE TREATMENT OF PD SYMPTOMS	179
6.6: DISCUSSION	181
6.7: SUMMARY	185
Chapter 7: Conclusions and Future Work	187
Bibliography	193

List of Figures

Figure 3.1. Schematic of hippocampal tissue model.....	51
Figure 3.2. Experimentally recorded excitatory postsynaptic potential.	52
Figure 3.3. Example of a <i>false bifurcation</i> from [143].	58
Figure 3.4. A co-dimension 1 bifurcation diagram in parameter B.....	71
Figure 3.5. Two-parameter numerical continuation diagrams.	74
Figure 3.6. Examples of waveforms from regions numbered in Figure 3.5....	75
Figure 3.7. Hippocampal EEG behaviour-types in noise driven model and data.....	76
Figure 3.8. Solution-types as a function of synaptic gain parameters (A, B & G) in noise driven model [91]......	77
Figure 3.9. Comparison of model with clinical data.....	79
Figure 3.10. Two parameter continuation plot of B and G with associated waveforms.....	80
Figure 3.11. Illustrating the deformation of waveform upon increasing parameter B.....	82
Figure 3.12. Output of stationarity algorithm.	85

Figure 3.13. Temporal evolution of multiple seizures from three TLE patients.....	87
Figure 3.14. Distributions of random vectors for statistical tests.	88
Figure 4.1. Flow chart describing the SMC-ABC algorithm.	101
Figure 4.2. Nevado Holgado model and parameter distributions.	109
Figure 5.1. Basal Ganglia connectivity.....	121
Figure 5.2. Connectivity schematic of first order BG model.....	124
Figure 5.3. Response of the 1 st order model to a brief cortical stimulation..	127
Figure 5.4. Deviation from observed firing rates for different model connectivities.	128
Figure 5.5. Performance of best model under the 8 experimental conditions.	129
Figure 5.6. Distributions of connection strength parameters in first order model.....	130
Figure 5.7. Connectivity schematic of full model of basal ganglia.	131
Figure 5.8. Second order model comparison to experimental data.....	135
Figure 5.9. Dependency of time constants on rate of change of firing rate and inputs.....	139

Figure 5.10. FF curve for the model striatum.....	142
Figure 5.11. Fit of <i>second order variable time constants</i> model to data.....	149
Figure 5.12. Distributions of free parameter values.....	153
Figure 5.13. Model validation time series.....	157
Figure 6.1. Three channel BG model schematic.....	165
Figure 6.2. Three channel cortical inputs.....	166
Figure 6.3. Time series of the model basal ganglia network selecting between inputs.....	169
Figure 6.4. As the model approaches the data, selection functionality improves.	172
Figure 6.5. Network changes in PD attempt to restore BG functionality.....	178
Figure 6.6. Change in selection functionality as DA and connection strengths change.....	180

List of Tables

Table 3.1. Model parameter values and biophysical interpretations.....	56
Table 3.2. Summary of segmentation algorithm.....	66
Table 3.3. Correlations between seizures for each patient.	89
Table 4.1. Parameter values and sources for the Nevado-Holgado model [50].	105
Table 4.2. Experimental data used to constrain free parameter in NH model [50]	106
Table 5.1. Table of model parameters.	147

Nomenclature

AMPA - α -Amino-3-hydroxy-5-methyl-4-isoxazolepropionic acid

BG - Basal ganglia

DBS - Deep brain stimulation

DDE - Delay differential equation

EEG - Electroencephalogram

GA - Genetic algorithm

GABA - Gamma-aminobutyric acid

GPe - Globus pallidus external segment

GPi - Globus pallidus internal segment

iEEG - Intracranial Electroencephalogram

MSN - Medium spiny neuron

NMDA - N-methyl-D-aspartate

NMM - Neural mass model

PD - Parkinson's disease

PSP - Post-synaptic potential

PSTH - Peristimulus time histogram

SMC-ABC – Sequential Monte-Carlo approximate Bayesian computation

SN - Substantia nigra

SNIC - Saddle node on invariant circle

SOM – Stochastic optimisation method

STN – Subthalamic nucleus

strD1 – MSN population of the striatum expressing mostly D1 receptors

strD2 – MSN population of the striatum expressing mostly D2 receptors

SWD - Spike wave discharge

TLE - Temporal lobe epilepsy

Chapter 1: Introduction

1.1: Background

The human brain contains about 86 billion neurons connected to each other by roughly 200 trillion synapses [1]. Oscillations between various populations of neurons are common and well documented, for example the alpha rhythm of the cortex that can be observed in the EEG [2]. However, there are oscillations that can emerge within networks of neurons that are pathological and highly detrimental to the normal functioning of the brain. This thesis is concerned with modelling the transition from healthy network states to the pathological oscillatory states in two different brain disorders; epilepsy and Parkinson's disease. To study these transitions, existing computational methods for modelling large systems of interacting populations of neurons are used and new tools are developed.

1.2: Aims and thesis overview

In Chapter 2 the literature surrounding the modelling of neural systems is reviewed. Firstly a broad overview of the differing levels of description at which models can be written is given, before focusing on the various methodologies for modelling the massed action of large systems of interacting populations of neurons. Since a key part of model development is the estimation of parameter values, a section is devoted to a review of the

many techniques that have been used for this purpose. The final section of the literature review chapter is an analysis of the ways that neural models have been used to draw biologically meaningful conclusions.

The broad aim of this thesis is to better understand the mechanisms responsible for the onset of pathological neural oscillations in epilepsy and Parkinson's disease. The aim of Chapter 3 is to explore the evidence for the dynamic evolution of focal onset epilepsy using clinical iEEG data and a bifurcation analysis of a mathematical model of hippocampal cortex. Focal-onset seizures have traditionally been conceptualised as having a highly circumscribed onset in an "abnormal" brain region, with evolution of the seizure requiring recruitment of adjacent or connected "normal" brain regions. Complementing this concept of the spatial evolution of seizures, the purpose of Chapter 3 is to explore the evidence for the dynamic evolution of focal epilepsy using bifurcation analysis of a neural mass model, and subsequently relating these bifurcations to specific features of clinical data recordings in the time-domain. The study is motivated by recent research in idiopathic generalised epilepsies which has suggested that the temporal evolution of seizures may arise out of gradual changes in underlying physiological mechanisms. It was found that spikes in the considered model arise out of so-called 'false' bifurcations, a finding consistent with other neural models with two timescales of inhibitory processes. These results were compared with previous studies of the model, before extending the results to characterise other more complex model behaviours. The

relationship between model dynamics and clinical recordings from patients with focal epilepsies is then explored. A novel algorithm was used to subdivide each recording into time-windows for which the data is approximately stationary. The bifurcation findings were then used to map out the evolution of seizures based on features of the clinical data from each of the epochs identified by the algorithm. Finally the similarity of the seizure evolution within patients was explored, using random surrogates to test for statistical significance.

In chapter 4 a Bayesian algorithm called sequential Monte-Carlo approximate Bayesian computation (SMC-ABC) is described. Since the algorithm has not previously been used in the field of neural modelling, its use is validated by replicating the results of an earlier study. The results indicate that SMC-ABC is an effective tool for finding the parameters of nonlinear neural models. The technique is used in the following chapter to find the parameters of a novel firing rate model of the basal ganglia.

Chapter 5 describes new computational methods of modelling large systems of interacting populations of neurons. It describes how to use mathematical models to rigorously test ideas about the function of different brain networks and structures. These methods are applied to modelling a group of structures called the *basal ganglia* and we test, and confirm, the idea that they are the structures responsible for action selection in the primate brain. One of the neural populations of the basal ganglia is the primary target of dopaminergic neurons. The death of these neurons in Parkinson's disease

gives rise to slowed movement and tremor, among other symptoms. In Chapter 6 the model is used to investigate the development of Parkinson's disease. The changes that are seen in the network structure of the basal ganglia are implemented in the model and conclusions are drawn regarding disease progression and possible treatments.

1.3: Contributions arising from the thesis

Contributions of the work in this thesis can be divided into two categories. Firstly, there are methodological advances that constitute improvements in the ways that neural systems can be studied. Secondly, the thesis and associated published work contains insights into the function of healthy brain systems and disease states. In chapter 3 a novel method of segmenting time-series data into temporal epochs in which the generating system is changing minimally is created. This method may prove to be of use for the analysis of complex time series data generated by many other kinds of nonlinear systems. The work of Chapter 3 also demonstrates that time domain analysis is at least as informative as the far more commonly used spectral analysis when looking at EEG data.

Chapter 3 also presents evidence that focal onset seizures may follow a characteristic evolution through a low dimensional phase space that is constant in different seizures in the same patient but different between different patients. This insight should inform future work on seizure prediction and suggest possible methods for seizure prevention.

Chapter 5 contains advances in neural modelling methodology. A principled method of testing an hypothesis of brain function using computational modelling is defined. Firstly a systems level model of the structure is created using connectivity that is known from experimental studies. Secondly, the full distribution of model parameters is found using inference techniques constrained by experimental data. A mathematical function is defined which quantifies the ability of the model to perform the hypothesised function. A positive correlation between the goodness of fit to the data and the ability to perform the function is taken as evidence that the hypothesis should be accepted. This is an approach that could be adopted in a wide variety of fields. Also in chapter 5, the use of the likelihood free inference technique of SMC-ABC is used for the first time in neural modelling and it is shown to be extremely well suited to the task.

A new method of creating firing rate models is created that expands the range of the possible dynamics that can be captured in high level models. This is accomplished by using second order dynamics to define the input/output relationships between neural populations and doing away with the assumption that neural populations always act at one constant characteristic time constant. These developments allow dynamical firing rate time series data to be used to accurately constrain model parameters. The above methodological advances are used to provide independent theoretical evidence that the basal ganglia perform action selection.

In Chapter 6, theoretical evidence is found that the pathological beta band network oscillations of Parkinson's disease occur, not as a direct result of the loss of dopamine, but due to the changes that occur in the network as the disease progresses. The model and subsequent analysis suggest reasons for the effectiveness of some treatments of Parkinson's, whose mechanisms of action are not yet fully understood.

Chapter 2: Literature Review

2.1: Overview of epilepsy

Epilepsy is a common chronic neurological disorder, affecting between 0.5-1% people in the world today. It is characterised by high amplitude, hypersynchronous neural activity in all (generalised seizures) or parts (partial seizures) of the cortex. 50% of people who have a seizure will not go on to have any subsequent seizures [3]. However, 20-30% of people diagnosed with epilepsy never experience a long-term remission. It has been suggested that seizures are self-promoting, each seizure making subsequent seizures more probable [4]. Findings from animal studies supports this view [5].

There are many classes of seizures and they have been categorised in different ways over the years. Absence (formerly known as petit mal) seizures are a form of generalised epilepsy in which the whole of the cortex displays pathological synchronous activity. Onset has no clear focus, beginning at the same instant in all areas of cortex. Those who suffer from absence seizures are usually children. They typically experience intermittent, brief interruptions in consciousness of less than about 10 seconds.

Complex partial seizures appear to have a specific location in the cortex which could be considered to be the origin of the seizure. The seizure then spreads, often to the same area in the contralateral hemisphere. The epilepsy

of patients suffering complex partial seizures often progress to engulf the whole cortex, becoming focal onset generalised seizures. These are the most common form of epilepsy and produce the symptoms most commonly associated with the condition. Seizures often begin with a series of peculiar behaviours such as ticks or twitches, which are the same from seizure to seizure in each patient. Sufferers may then experience fitting, uncontrollable muscular contractions over the whole body lasting up to a few minutes. This is followed by a post-ictal phase during which consciousness may be regained, though the brain activity, as shown by EEG recordings, often does not return to the pre-ictal state until many minutes later. Sufferers are often exhausted by the episode and a period of sleep follows an event.

First line treatment for epilepsy is medication. Anti-epileptic drugs (AEDs) work by affecting the processes involved in the recurrent firing of neurons. Sodium channel blockers and calcium current inhibitors decrease neurons' propensity to fire an action potential by blocking the flow of depolarising ions through the channels in the cell membranes. Gamma-aminobutyric acid (GABA) enhancers work by blocking the reuptake of GABA, the brain's inhibitory neurotransmitter, thereby producing an overall decrease in network activity.

However, a large trial of antiepileptic drug treatment in recent-onset idiopathic generalized epilepsies (IGEs) and unclassifiable generalized epilepsies showed that 34-49% failed to achieve 12-month remission with first-line medication [6]. 23% of patients in the same long term study were

still not seizure free after 5 years. While the sites of each drug's action are well known, we lack a complete understanding of how cellular level processes, with which the drugs interfere, give rise to the macro-scale behaviour of an epileptic seizure. The lack of understanding of the fundamental mechanisms underlying seizures means that it can be many years of trying different drugs before an effective drug is found.

In cases where drug treatments have failed, a surgical intervention is sometimes possible. If the focus (point of origin) of the seizure is in a non-vital area of cortex, then it can be removed. However, a meta-analysis of long term outcomes of surgery for epilepsy showed that 34% of patients who underwent temporal lobe resections still experienced seizures after the procedure. This figure rises to 63% for frontal lobe resections [7].

The primary goal of all neuroscientists involved in the study of epilepsy is to understand the basic mechanisms underlying epilepsy to enable the elimination and prevention of epileptic seizures in humans. On a theoretical level we need to gain an understanding of pathological neural population behaviour as a dynamical nonlinear system. If we can use available data to constrain models of the neural substrates of seizure generation then we can use the physiological interpretation of parameters to generate hypotheses to drive experimental research and suggest new sites for drug interventions.

The mechanisms of epilepsy are mainly studied in animal models and computational models. Data used for the analysis of computational models comes from electroencephalograms (EEGs). A mesh of electrodes is

positioned over the patient's head. Each electrode records the electrical field potential from the area of cortex underneath it. EEGs can be recorded either from the outside of the skull or intracranially by removing a section of skull and positioning the electrodes directly onto the surface of the brain. EEG recordings represent a challenge to modellers due to high levels of noise, the difficulty in distinguishing the noise from the behaviour of interest and the interplay between complex spatial and temporal effects. For this reason absence epilepsy has been a popular choice for computational models. The EEG of sufferers of absence seizures display a highly uniform pattern of oscillations arising virtually instantaneously across the entire cortex. Thus spatial components can be safely neglected and the time evolution of the seizure waveform can be studied in a simpler model.

The EEG of patients suffering from subsyndromes of IGEs often display a characteristic wave form consisting of one or more quick bursts of activity followed by a quiescent phase, with the whole cycle repeated at a frequency of about 2-4Hz. This behaviour has become known as spike-wave discharge (SWD). Its ubiquity in generalised seizures has meant that it has been well studied in a variety of animal models [8]–[10]. Results from the study of these models have led to the conclusion that both thalamus and cortex are required for the generation of the classic SWD. Lesion studies of genetic absence epilepsy rats from Strasbourg (GAERS) have shown that SWD behaviour is not possible without both of these structures [11]. In the feline generalised penicillin epilepsy (FGPE) model, the large dose of the weak

GABA_A antagonist penicillin, results in a typical 3-4Hz SWD, which has been simultaneously recorded in both thalamus and cortex [12], [13].

2.2: Overview of Parkinson's disease

Parkinson's disease (PD) is a progressive neurological condition in which a particular group of neurons gradually die. The affected neurons are located in a subcortical nucleus known as the substantia nigra (SN). Many of the neurons of the SN are dopaminergic and therefore their gradual death results in a decline of the levels of dopamine transmission to the SN's afferent nuclei.

The dopaminergic neurons of the SN project to the basal ganglia [14]. The basal ganglia (BG) is a group of subcortical nuclei that receives inputs from most parts of the cortex and from many subcortical structures via thalamic relays. The output of the BG has been shown to be a tonic inhibition of the same structures from which the BG receives its inputs. The BG is composed of the striatum, the subthalamic nucleus (STN), and the globus pallidus. The dopaminergic neurons of the SN project to all of these nuclei but by far the highest proportion of projections are to the striatum. The loss of the dopaminergic innervation of the BG has profound effects on the functionality of this network of structures.

The symptoms of PD can be divided into three categories; cognitive symptoms; autonomic symptoms; and motor symptoms. Cognitive symptoms include depression, anxiety and cognitive impairment [15], [16].

Autonomic symptoms include dysphagia (difficulty swallowing), urinary incontinence, constipation, excessive sweating and erectile dysfunction [17]. However, the most common and most obvious symptoms of PD are motor deficits. Sufferers experience bradykinesia (slowness of movement) leading to a shuffling awkward gait, muscle stiffness and tremor, usually beginning in a hand or arm [18]. Tremor is most likely to occur when at rest.

Treatments of PD can be divided into two categories, drug treatments and surgical treatments. The reason for the death of the SN dopaminergic neurons remains unknown and there is currently no cure for PD. Treatments have therefore focused on alleviating the symptoms of the disease. The drug treatments for PD focus on mimicking the effects of dopamine. Levodopa is a widely prescribed drug for PD which is absorbed by neurons and is turned into dopamine thus compensating for the loss of the natural dopamine. However, while Levodopa has a very positive effect when first prescribed, as the disease progresses the drug leads to its own motor deficits including sudden and uncontrolled jerky movements (dyskinesia).

Dopamine agonists are another form of drug treatment and also act as a substitute for dopamine by binding to and activating the same receptors as dopamine would have in the healthy brain. They are often prescribed alongside Levodopa in order that the dosage of the later can be reduced. However, dopamine agonists have been linked to the development of compulsive behaviours such as gambling and hyper-sexuality and disinhibition. Monoamine oxidase-B inhibitors block the effects of the

chemical pathway that destroys dopamine in the brain and is a drug that is used to treat early stage PD as an alternative to Levodopa. All drug treatments suffer the same drawbacks in that they have a blanket effect on the many parts of the brain that use dopamine and are not targeted on the specific nuclei that are innervated by the SN. They also lose effectiveness over time as increasing SN cell death occurs.

There are also two surgical treatments for PD; deep brain stimulation and pallidotomies. In deep brain stimulation (DBS) an electrode is surgically implanted into one of the nuclei of the BG (usually the STN) and a pulsatile current is used to stimulate the area around the electrode. This treatment is highly effective in alleviating the motor symptoms in some patients with advanced PD.

Paradoxically the effects of DBS are similar to the effects of lesioning the STN. There are four main classes of possible explanations for why the stimulation of an excitatory should lead to an effective inhibition [19]. 1) The stimulation may change the behaviour of the voltage-gated ion channels such that action potentials cease to occur (depolarisation block) [20]. 2) Depletion of neurotransmitters at the axonal terminals of the stimulated neurons [21]. 3) The stimulation may affect the axon terminals of inhibitory nuclei that innervate the STN causing the STN neurons themselves to be inhibited [22]. 4) Stimulation of the STN results in an increased inhibition of BG output nuclei due to the way that the network is changed in PD [23]. Experimental and theoretical research is ongoing to find the mechanisms of action of this

treatment. This thesis is concerned, in part, with developing modelling tools for the study for this treatment. Neural systems are extremely complex, with vast numbers of nonlinear dependencies at varying scales interacting to give rise to the observed behaviour. Mathematical modelling is the primary means of ascertaining the parameters and variables that are of the greatest importance to generating the observations, and is also a key method for generating hypotheses that can be tested experimentally.

2.3: Computational models of neural structures

In this section a general overview of the techniques used for the modelling of neural systems is given. Then a more in-depth review is undertaken of specific models of both epilepsy and Parkinson's disease at all levels of description. The aim of this section is to critically evaluate available models and focus in on the most appropriate model type for the research questions addressed in this thesis, namely neural mass models for the modelling of epilepsy in cortex and firing rate models for the modelling of basal ganglia.

Computational models are mathematical models that require the processing power of a computer for their analysis. Complex nonlinear models can be analytically intractable so computers can be used to solve the system numerically to an extremely good approximation. Experiments can be run on the model, parameter dependencies explored and hypotheses of system function generated by manipulating the mathematical structure or parameter values in the model. Computational modelling is extremely important in the

field of neuroscience as the nervous system is immensely complex and highly nonlinear [24]. Experimental manipulation and observation is hampered by many confounding factors such as the fact that animal models may not generalise well to humans or the many and complex effects of various anaesthetics [25], [26]. Computational models allow us to reduce the dimensionality of the system and to isolate and analyse individual elements to generate predictions that can be tested experimentally.

2.3.1: Modelling of epilepsy

The SWDs of epilepsy have been intensively studied in many computational models at varying levels of description. Destexhe [27] was the first to model these pathological oscillations. Multiple neurons were individually modelled using an Hodgkin-Huxley formalism. Parameters were found by fitting model output to experimentally recorded postsynaptic currents [28]. It was found that the slowly acting GABA_B response and thalamocortical feedback were both essential to the generation of SWDs. Their model is too detailed to allow a complete search of the parameter space for epileptic dynamics but their result has been confirmed in various studies of models of generalised seizures with far smaller parameter spaces [29], [30]. More generally it has been shown that SWD dynamics can be observed in systems which have two distinct time scales, whether or not the time scales are related to GABA_A and GABA_B response, resembling the dynamics of *fast-slow* systems as studied by Brons in the early 1990s [31].

A detailed model of cortical tissue was created in [32]. This study focused on the possible role of axon-axon gap junctions in the generation of a fast (70Hz) oscillation that often precedes seizure onset. It was found that gap junctions were a possible candidate for the generation of these oscillations and that therefore gap junction blockers may be a possible treatment for focal epilepsy. As with the Destexhe model [27] this model contains a great deal of physiological detail, modelling thousands of individual neurons. While this makes these models suitable for testing the effects of changing intracellular parameters, it is less suitable for examining network level effects. For this reason much of the current work on the modelling of epilepsy has been done using models of the mass action of large populations of neurons [30], [33], [34]. These models will be discussed in a later section.

2.3.2: Modelling of the basal ganglia and Parkinson's disease

Modelling of PD has focused on the BG since that is the structure that is principally innervated by the dopamine neurons of the SN. It has been observed that the motor symptoms of PD coexist with an increase of beta frequency (12-30Hz) oscillatory activity in the output of the BG [35]–[38]. This observation has led many to conclude that the origins of the tremor in PD are in one of the feedback loops involving the BG. The BG is composed of four populations of neurons. The striatum and STN are the BG's input nuclei, receiving inputs directly from various cortical areas and many subcortical areas via the thalamus [39],[40]. The BG's output nucleus is the GPi (SNr in rodents) and projects tonic inhibition to the same cortical locations from

which the BG receives its inputs [41], forming loops. In the case of cortical loops, the GPi projects back to the cortex via thalamic relays [41]. Within the BG three pathways have been identified as being of particular importance; the direct pathway (Striatum to GPi); the indirect (striatum to GPe to STN to GPi) [42]; and the hyperdirect pathway (STN to GPi) [43],[44]. The STN is reciprocally connected to the GPe [45]. While other pathways exist much of the focus of BG modelling has focused on these connections. Other connections will be examined later in the thesis.

Feedback loops in the BG are a key feature of interest and have now been widely studied using computational models. There are two feedback loops which have been thought to be candidates for the generation of oscillatory activity in the BG output nuclei: cortex-BG-thalamus-cortex and GPe-STN. A study of the GPe-STN feedback loop was conducted by [46]. This study found that increasing the strength of the cortex-STN connection increases oscillations. However, many of the other conclusions of this study rely on the assumption that there are significant self-excitatory connections within the STN. Experimental evidence for these connections is not sufficiently strong to permit this assumption [47], [48].

Similarly a conductance based study of the STN GPe feedback loop [49] found that the system is capable of generating oscillations in the theta range. However, this study neglected transmission delays between nuclei which have since been shown to be critical to the frequency of oscillations.

A later study by [50] used a first order firing rate model of the same feedback loop to investigate the conditions necessary for the generation of Beta oscillations. By including axonal transmission delays between the two nuclei it was found that the self-excitation within the STN was not necessary to explain experimental observations of mean firing rates and oscillation frequency. Thus it can be concluded that the GPe-STN feedback loop is a possible candidate for increase in power of beta band activity in the BG of Parkinson's sufferers. Similar conclusions were reached by [51], who created a neural mass formulation of the whole basal ganglia-thalamo-cortical loop.

Due to the intrinsic and extrinsic connectivity of the BG and its tonic inhibitory output, it has long been thought that the BG may be the locus for action selection in the vertebrate brain [52]–[56]. The typical motor symptoms of PD such as difficulty executing voluntary actions and slowed movements could easily be considered to be deficits in the functionality of a selection mechanism. In the study of PD it is therefore important that computational models consider both the function of the healthy BG and the change in network dynamics that occurs with disease progression.

Unfortunately there have so far been no models that address the issues of pathological oscillations and BG functionality simultaneously and it is this gap with which the latter half of the thesis is concerned. [55] have come the closest to addressing this problem by creating a model of the BG using integrate and fire neurons. While this study helps to illuminate the origins of alpha and gamma band activity in the healthy BG, they do not go on to

address the possible mechanisms for the rise in beta band activity in PD. The high amount of biological detail in the model may make finding the many parameters of the diseased state extremely difficult. The problem may be better addressed by creating a model of mass action similar to that of [50].

One popular and fruitful model of BG functionality written at the firing rate level of description is [53], [54], the GPR model. While the model in this study is highly abstracted it has served as the platform for much of the subsequent work on the modelling of BG function, such as [57], another popular model of selection in the BG. It may be useful to extend the GPR model to better quantitatively represent BG firing rates and to use it to analyse the effects of the changes that occur in the network as PD advances.

Frank has proposed a slightly different hypothesis of BG function. It is proposed that the BG functions not as a selection mechanism, but as a gating mechanism [58]. The disinhibition of the thalamocortical circuits by the BG allows the updating of information currently stored in working memory. Frank's computational model of this mechanism is a plausible mechanism for how the BG interacts with working memory [59]. While the hypothesis is not the same as the hypothesis of action selection it should be noted that the action selection hypothesis is chiefly concerned with, and has been modelled as, a motor circuit function. It may be that BG-thalamus-frontal cortex loops function in a slightly different way to BG-thalamus-motor cortex loops.

2.4: Models of mass action in the brain

Though the state space of a fully described neural system is vast, the actual observed behaviour is restricted to a relatively low-dimensional sub-space. Many of the variables may change over timescales much (shorter/) longer than the characteristic timescale of the phenomena of interest. These variables could be considered to be (instant/) constant over the time scales of interest and can therefore be modelled as fixed parameters (*quasi-steady state* approach) [60]. Other variables may strongly covary and so can be lumped together as a single variable [61]. In this way it is possible to greatly reduce the dimensionality of the system to a manageable number, while still studying the problem of interest. The advantage of this model reduction is that analysis is greatly simplified creating the possibility of insights into function.

This section begins with a general discussion of the main methods for the modelling of the aggregated activity of large populations of neurons; neural field models, neural mass models and firing rate models. Following this, there is a full review of the way these techniques have been applied to the modelling of both epilepsy and Parkinson's disease, allowing the correct modelling framework to be chosen for the study of both epilepsy and PD.

2.4.1: Mass action models in general

The first attempt to model the aggregated responses of populations of excitatory and inhibitory neurons was made by [62] who demonstrated that

many features of aggregated neuronal dynamics such as hysteresis loops and limit cycles can be captured using a pair of nonlinear differential equations, with one equation defining the proportion of excitatory cells that are active and the second defining the number of inhibitory cells that are active. Similar work was done by [63] who derived a lumped parameter model to explain the alpha rhythm of the EEG, and Nunez, who derived the brain wave equation [64]. These studies form the foundation of most models of mass action in the cortex. The models have been built upon and analysed in a multitude of ways to be discussed later in this chapter.

2.4.1.1: Spatially extended models

Models of mass action that include spatial components have been developed for the purpose of modelling the propagation of neural activity across the cortex. Spatial dependence is accomplished by modelling two, either discrete or continuous spatial dimensions directly in the equations for each neural population (neural field models) [65]. A third discretised depth dimension is sometimes included to model the different layers of cortex [66]. The rationale behind this method is that within any given macro-scale piece of neural tissue there will be such a large number of randomly connected neurons that statistical methods can be used to derive continuous field equations in the form of partial differential equations. A weighting function describes the connectivity structure of the tissue. For example, if local connections are, on average excitatory, but longer-range connections are inhibitory, then a mexican-hat function like a *difference of Gaussians* would be an appropriate

choice. Often a uniform homogenous connectivity structure is assumed. The solutions to the system of partial differential equations can be steady states, travelling wave fronts, bumps or stationary waves (known as *breathers*). Models using this method generally neglect depth and boundary effects and treat the cortex as an infinite two-dimensional sheet [67].

Neural field models seem to be a natural choice to study the spread of the pathological oscillations of epilepsy as they travel across the cortex. Primary data on epilepsy is gathered by EEG, in which an array of recording electrodes are placed at spatially distinct locations over the head of the patient. Field potentials of the area of cortex underlying each electrode are recorded. What is measured by the EEG can therefore be thought of as an averaged field potential of all the neurons under each electrode.

One of the most successful neural field models of the EEG is [68] though this study is concerned with modelling the effects of anaesthesia on the EEG and does not address epileptic states. The only neural field study that produces SWDs is [69], whose model of the cortex is based on the model of [70].

Neural field models are problematic to implement since their assumptions create a large disconnect with physiology. For the sake of making the models analytically tractable potential to firing rate operators are often approximated as a Heaviside function [65]. The assumption that connectivity kernels are homogeneous is particularly limiting. Work is still ongoing by groups in Exeter and Nottingham to map known connectivity structures onto

the PDEs of the neural field models in order that models can be built that accurately describe the spatial propagation of focal onset seizures.

2.4.1.2: Neural mass models

Neural mass models can be derived from a set of neural field equations simply by removing the dependence on spatial location, turning the partial derivatives into time derivatives [71]. Neural mass models utilise a “rate to potential” transfer function, conceptually located at the synapse of an average neuron. This changes the firing rate of the afferent nucleus into a post synaptic potential and is typically modelled by a biexponential [63], [71] or an alpha function [72]. There is a unique transfer function for each receptor type in each neural population. The PSPs are linearly summed and transformed into a firing rate by a “potential to firing rate” operator conceptually located at the soma of the average neuron (see [73] for a review of these operators). The usual choice for this function is a sigmoid, which is more physiologically realistic than the Heaviside function that is often used in neural field formulations. The form of the “potential to rate” and “rate to potential” operators embodies the mean cellular dynamics from synapse to soma.

Epilepsy is suited to analysis using models of this type since it is a dynamical disorder of the brain characterised by hyper-synchronous neural activity across large areas of cortex [9], thus spatial dependencies can often safely be neglected. Also, the number of nuclei involved in modelling the cortex is relatively small (a population of pyramidal cells whose activity defines the

simulated EEG, and either two or three distinct populations of interneurons) so the dimensionality of the system is sufficiently small that numerical and analytical analyses are possible.

This approximation has proved extremely fruitful in the modelling of epileptic EEGs. Jansen & Rit proposed a lumped parameter model of a single cortical column [34] based on the work of Lopes da Silva [74]. They included an additional population of excitatory interneurons in a second feedback loop. Thus their model is a population of pyramidal cells with two feedback loops, one inhibitory, one excitatory. Their model is capable of replicating many of the waveform features of the EEG and, when two models are connected together with transmission delays between them, it is capable of replicating the spatial distribution of alpha and beta rhythms. As with the Lopes Da Silva study, there is no analysis of epileptic states. The Jansen & Rit model [34] has been studied a great deal and its properties are well understood. Many other models are based on it. Wendling [75] created a model of hippocampal cortex which includes an additional population of inhibitory interneurons mediated by GABA_A receptors with a longer time constant. Their model is therefore composed of the pyramidal cell population, one excitatory feedback loop of interneurons, and two inhibitory feedback loops of interneurons, one with a short time constant and one with a long time constant. The additional inhibitory population enables the model to replicate the spectral properties [76] and the features of the shapes of the waveforms in the time domain (see [77] and Chapter 3). The success of these

models, which are all based on the pyramidal cell population and a pair of feedback loops, demonstrates that the neural mass formulation is an adequate framework for capturing the network level activity in cortex.

David and Friston have also analysed and augmented a Jansen and Rit model [78]. They used dynamic causal modelling to find the parameters of a generative neural mass model of the cortex-BG-thalamus-cortex loop driven by noise. Their principle findings were that coupling strength and propagation delay are key determinants of the spectrum of the EEG and strong coupling between areas of cortex induces phase locking.

Suffczynski et al [79] created a neural mass model of thalamic population activity including cortical feedback. It is a slightly more detailed version of the model put forward in Lopes Da Silva (1974). Since the model is primarily concerned with thalamic activity, much of which is characterised by short duration bursts of rapid activity, the variable in the model is different to that in the Lopes Da Silva study. As mentioned above, the Lopez Da Silva model uses the *proportion of active cells* as its variable. The Suffczynski study uses *action potential density* as its variable in order that the bursting behaviour of the thalamus can be captured. One drawback of their model is that it does not explicitly include a term that would correspond to the EEG. It is therefore not of direct use for the modelling of epilepsy. However, since the thalamus is responsible, at least in part, for the spread of activity across cortex, a detailed neural mass formulation may prove to be valuable as a part of a

more extensive model that includes more detailed models of cortical populations.

One such model that includes the thalamo-cortical loop as well as a term that could be interpreted as the EEG signal is that of [71]. This study begins by deriving a set of neural field equations for the cortical sheet coupled with a spatially independent model of the nuclei of the thalamus. Their model is concerned with the analysis of absence seizures which appear across the whole cortex virtually simultaneously [80], thus the spatial components are neglected creating a neural mass model. They go on to conduct a bifurcation analysis of the model using the cortex to thalamus coupling strength and the time delay of the slow GABA_B transmission as bifurcation parameters. They show that the waveform profiles of SWDs in absence epilepsy are dependent mainly on these parameters and that transitions between oscillatory solutions with different numbers of maxima per cycle are due to false bifurcations [81]. However, this formulation has only a single neural mass to represent the cortex, and so this model would require significant reworking if it were to be made to represent the dynamics of focal onset seizures.

Neural mass models assume that no dynamics occurs between the synapse and the soma of each average cell. This is not always the case. It has been shown that the membrane time constant, which governs the transmission between synapse and soma, is in fact variable by a factor of ten: when cells are active the membrane time constant is dramatically smaller, increasing the rate of information transfer [82], [83]. In cases where this assumption is

approximately true neural mass models are an extremely effective way of capturing very detailed physiology in an extremely compact form. However, attempting to fit parameters to a neural mass model of a system for which this assumption is invalid would yield unreliable conclusions.

The details of BG dynamics studied in [84] demonstrate that the neural mass model would be insufficient to explain the firing rate changes that are seen in the pallidum. Under a neural mass formulation the only mechanism that could reasonably explain the observation that GP firing rates make a very gradual return to their tonic rates would be only be explainable as a consequence of the receptors that function over longer time periods, NMDA or GABA_B. However, recordings of GPi following application of the NMDA antagonist, *cpp*, show that the elevated GPi firing rates persist. In that example NMDA therefore has a minimal effect on the mean firing rate. This is a possible issue with a recent study by [51] in which a neural mass model of the cortex-BG-thalamus-cortex system was created and its parameters found using spectral data recorded from anaesthetised rats. It may be useful to find a way to capture input/output firing rate dependencies directly without having to model intracellular processes at all.

Neural mass models require a separate differential equation for each receptor type, meaning that to model a single neural population containing AMPA, NMDA, GABA_A, GABA_B receptors would require at least four second order differential equations. To model the systems in which the number of interacting populations is even slightly larger than the models described

above would require a much larger number of equations. The parameter space associated with such a model would be prohibitively large. It is therefore desirable to reduce the dimensionality of the model still further. One method for accomplishing this is to employ a firing rate model.

2.4.1.3: Firing rate models

Firing rate models are particularly well suited to modelling certain types of experimental data. In many experiments the incidence of action potentials are recorded and other intracellular variables such as membrane potentials or synaptic currents are hidden. This is the case for the majority of experiments that record activity in the BG. It would therefore be difficult to accurately constrain a model that explicitly included these variables. So while firing rate models contain less physiological detail, they can be more accurate in reflecting the biology in cases where the data is insufficient to place bounds on the unobserved variables. When modelling the BG, a firing rate model would therefore be more appropriate than a neural mass formulation since the data is often in the form of peristimulus time histograms (PSTHs) of spike events i.e. population average firing rates.

Firing rate models can be derived in a number of ways. A simple heuristic derivation has been put forward by [85] in which the firing rate of a given cell is dependent on the potential at the soma. The potential at the soma is in turn dependent on post synaptic potentials that are governed by a bi-exponential impulse response function. Their derivation begins with a neural mass formulation then reduces the dimensionality of the model by making

various approximations. One key assumption is that the timescales of activity at the synapse are negligible when compared to the membrane time constant of the post-synaptic cell. While there are many other methods for deriving firing rate models, all make use of this assumption [85]–[87]. Unfortunately this assumption has been shown to not be valid in many situations [82], [83] and this is an issue which will be addressed in Chapter 5.

2.5: Parameter estimation for neural models

In order to make reasonable hypotheses for clinical studies based on the results of experiments run on computational models, one has to be confident that the structure of the model reflects the neural architecture and that the parameters of the model are within biophysically plausible ranges. This can be relatively easy when a parameter is clearly defined, such as the conductance of an ion channel for example. It is much harder when the parameters are not directly measurable. This is generally the case with the parameters of mass-action models, since a parameter such as “connection strength between two neural populations” is the aggregated activity of millions of synapses spread across thousands of neurons.

One approach is to vary the parameters to fit the model’s behaviour to clinically obtained data, such as the EEG of epileptic patients. However, this is a nontrivial task due to the nonlinear nature of the system. In all but the simplest cases, the error function is unknown and so traditional methods such as gradient descent are unavailable; Random walks and exhaustive

search methods are unusable due to the extremely high dimensionality of the parameter-space.

A usual method has been to adopt a two-pronged approach. Firstly, estimate and fix parameters that have a physiological interpretation and second, to use some method to search the system's parameter space to find regions where model behaviour is qualitatively similar to real EEGs. This was the approach taken in the previously cited Lopez da Silva [63], Jansen and Rit, [88] and Wendling [75] class of models. Parameters found to give rise to the behaviour of interest were inherited by the future studies since this is an obvious way to reduce the dimensionality of the parameter space.

Different studies have lent more heavily on one or other of the approaches. Some rely mostly on published data to constrain parameter estimates, for example Robinson [89], while others use sophisticated optimisation methods to find reasonable parameter sets using relatively sparse data [68]. A good example of the first approach was taken by Robinson [89], who applied multiple constraints on parameters from the biological literature and combined them with model constraints to give a more accurate model fit. Monte Carlo methods were used to fit the highly constrained model to data. Bojak and Liley on the other hand use only Fourier power spectrum data and maximum and minimum mean firing rates as data to assess the validity of parameter sets estimated by a swarm optimisation method [90].

An interesting approach to parameter estimation was taken by [76]. Most parameter values were inherited from previous studies [75], [91] and their

values were fixed. The connectivity strength parameters, of which there are three, were allowed to vary. An evolutionary algorithm was used to find parameter sets that optimise the model's fit to the spectral properties of clinical data. Optimum parameter sets were found for different time periods, before during and after seizure. An assumption inherent in this approach is that the time evolution of a seizure is governed by changes in a small subset of the neural system's parameters. Thus the evolution of a seizure through time could be plotted as a path through parameter space, some regions of which would contain normal steady state or alpha rhythms, and some regions would give rise to the pathological oscillations of epilepsy.

The most advanced work that has been built on this assumption has been done by [92]. A multi-objective genetic algorithm was developed capable of recognising the precise features of individual waveforms such as the size and number of spikes in a cycle of SWD. They used it to plot paths through parameter space for different seizures in the same patients. This method retains much more of the information contained in an EEG time series than using the spectral methods used by [76].

In mathematical modelling what is often required is some measure of our belief in a particular set of parameters given the available data. This makes Bayesian inference an ideal tool for the purpose since this naturally arises from the Bayesian framework. Rather than extracting parameter values directly from data as is the case in frequentist estimation methods or the evolutionary methods discussed above, the Bayesian approach yields a

subjective belief in different parameter values. Bayesian inference therefore yields distributions of possible parameter values rather than one *best* parameter set. This is of particular use in neural modelling because the spread of the posterior distribution could be regarded as a measure of the robustness of the model to small perturbations in each parameter.

Dynamic causal modelling (DCM) is a framework that uses the Bayesian *expectation maximisation* algorithm for finding the most likely model connectivity and parameter values that explain experimental data [93]. It has been used in many applications. Of particular interest to this thesis is its use in neural mass modelling [51]. However, DCM is not universally accepted as giving an accurate picture of the underlying, and unknown, neural substrate. It has been demonstrated that DCM does not consistently identify the true model from a set of candidate models [94]. DCM is also limited to low order bilinear models and is not universally applicable. It is also highly much harder to implement than some likelihood free inference techniques that do not suffer this disadvantage.

With the exception of DCM, Bayesian approaches to parameter estimation have not been widely used in neural modelling primarily because of the difficulty in calculating the likelihood function. The likelihood function is defined as the probability of obtaining the observed data given a particular model and set of parameters. In all but the simplest models this can be extremely difficult to calculate. Fortunately there is a growing trend for the use of so called likelihood-free inference techniques in which the likelihood

distribution is approximated by sampling from the posterior. Various algorithms have been proposed that use this basic idea. The most basic, which was proposed by [95], uses a simple rejection algorithm to select samples from the prior that satisfy some acceptance criterion. However, in cases where the parameter space is high dimensional and the data used to constrain the search is highly informative, this method alone is very inefficient.

Approximate Bayesian computation methods address this inefficiency either by using conditional density estimation [96], [97], by using Markov-chain Monte-Carlo sampling [98] or a sequential Monte-Carlo method [99]–[101]. For a full discussion of approximate Bayesian computation methods see [102]. ABC has not been used to date in neural modelling: this thesis proposes the novel use of ABC in estimating neural connection strengths, which could prove to be highly advantageous across the field of computational neuroscience, exploiting the many computational models that already exist to drive this simple Bayesian estimation framework.

2.6: Analysis of dynamics with neural models

2.6.1: Bifurcation analysis

When the number of parameters which are allowed to vary is as low as three, it is natural to attempt to explore the model's behaviour at all parts of the parameter space. Wendling et al [91] attempted to do this by qualitatively classifying the model's behaviour at every discrete location of the parameter

space. While this approach gave rise to simulated EEGs which looked similar to clinically recorded EEGs, it lacks rigor. Since the system is unknown and non-linear, interesting dynamics can occur in arbitrarily small regions of parameter space. These regions would be missed if the discretised sampling used in the exhaustive search technique used by Wendling were too large. Also, the Wendling model [91] has a Gaussian noise as an input. This means that the observed model behaviour could be, in part, due to the varying sizes of the basins of attraction of coexisting stable limit cycles. The noise may serve to kick the model between different limit cycles. While this may be the case in the real system too, it would be more instructive to analyse the mechanisms separately.

A tool for accomplishing this task is bifurcation analysis. The first study to use this tool for looking at the behaviour of a cortical model was [103], who analysed the Jansen & Rit model [88]. The model cortical column has an input parameter that was varied smoothly and the value of a system variable was recorded, yielding a 1 parameter bifurcation diagram. It was shown that the transition from normal background activity to spike-and-wave-like epileptic activity was caused by a Hopf bifurcation in the Jansen & Rit model. They were also able to give support to the values of the fixed parameters, and the ranges of the variable parameters by conducting the bifurcation analysis for different values. It was found that the variety of behaviour exhibited by the model was significantly reduced when parameters varied significantly from the ones given by Jansen and Rit [88].

The tools of bifurcation theory allow a far more thorough exploration of parameter space than is possible by just simulation alone. If the dimensionality of the parameter space to be explored can be reduced to two or three, bifurcation theory allows for the model behaviour to be completely described within this space without having to run simulations at infinitely small parameter gradations. Beginning from an equilibrium state, a single parameter is smoothly changed until the conditions are detected that indicate a Hopf bifurcation has taken place. The Hopf bifurcation itself can then be tracked through the two dimensional parameter space yielding a line through the space which divides the region of parameter space for which the model gives a steady state solution from the region which gives rise to oscillating solutions. All types of bifurcations can be tracked through parameter space, and so it is possible to gain a complete understanding of model dynamics on the chosen subspace.

Marten et al [71] analysed their thalamocortical neural mass model in this way, mapping model behaviour in a two dimensional parameter subspace. They identified from simulation that cortex-thalamus coupling strength and the GABA_B delay time were the parameters whose variation led to the most interesting range of model behaviour. They also found that interesting changes in the time series of the model output could not be explained by bifurcations. The appearance and disappearance of additional spikes in the time series was found to be the result of “false” bifurcations. In false bifurcations, the change of a parameter results in a smooth change in the

vector field of the system, but the change appears discontinuous when the state space is projected onto the observable subspace. Marten et al [71] used co-location to continue false bifurcations in a similar way to normal bifurcations and so were able to fully map model behaviour across the two dimensional parameter space and envisage the abrupt changes in the EEG of an absence seizure as a smooth path through parameter space. No similar time domain analysis has yet been done on any of the neural mass models of cortex. A study of this kind may shed light on the mechanisms underlying the dynamics of focal onset epilepsies.

Jansen & Rit models [88] of cortical tissue have been extensively studied using bifurcation analysis. Spiegler et al. conduct a bifurcation analysis of a modified Jansen & Rit model [104]. Extrinsic input to the neural mass model comes from three sources, instead of one as in the original model (and also the Grimbert & Faugeras analysis [103]). The inhibitory interneuron population, the excitatory interneuron population and the pyramidal cell population all receive independent inputs. Inputs are constants measured in mV, without noise. The pyramidal input is the main bifurcation parameter used in the paper. Codimension-one bifurcation diagrams are calculated and classified according to the nature and order of their Hopf bifurcations. This was done for every combination of the remaining two inputs (where the two remaining inputs are coarsely discretised). A similar analysis is done using the excitatory and inhibitory dendritic time constants as the secondary

variables. The authors build a comprehensive account of the behaviour of this modified model as a function of all three possible inputs.

Touboul et al. [105] also conduct a thorough bifurcation analysis on mainly the Jansen & Rit [88] neural mass model of cortex, but also include a brief analysis of the Wendling model [72] of hippocampal cortex. Their approach is to reduce the dimensionality of the model by performing a change of variables to yield a dimensionally smaller system whose parameters are dimensionless. This leads to a distortion of the bifurcation diagrams when compared to similar analyses of the full models, but the differences are qualitative only.

Bifurcation parameters are mainly the extrinsic input to the neural mass (from areas of cortex outside the modelled area), and a dimensionless global connectivity parameter. Their thorough bifurcation analysis in these parameters includes bifurcations up to codimension-three.

While the Speigler [104] and Touboul [106] studies are successful at describing the solutions of their models for different values of extrinsic input, this information may prove to be of limited value. If we are interested in the emergence of focal onset epileptic oscillations then manipulating external inputs to the system to show behavioural transitions is not the most informative approach. What is of interest is the intrinsic oscillatory properties of the piece of cortical tissue being modelled, independent of external input. Therefore a more fruitful approach may be to fix all inputs to a physiologically plausible background level and then identify which of the

model's internal parameters can be varied to cause the system to make the transition to oscillatory solutions. This was the approach taken in Nevado Holgado et al. [50], in which conditions for the generation of beta oscillations in the globus pallidus- subthalamic feedback loop were assessed analytically.

One study of a cortical neural mass model has used internal system parameters as the bifurcation parameters. In an appendix to [105] the authors analyse a dimensionally reduced version of the Wendling model of hippocampal tissue [75]. However, the analysis is brief and the parameter ranges are small when compared to the ranges used by Wendling et al. in their 2005 study [76].

A bifurcation analysis of a model of cortical tissue may help illuminate the mechanisms of focal onset epilepsies in the same way that bifurcation analysis of neural mass models of the thalamocortical loop has yielded interesting hypotheses regarding the mechanisms of absence seizures. Also, little attention has hitherto been given to the temporal features of the EEG of focal onset epilepsies. Rather parameters have been fit using spectral properties of the data. This method is less suited to studying dynamic evolution as theoretical results from nonlinear dynamics have shown that temporal information cannot be recovered from spectral information alone [107], [108]. Thus far, the theoretical methods for dealing with focal onset epilepsies have not been taking full advantage of all the information contained in the EEG.

There have also been bifurcation analyses of models of the BG. Most notably the study of [50] in which conditions for the generation of the beta oscillations associated with Parkinson's disease were analytically derived from a bifurcation analysis of their firing rate model of the STN-GPe feedback loop.

2.7: Summary

There has been much success in the theoretical study of absence epilepsy using time domain analyses and bifurcation analysis of neural mass models of the thalamo-cortical loop [71], [109]. While there have been studies that use neural mass formulations to examine the dynamics of the much more common focal onset seizures, these studies have used spectral properties of EEG data from temporally broad segments of the seizure EEG [91], [110]. The work on absence seizures indicates that an analysis using temporal features may better illuminate the changes in the neural substrate. In studies that conduct bifurcation analyses on models of cortex the principle parameter that is varied is the extrinsic input to the model [104], [106], [111], [112]. However, recent work has led to the hypothesis that the evolution of seizures is due to gradual changes in underlying system parameters rather than simply strength of external inputs. There is therefore scope to analyse neural mass models of hippocampal tissue in the time domain and to conduct a full bifurcation analysis on the models to explore which parameters are responsible for the variation in the waveform profiles as seizures progress.

There have been many computational models demonstrating that the basal ganglia is capable, in principle, of performing action selection [53]–[56]. There have also been many models of the generation of beta oscillations in the STN-GPe feedback loop of the basal ganglia that has been shown to occur with the advance of Parkinson’s disease [46], [50]. However, as yet there has been no model that has been capable of quantitatively examining the selection functionality of the basal ganglia alongside the generation of the pathological oscillations of Parkinson’s. The only model that has addressed oscillations and functionality simultaneously is that of [55], but this study does not address the transition to the parkinsonian state, only oscillations in the healthy condition. Their model is also far too physiologically detailed to permit any kind of numerical or analytical analysis. There is therefore scope to create a population activity level model of the basal ganglia and use it to quantitatively study the dynamics of healthy function and also how functional deficits present themselves as Parkinson’s disease advances.

Chapter 3: The dynamic evolution of focal onset epilepsy

3.1: Introduction

Focal-onset seizures typically show a dynamic evolution of the clinical features of the seizure, progressing through a sequence of subjective and behavioural phenomena in a manner that is highly stereotyped for an individual patient, and often broadly similar between different patients with seizure onset in the same anatomical site [113], [114]. The accompanying EEG features also dynamically evolve through the seizure. Focal-onset seizures are conventionally conceptualised as having a highly circumscribed onset in an “abnormal” brain region, with evolution of the seizure requiring recruitment of adjacent or connected “normal” brain regions. The emergence of focal seizure activity is increasingly recognised to occur in a network of interconnected regions. The dynamical evolution of clinical seizure features and EEG features must presumably be explained by the fundamental mechanisms of seizure onset, spread of seizure activity to connected brain regions within the seizure network, and spontaneous seizure termination. These fundamental mechanisms are not yet known.

Human focal-onset epilepsy may be associated with onset in medial temporal regions in or adjacent to the hippocampal formation, or in neocortical

regions. A wide range of pathologies may be identified using *in vivo* MRI or *ex vivo* histology, including hippocampal sclerosis, cortical malformations, focal cortical dysplasia, tumours, and the consequences of traumatic brain injury; in some instances no specific pathology can be identified. In contrast to absence seizures in idiopathic generalised epilepsy, where the cortico-thalamic loop has been implicated in several studies [71], [115]–[121], the generators of seizure discharges in EEG are not so fully described in focal-onset seizures.

In human temporal lobe epilepsy (TLE), EEG may be obtained from scalp electrodes or intracranial electrodes (termed intracranial EEG, iEEG). If seizure onset is in the hippocampus, typically the scalp EEG remains normal at seizure onset, because signals from the hippocampus are not detectable at the scalp, but a 5-9Hz rhythm gradually appears in anterior temporal regions ipsilateral (sometimes contralateral) to seizure onset, and evolves over seconds, becoming slower and more diffuse later in the seizure [122], [123]. The pattern of intracranial onset is complex, typically showing localised higher frequency activity at 10-20Hz in the hippocampus, which spreads and slows, being visible at the scalp only when neocortical regions are involved [124]. Seizure onset from a focus in neocortex often may show a low voltage higher frequency onset in the 20-40Hz range, which increases in amplitude and slows [124], [125], and may be visible with scalp EEG as well as intracranial EEG. The evolving patterns of ictal EEG discharge suggest that

the underlying networks which generate the ictal activity progressively alter over the course of the seizure.

The commonest focal onset human epilepsy is temporal lobe epilepsy (TLE), most often due to a specific pathology termed hippocampal sclerosis (or its less severe variant end-foolium sclerosis). The pattern of abnormality is typically restricted to the hippocampal formation with limited evidence of neuropathological abnormality elsewhere in the brain [126]. Evidence suggests that microscale mechanisms in local microcircuits may be responsible for seizure onset, but the manifestation of the seizure depends on activity emerging in large-scale macroscopic brain networks. Several animal models of human TLE with hippocampal sclerosis exist and have been extensively studied. For example, unilateral electrical stimulation of the excitatory input through the perforant path results in status epilepticus which is followed by the emergence of spontaneous temporal lobe seizures [127]. In this model, seizures may appear to be generated from hippocampus (ipsilateral or contralateral to the stimulation) or entorhinal cortex, but the generation of the seizure appears to be critically dependent on the involvement of both local and larger-scale networks. In several *in vitro* and *in vivo* temporal lobe epilepsy models, emergence and expression of the seizure depends on intact connectivity between hippocampal and interconnected cortical regions such as entorhinal and perirhinal cortex [128]. This evolving change in the underlying networks generating seizures has recently been illustrated in three dimensions in the human brain [129]. In this study, iEEG

power in a frequency band typical of seizure activity was directly measured using a very large number of intracranial electrodes in a small number of patients, and a three-dimensional map of the temporal evolution of this iEEG power was created by interpolating between electrodes. This map showed that the brain networks supporting seizure activity gradually evolved from mesial temporal structures to temporal and insular neocortex.

Although these lines of evidence support the idea that the dynamic evolution of the seizure requires spatial extension of seizure activity into progressive larger circuits, experimental electrophysiological techniques are typically limited to the study of small brain regions and limited numbers of neurons, therefore may interrogate local microcircuit phenomena but may not reveal larger-scale brain network activity involved in generating seizures. The technique of ^{14}C -2-deoxyglucose autoradiography [130] can reveal the regional metabolic rate throughout the brain in the period following injection, and hence infer the network of brain regions active during a seizure. In a TLE model, seizures with highly focal motor and behavioural features were associated with increased activity restricted to the medial temporal lobe and its direct connections, but the evolution of the seizure into a more generalised pattern in the same model was associated with activity in a network including medial temporal lobe, thalamus, basal ganglia and neocortex [131]. This increased metabolism during the acute seizure may be reflected in structural alterations evolving over months to years in a network of brain regions in experimental TLE, revealed with MRI, including

hippocampus, thalamus, striatum, and specific neocortical regions [132]. In human TLE, seizure-related regional cerebral blood flow increases (assumed to reflect increased neuronal firing) have been seen in temporal lobe and ipsilateral basal ganglia [133], and the temporal evolution of the anatomical extent of these blood flow changes throughout the brain has been described [134].

In summary, there is clear evidence of a dynamic evolution of the clinical features of the seizure and accompanying EEG in focal-onset epilepsy. In experimental systems, localised seizure onset evolves to more widespread involvement of macro-scale brain circuits, accompanied by associated changes in behavioural seizure features; some evidence exists also in human focal-onset epilepsy that the dynamic evolution of the seizure and EEG is accompanied by progressive involvement of more extensive brain circuits. Given the challenging richness and complexity of experimental data, and the persistent obscurity of the mechanisms responsible for seizure onset, evolution and termination, a modelling framework is here described through which EEG data can be interrogated. Prior work in absence epilepsy [71], [109], [118], [119], has illuminated the underlying mechanisms of seizure activity seen on scalp EEG. As yet however, there has been no similar analysis conducted on the far more common condition of focal onset epilepsy. This has been largely due to the complexities of fitting model parameters to data drawn from a system that is undergoing constant changes over the time course of the seizure. In the work that follows this issue is addressed and a

formal model-driven analysis of intracranial EEG (iEEG) is described that can explain features of focal-onset data, in particular transitions from one pattern to another during the seizure discharge.

3.2: Materials and Methods

3.2.1: Intracranial EEG recordings

Intracranial EEG data were obtained from 3 patients undergoing iEEG at King's College Hospital, London. In these cases, conventional antiepileptic drug treatment had failed to control seizures despite trying a range of medications at appropriate doses; hence these patients were being evaluated for surgery in which the putative focal source of seizure activity would be resected. A first phase of investigation with magnetic resonance imaging, neuropsychometric testing and seizure recording with simultaneous video and scalp EEG had failed to adequately localise the seizure onset zone, therefore the conventional next step of iEEG was undertaken to better localise seizure onset. The data used here were obtained during conventional clinical investigation entirely independent of the study described here. iEEG data were examined by the clinical team, seizures identified and appropriate segments copied, and shared with this study in an entirely anonymised form without video. The local Research Ethics committee of King's College Hospital approved use of these data for this study.

The patients, all female, were aged 26, 55 and 61. All three subjects had the clinical syndrome of temporal lobe epilepsy, and all were studied with

bilateral subdural electrode strips covering inferior and medial temporal lobe. Commercially-made intracranial electrodes approved for human use were used (AdTech Medical Instruments Corporation, WI, USA). Strips of electrodes consisted of 8 platinum-iridium disc electrodes 4mm in diameter arranged in a single row at intervals of 10 mm centre to centre, embedded in a strip of polyurethane 0.7 mm thick. Intracranial EEG data were recorded using a Nervus Medelec System (Medelec, Oxford Instruments, Witney, UK). Data were digitized at 256 Hz with a 22 bit analogue-to-digital converter, band-pass filtered in software (0.3 Hz – 70 Hz).

Large-scale brain activity recorded using such strips is typically thought of as the summation of the ionic interactions of large populations of neurons; predominately pyramidal cells, which integrate both excitatory postsynaptic potentials (EPSPs) and inhibitory postsynaptic potentials (IPSPs) and output extracellular currents [135]. These currents may be summed due to the perpendicular alignment to the scalp of the pyramidal cell dendritic tree.

Patient 1, aged 55, had two patterns of seizure. The first pattern emerged from right medial temporal regions, and consisted of motor arrest followed by automatisms (involuntary semi-purposeful motor activity) involving the right hand. A second pattern emerged from left mesial temporal electrodes, and consisted predominantly of motor arrest accompanied by oral automatisms (lip-smacking and chewing movements). Patient 2, aged 26, had a single pattern of seizure emerging from left medial temporal electrodes; this consisted of motor arrest followed by prolonged involuntary repetitive

vocalisation, and posturing of both arms. Patient 3 also had a single pattern emerging from left medial electrodes, consisting of arrest, automatisms of the left hand, dystonic posturing of the right arm, chewing, and dysphasia for a few minutes after the seizure. In all patients, different seizures emerging from the same onset zone tended to be very similar within patients, with the same overall pattern and evolution of features, but differing duration (see below). Although it would be of great interest to relate the evolving clinical seizure characteristics to the bifurcation analysis of our model, these clinical features are challenging to robustly characterise and classify, hence this is not attempted here.

3.2.2: A neural mass model for intracranial EEG recordings

There are a number of approaches that can be considered for defining a generative model of (i)EEG and the interpretation of EEG signals from biophysical principles remains an active area of research. One approach is to consider large-scale neuronal networks whose output mimics that of EEG (for example [27], [136]). A challenge with such an approach is that the model complexity typically precludes any attempt at formal analysis, making it difficult to identify the underlying mechanisms responsible for features observed in the data. This makes an approach based around matching features of model output to iEEG recordings difficult. As an alternative to this detailed approach, a continuum-based approximation using a neural mass formulation was used.

The neural mass framework can be traced back to fundamental studies [74], [137] in the 1970s. Freeman in his work on olfaction observed that the population response to an electrical impulse observed a bi-exponential response consisting of a steep rise and a more gradual decline. Similarly Lopes da Silva and colleagues used the neural mass formulation (described therein as a 'lumped parameter model') to explain the alpha rhythm of the human EEG. More recently, in the 1990s, Jansen and Rit [138] introduced a neural mass model (NMM); the output of which they relate to visual evoked potentials recorded using EEG.

NMMs are employed as a means of capturing the bulk properties of interacting populations of different types of neurons. The response of each neural population is governed by a differential equation. The equations are coupled together according to the schematic structure of the model and solved numerically using a program such as MatLab. NMM have no spatial component, thus they must be conceptualised as representing a large number ($O(10^4)$ - $O(10^8)$) of neurons but in an area of tissue small enough such that axonal transmission delays can be safely neglected. This makes NMMs particularly well suited to the modelling of systems for which the output represents a scalp or intracranial EEG signal, as each electrode gathers the aggregated potential of neural activity from the small area of tissue under it. The reader is referred to [67], [139] for full analytical discussions of neural modelling, including spiking neuron models, NMMs and neural field models.

3.2.3: A generative neural mass model of hippocampal cortical tissue

A generative neural mass model was examined which has previously been shown to qualitatively replicate the EEG of human TLE sufferers. The model was constructed as in studies by Wendling [72], [91]. The model output represents the mean field potential of a population of hippocampal pyramidal neurons. The potential of this population is given by the aggregated contributions of the three feedback loops of interneurons connected to it; one excitatory population; and two inhibitory populations. One population is classed as slow inhibition, reflecting dendritic projecting GABA_A interneurons; the other population is classed as fast inhibition, reflecting somatic projecting GABA_A interneurons (See Figure 3.1).

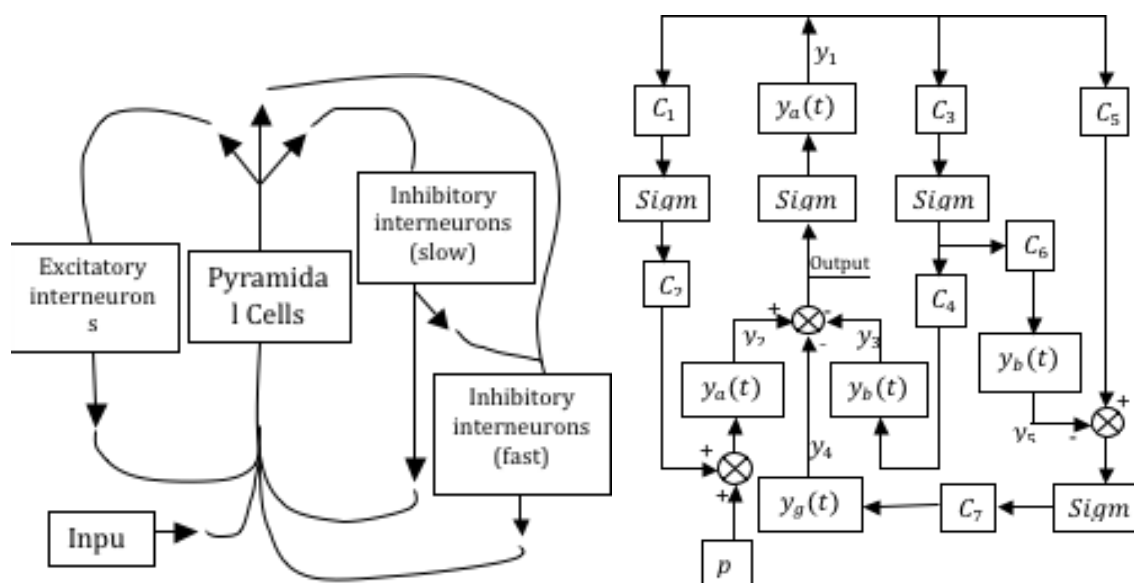


Figure 3.1. Schematic of hippocampal tissue model.

Left: Schematic of neural mass model as defined by [75]. Main population of pyramidal cells interact in feedback loops with three populations of interneurons; one excitatory and two inhibitory interneuron populations with GABA_A projections. One inhibitory population synapses on the dendrites of the pyramidal cells, the other directly onto the soma. This difference in morphology results in two distinct time-scales in the model. The slow inhibitory population also inhibits the fast acting inhibitory population as well as the pyramidal cells. **Right:** Block representation of the model showing relative locations functions. Sigmoids can be thought of as cell bodies, transforming the membrane potential of each population into an output firing rate. Transfer functions represent synapses between populations with C parameters representing connection strengths between populations. Model output is the aggregated activity of all three feedback loops.

In vivo, the firing of action potentials in presynaptic cells gives rise to changes in the membrane potential of the postsynaptic neuron. The model of Wendling et al [72], [91] captures this behaviour by allowing the dynamics of the membrane potential of each synapse to be governed by a second order ordinary differential equation (ODE). Experimental studies have shown that presynaptic action potentials cause the dynamics of postsynaptic membrane

potentials to look similar to alpha functions (see Figure 3.2). By assuming that the temporal width of action potentials is negligible, Wendling et al [72], [91] then model synaptic dynamics as a second order ODE whose solution when being driven by an impulse is given by an alpha function [33] of the form of Equation 3.1. This function transforms the summed firing rate inputs of each synapse into an average post-synaptic potential (PSP). The model also assumes PSPs are linearly summed.

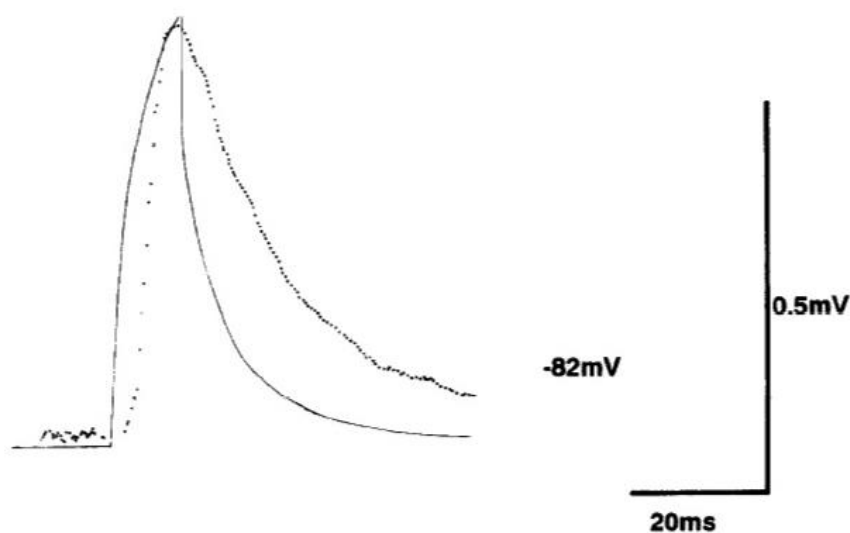


Figure 3.2. Experimentally recorded excitatory postsynaptic potential. Figure reproduced from [140]. Dotted line: Spike triggered EPSP recorded from a neocortical pyramidal neuron. Can be well approximated by an alpha function such as Equation 3.1. Solid line: Postsynaptic response to injected current (not relevant in the current context).

In order to accurately represent physiology, it is required that the post-synaptic potential's response to a pre-synaptic action potential, should have the form of an alpha function (see Figure 3.2). Thus the mean post-synaptic membrane potential y of the n^{th} synapse is given by

$$y_n = \frac{h_n t}{\tau_n} \cdot e^{-t/\tau_n} \quad (3.1)$$

where h_n is the synaptic gain of the n^{th} synapse, which can take one of three values; either A , B or G .

- A is the synaptic gain in the excitatory feedback loop.
- B is the synaptic gain in the slow inhibitory feedback loop.
- C is the synaptic gain in the fast inhibitory feedback loop.

τ_n is the time constant for each synapse and can take one of three values; a , b or g .

- a is the time constant of excitatory synapses.
- b is the time constant of slow inhibitory synapses.
- c is the time constant of fast inhibitory synapses.

The transfer function (Equation 3.1) is the solution to the second order homogeneous ODE,

$$\frac{d^2 y_n(t)}{dt^2} + \frac{2}{\tau_n} \frac{dy_n(t)}{dt} + \frac{y(t)}{\tau_n^2} = 0, \quad (3.2)$$

in which, once again, y_n is the potential of the postsynaptic membrane of the n^{th} synapse. Setting the right hand side equal to the input to the synapse yields

$$\frac{d^2 y_n(t)}{dt^2} + \frac{2}{\tau_n} \frac{dy_n(t)}{dt} + \frac{y(t)}{\tau_n^2} = \frac{h_n x_n(t)}{\tau_n}. \quad (3.3)$$

where $x(t)$ is the firing rate of the postsynaptic neural population in spikes per second. The population's firing rate, x , is related to its presynaptic inputs, v , by a sigmoid function,

$$x(v) = \frac{2e_0}{1 + e^{r(v_0 - v)}} \quad (3.4)$$

Where $2e_0$ is the maximum firing rate, v_0 is the firing threshold potential, and r is the slope of the sigmoid at $v=v_0$. v is the weighted summation of the potentials of the presynaptic nuclei and is therefore given by

$$v = \sum_m C_{mn} y_m. \quad (3.5)$$

Where y_m is the potential of the m^{th} presynaptic nucleus, and C_{mn} is the connection strength between the m^{th} nucleus and the postsynaptic nucleus. Equation 3.4 is known as a *potential to firing rate function*, and transforms the membrane potential of the neuron (which is affected by the activity of the neuron's synapses) into the firing rate of the neuron. Since neurons have physiological bounds to their firing rates both above and below, with smoothly graded activity between these bounds, a sigmoid function is very often used to capture this transformation. See [73] for a detailed discussion of potential to firing rate functions.

Given that the dynamics of each synapse of the generative model is governed by Equations 3.3 – 3.5, the following set of ODEs describes the complete model.

Materials and Methods

$$\begin{aligned}
\ddot{y}_1 &= \frac{A}{a} S\{y_2 - y_3 - y_4\} - \frac{2}{a} \dot{y}_1 - \frac{1}{a^2} y_1, \\
\ddot{y}_2 &= \frac{A}{a} (p + C_2 S\{C_1 y_1\}) - \frac{2}{a} \dot{y}_2 - \frac{1}{a^2} y_2, \\
\ddot{y}_3 &= \frac{B}{b} C_4 S\{C_3 y_1\} - \frac{2}{b} \dot{y}_3 - \frac{1}{b^2} y_3, \\
\ddot{y}_4 &= \frac{G}{g} C_7 S\{C_5 y_1 - y_5\} - \frac{2}{g} \dot{y}_4 - \frac{1}{g^2} y_4, \\
\ddot{y}_5 &= \frac{B}{b} C_6 S\{C_3 y_1\} - \frac{2}{b} \dot{y}_5 - \frac{1}{b^2} y_5,
\end{aligned} \tag{3.6}$$

The dependence of y on t is universal and has therefore been dropped from the notation. y_1 - y_5 are the output potentials in millivolts of the linear transfer functions. Refer to the right hand panel of Figure 3.1 for a graphical representation of the meaning of y_1 - y_5 . The potential to firing rate sigmoid function defined in equation 3.4 is showed as S . Inputs to this sigmoid function are given in $\{\dots\}$. p represents the input to the system from areas of cortex outside the region described by the model, here modeled as a constant of 90 spikes per second (justification below). The average number of synaptic contacts between the main pyramidal cells and the populations of interneurons is parameterised by the dimensionless connectivity constants C_1 to C_7 . See Figure 3.1 for a schematic illustration of the relationships between system variables and parameters and Table 3.1 for a list of parameter values. Each of the above second order ODEs can be split into two first order ODEs, yielding a full system of 10 first order ODEs. This set of

equations was solved numerically using the MatLab ODE solver, ode45, which uses a variable step Runge-Kutta method.

Model output is given by, $\mathbf{y}_2 - \mathbf{y}_3 - \mathbf{y}_4$ since this is the summed activity of all three feedback loops.

Parameter	Interpretation	Value
A	Mean excitatory synaptic gain (mV)	Varied
B	Mean slow inhibitory synaptic gain (mV)	Varied
G	Mean fast inhibitory synaptic gain (mV)	Varied
a	Inverse average time constant - excitatory feedback loop	0.01 s
b	Inverse average time constant - slow inhibitory feedback loop	0.02 s
g	Inverse average time constant - fast inhibitory feedback loop	0.002 s
C1	Connectivity strength – pyramidal to excitatory	C
C2	Connectivity strength – excitatory to pyramidal	0.8 C
C3	Connectivity strength – pyramidal to slow inhibitory	0.25 C
C4	Connectivity strength – slow inhibitory to pyramidal	0.25 C
C5	Connectivity strength – pyramidal to fast inhibitory	0.3 C
C6	Connectivity strength – slow inhibitory to fast inhibitory	0.1 C
C7	Connectivity strength – fast inhibitory to pyramidal	0.8 C
v0,	Firing threshold potential	6 mV
e0	Half of maximum firing rate of neural masses	2.5 s ⁻¹
r	Slope of potential to rate sigmoid function at v=v0	0.56 mV ⁻¹

Table 3.1. Model parameter values and biophysical interpretations. Fixed parameter values were established in [138]. C = 135

3.2.4: Bifurcation theory and numerical continuation

Of particular interest is the understanding of the mechanisms that underlie the transition from one solution type to another within the generative model. Bifurcation theory, which is concerned with the study of changes in the structure of solutions of parameterised differential equations, provides a natural suite of tools for understanding such transitions. Essentially, bifurcation theory enables us to neatly divide regions of model parameter

space into different solution types that can in turn equate to the dynamic waveforms of activity recorded using iEEG. A substantial literature on bifurcation theory has built up in recent years and the reader is referred to [141] for a detailed discussion of the approaches that follow.

A common type of bifurcation is the so-called Hopf bifurcation, which describes the transition from steady-state dynamics to oscillatory behaviour. Such a transition is frequently observed in seizure recordings, where inter-ictal activity resembles a noisy steady state, with the commencement of seizure activity heralded by a transition to oscillations whose amplitude is much larger than the amplitude of the noise driven fluctuations of the inter-ictal state. These oscillations typically have a lower frequency than the preceding inter-ictal activity.

There is another type of transition that commonly occurs in systems with multiple time-scales of activity. This is where the geometry of the vector field itself changes upon smooth variation of a model parameter(s). This corresponds to the appearance of an inflection point in the time-profile of the solution and consequently an extra maxima and minima of the wave profile as variation of the system parameter continues. This type of transition is in contrast to a bifurcation, where the change in behaviour occurs abruptly, resulting in a change of structural stability. However, the transition can appear abrupt if one considers a projection of the system into a lower-dimensional space, hence the term 'false' bifurcation, which was coined by [142] who studied a related phenomenon in fast-slow systems. Within the

context of epilepsy, this type of solution has been used to describe the onset of spikes in a variety of neural models (e.g. [69], [71], [118],[143]. See Figure 3.3).

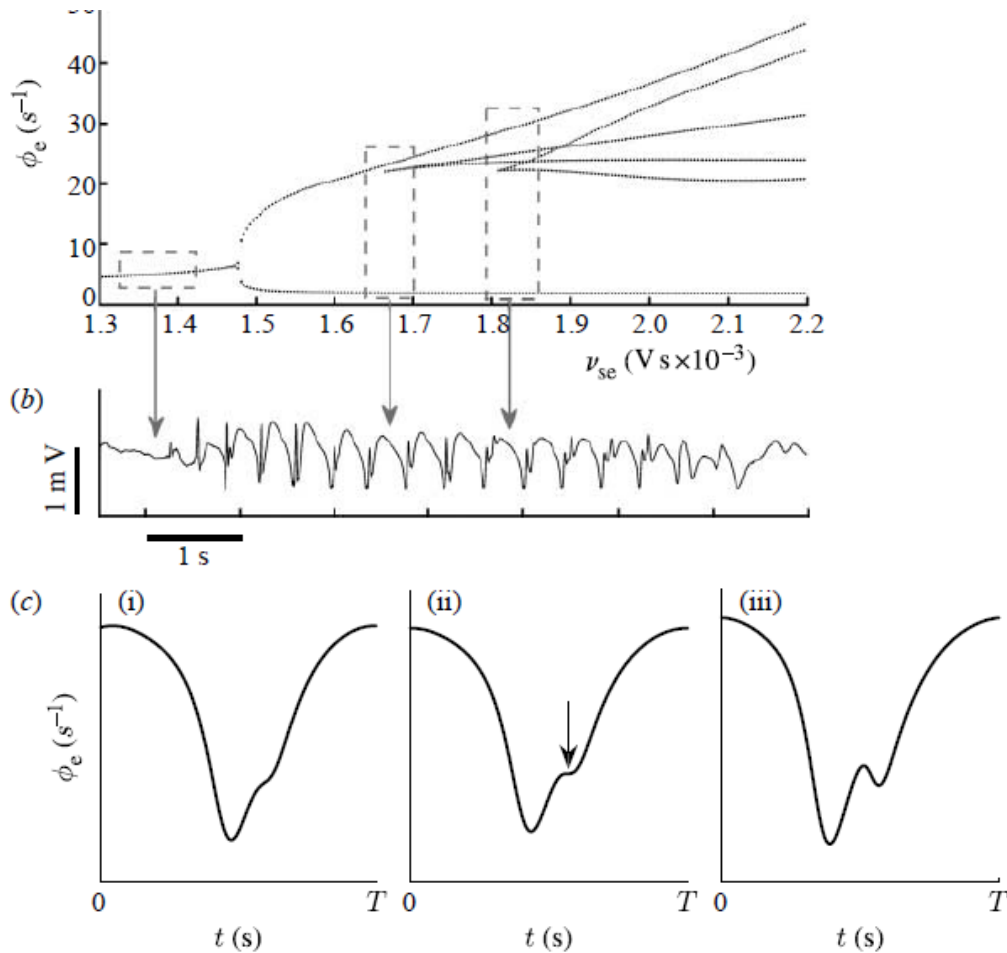


Figure 3.3. Example of a *false bifurcation* from [143].

[143] describes a model of the corticothalamic loop for the study of absence epilepsy. The *spikes* that are ubiquitous in the waveforms of the EEG recorded from absence epilepsy sufferers arise in the model via a false bifurcation; an inflection in the vector field giving rise to what appears to be an abrupt change in system behaviour when viewed in a particular projection. The bifurcation parameter in this case is the cortex-thalamus coupling strength.

To map out curves in parameter space corresponding to these bifurcations, a technique was used called numerical continuation. Described in detail in the

book of [144], continuation techniques are a method for mapping out bifurcation curves in multi-dimensional parameter spaces by essentially formulating the bifurcation in terms of a linear algebra problem, finding an initial solution and then continuing the branch of solutions as parameter(s) are varied. For example, the condition for the presence of a Hopf bifurcation is that the eigenvalues of the Jacobian matrix of the system are a complex conjugate pair with zero real part. Continuation software such as XPPAut [145] or DDE-biftool [146] can vary parameter(s) such that the condition is always satisfied. In this way the continuation software can map out the manifold of the Hopf bifurcation in parameter space. Other bifurcations have their own linear algebraic conditions which may also be continued. In a similar fashion one may also continue branches of false bifurcations by continuing the branch of solutions in parameter space corresponding to a zero first and second derivative (those required for an inflection point) [81].

This paper is related, in part, to the work of [103], who conducted a one-parameter bifurcation analysis of a similar model [138]. Model behaviour was examined as a function of the extrinsic input parameter (p), with all other parameters fixed. It was found that the transition to epilepsy-type oscillations occurred as a result of a Hopf bifurcation at an input value of approximately 90Hz. This work was extended by [104] who systematically studied the effects of changing five parameters (the denritic time constants of the inhibitory and excitatory interneurons and the levels of extrinsic inputs onto all three neural populations) in a modified Jansen & Rit model. This

work is related to earlier studies of variation in extrinsic inputs by [78], [105].

In the present study it is assumed that the average level of input to the area of cortex represented by the model can be regarded as a constant. Inputs to the neural mass model from other areas of cortex (p) have previously been modelled as a constant with the addition of Gaussian white noise. This is primarily to account for other neural activity not explicitly incorporated within the model. However, the current analysis is concerned with the contribution of deterministic mechanisms to the dynamic waveform. Hence, in the interests of capturing the richest variety of dynamics that can be supported by the model, the level of input (p) is instead set constant close to the location of the Hopf bifurcation identified by [147] at 90Hz.

There has been some success using bifurcation and continuation techniques for the study of generalized epilepsy. Marten [71], [118] was able to map solution-types of a neural mass model of the thalamocortical loop (in which typical absence seizure arise) on a two dimensional parameter subspace. Numerical continuation was used to find regions of parameter space separated by lines of Hopf bifurcations and false bifurcations. A similar analysis on the model defined above was conducted. A combination of DDE-Biftool and XPPAut was used to perform numerical continuation.

3.2.5: Relating model solutions to clinical data

Recent work on the modelling of absence epilepsy data has demonstrated that changing features of the EEG could be due to smooth changes in a relatively small number of the underlying system parameters [109]. The characteristic spike and wave discharges (SWD) that are a hallmark of absence seizures, have a frequency of 2-4Hz and are highly synchronous across the entire cortex. In this study, segments of ictal EEG were split into individual spike-wave cycles and model parameters were fitted to each cycle. Features of each cycle (the number of spikes, their ordering and position in phase) were used to determine model parameters, by minimising the distance between the features of the model output and the equivalent features obtained from each spike-wave cycle of the clinical data. The variation of these parameters from cycle to cycle of the overall SWD gives rise to the path through parameter space. SWD are naturally suited to this type of analysis, given the uniformity of EEG and the high signal to noise ratio. In TLE however, there is no such uniformity. The neural activity in TLE originates from a localised area of cortex before spreading to neighbouring regions. Onset can often appear gradual with no clear moment of genesis, and waveforms are not nearly as uniform or synchronous as they are in absence seizures. Thus clearly identifying individual cycles from iEEG data of a TLE seizure is impossible. Consequently, if the hypothesis that the temporal dynamics of TLE are due to smooth changes in system parameters is to be explored, a principled way to segment the data must first be found.

To consider this problem a *selection algorithm* was created, the aim of which is to identify epochs of data across which the parameters of the model are changing minimally. The underlying assumption being that within an epoch parameters are approximately constant, whilst across epochs there may exist gradual variations in parameters and that there is some consistency in this parameter evolution across different seizures from the same patient. This would present evidence for a gradual variation in neural mechanisms that underpins the transition from inter-ictal to ictal dynamics.

It is required that epochs of the iEEG data be identified that are sufficiently small that the model parameters can be regarded as constant over the duration of the epoch, but sufficiently large that a few cycles of any oscillations which may be present can be seen. For instance, if a powerful oscillation exists at 2Hz, and 4 cycles per epoch are required, then it is necessary to select an epoch with a width of about 2 seconds duration.

First the noisy iEEG signal is de-noised by a simple Butterworth low pass filter set at 30Hz to eliminate high frequency noise. MatLab's continuous wavelet transform function (using Morlet-wavelet *cgau4*, and a logarithmic frequency scale from 0.1-30Hz) is then used to calculate the relative power of each frequency at every time step. The matrix of power values is then normalised at each time step to yield the power of each frequency relative to the total power at each time step. It is assumed that the most salient frequency at each instant of the time series is that for which the relative power is maximal. However, the power spectrum at each instant is not

necessarily simple: It may have multiple peaks at different frequencies, or show low-frequency artefacts. For this reason one cannot simply use the frequency for which the power is at a maximum: rather a “centroid frequency” is defined. The centroid frequency of the power spectrum at each instant is calculated by a simple scalar product of the vector of discretised frequencies with the power at each frequency, divided by the total power at that time step. This yields an average frequency which is weighted by the relative power at each frequency. This centroid frequency can be used as a guide for determining the minimum size of the time window that is required to include full cycles of the oscillations with the most power. The reciprocal of the centroid-frequency is approximately the time taken for a single cycle of the most powerful oscillations at that instant in time. This value is multiplied by the number of cycles that are required to be seen in each window to yield the size of the time window needed at each time step. Each and every time step therefore constitutes the centre of an epoch of data, whose temporal breadth is given by the above process.

Since the task is to find the epochs within which the data is at its most stationary, the variance of the spectral properties within all the epochs are then calculated. The variance of the centroid-frequency within each window is calculated and recorded for each time step, as is the variance of the maximum of the power. This yields two vectors whose length is the same as the number of data points in the iEEG. Each element of the first vector is the variance of the centroid-frequency within the epoch of data which is centred

on that time point. Each element of the second vector is the variance of the maximum power within the epoch of data which is centred on that time point. The log of both these vectors is taken. Both vectors are then normalised to unity by dividing each element by the maximum variance in each vector. This gives two vectors of dimensionless measures of variance of frequency and power at each sampling point in the data. These are then added together to yield a *total variance* function. The minimas of this function are the time steps which are the centres of the epochs in which both the frequency and amplitude show minimum variation. It should be noted that, due to the way the total variance function is calculated it is non-smooth, local minima are plentiful. Applying a one second moving-average smoothing procedure to the vector removes local minima. It is also necessary to include a threshold level of the dimensionless variance since local minima still exist for high levels of total variance. The threshold is set at a level which selects only epochs whose total variance is relatively small, in this case 4% of the maximum of the normalised variance (which is two by definition since it is the sum of two quantities which have been normalised to one). In cases where two time windows overlap the window with the lower value of total variance is preserved and the other window is deselected.

This method of time series segmentation is a solution to the problem of how to divide the data into near stationary epochs to which model output can be compared. In this study the evidence for the dynamic evolution of TLE is explored by categorising the profile of waveforms within each epoch of iEEG

using features in the time domain which can be mapped to an equivalent region of parameter space obtained from our bifurcation analysis where the model output has equivalent features. Numbering each epoch according to its dynamic behaviour (see Figure 3.10, right), gives rise to a sequence of length n (being the total number of epochs) from which the consistency of seizure evolution is explored, by studying the consistency of this “seizure sequence” for different seizures.

Table 3.2. Summary of segmentation algorithm

Step	Aim	Procedure
1	Denoise data	Apply 30Hz Butterworth low pass filter to the data, $D(t)$.
2	Calculate the relative power, $P(f,t)$ of each frequency, f , as a function of time, t . * i.e. Calculate the scalogram of $D(t)$.	Apply MatLab's continuous wavelet transform function to $D(t)$, with Morlet-wavelet $cgau4$, and a logarithmic frequency scale from 0.1-30Hz, f .
3	Calculate normalised power values, $Q(f,t)$.	$Q(f,t) = \frac{P(f,t)}{\max(P(f,t))} \Big _{t=T}$
4	Calculate centroid frequency, $F(t)$.	$F(t) = \frac{f \cdot Q(f,t)}{\sum_f Q(f,t)} \Big _{t=T}$
5	Calculate width of time window, $S(t)$, required to see m cycles of oscillations of frequency $F(t)$	$S(t) = \frac{m}{F(t)}$
6	Calculate variance of power, $VP(t)$, in each time window, $S(t)$.	$VP(t) = \text{var}(\max(P(f,t))) \Big _{t=S/2}^{t+S/2}$
7	Calculate variance of centroid frequency, $VF(t)$, in each time window, $S(t)$.	$VF(t) = \text{var}(F(t)) \Big _{t=S/2}^{t+S/2}$
8	Create a metric of the total variability of the signal, $V(t)$, at each time point.	$V(t) = \frac{\log(VP(t))}{\max(\log(VP(t)))} + \frac{\log(VF(t))}{\max(\log(VF(t)))} \Big _{t=T}$
9	Smooth $V(t)$ to remove local minima.	$V_{smooth}(t) = \bar{V}(t) \Big _{t=0.5}^{t+0.5}$
10	Apply threshold to remove high minima	If $V_{smooth}(t) > 0.08$, $V_{smooth}(t) := 0.08$ element-wise for all t in T .
11	Find minima	Find minima of $V_{smooth}(t)$
12	Define segments, K .	$K(n) = D(t) \Big _{t=n-S(t)/2}^{t=n+S(t)/2}$ Where n takes all the values in N . Where N is the set of all times at which V_{smooth} is a minimum.
* Where t takes all values in T , where T is the set of all sampling times in seconds.		

Ultimately, it may be illuminating to precisely fit model parameters to TLE data (rather than based on bifurcation regions) using a tool based on temporal feature detection such as that used by [109] for absence seizures. One of the challenges with pursuing such an approach is the heterogeneity of

waveforms in TLE in contrast to the relatively consistent patterns observed in SWD. There have been some attempts to fit parameters of a neural mass model from clinical recordings in TLE [76]. However, the authors primarily used coarsely discretised spectral properties of temporally broad segments of the iEEG as input to their parameter fitting algorithm. This method is less suited to studying dynamic evolution as theoretical results from nonlinear dynamics have shown that temporal information cannot be recovered from spectral information alone [108], [148], [149].

3.3: Results and Statistical Analyses

Results are presented in three parts. In the first part bifurcation theory and numerical continuation is used to understand transitions in the dynamic behaviour of the model within regions of parameter space considered in earlier studies of the same model [91]. In the second part, the boundaries of the considered parameter space are expanded and bifurcations to more complex wave morphologies containing poly-spike solutions are described, that are strongly reminiscent of the transitions observed in other neural-mass models [119], [150]. These poly-spike complexes are frequently observed in clinical data during focal seizures (this study), as well as in generalized epilepsies [71], [118]. In the third part, changes in data features from clinical recordings to variations in the waveform profiles of the solutions of the model determined from the bifurcation structure are mapped. In this part multiple recordings from a number of patients are

considered to evaluate the consistency of seizure evolution both within and between patients.

3.3.1: Bifurcation analysis: Part I

Initially, the bifurcation analysis of the model will draw direct comparisons with the qualitative analysis of the noise-driven model in [91]. Consequently, the ranges of the free parameters (A , B , G) are restricted to those used in that study ($[3\text{mV}, 7\text{mV}]$, $[0\text{mV}, 50\text{mV}]$, $[0\text{mV}, 30\text{mV}]$) respectively. These parameters correspond to the connectivity strengths of the excitatory interneurons (A), and the slow and fast inhibitory interneurons (B , G) on the pyramidal cell population respectively. In their work Wendling and colleagues presented a number of numerically generated activity maps within which they identified six primary behaviour types and explored the regions of A , B and G for which these behaviour types occurred. The purpose of the next part is to explain these behaviour types in terms of underlying changes in system dynamics.

Simulation of the model for mid-range values of A ($A=5\text{mV}$) and G ($G=20\text{mV}$) show that an equilibrium solution gives way to an oscillatory solution as the value of parameter B is increased (Figure 3.4). Parameter B represents the mean synaptic gain of the slow dendritic GABA_A inhibitory population on the pyramidal cell population. Oscillations begin with arbitrarily small amplitudes and a fixed period. Transition to oscillatory behaviour occurs as a result of a supercritical Hopf bifurcation at a B value of approximately 12mV.

An analysis of the eigenvalues in this region shows a pair of complex conjugate eigenvalues crossing the imaginary axis, confirming the existence of the Hopf bifurcation.

Further increasing B leads to another sudden change in the type of solution. At higher B values ($B = 20\text{mV}$ in the case illustrated in Figure 2) a spike appears in the time series of the simulated EEG, accompanied by a change in the profile of the waveform. This change cannot be considered a true bifurcation, however, since the discontinuity exists only in the particular state-space projection with which represents the EEG signal. Consequently, this behaviour has been termed a false bifurcation [142] (see [81] for a description of continuation method). The location of the false bifurcation coincides with that given in [91] for the emergence of “sustained discharge of spikes” class of model behaviour.

At high values of B ($B > 38\text{mV}$ in the case illustrated in Figure 3.4) the system returns to an equilibrium solution. The transition from spike and wave behaviour to this new equilibrium solution has different properties to the Hopf bifurcation that was seen at the low B value. Close to the transition the amplitude of the oscillation is large, and the period becomes arbitrarily high. The waveform becomes increasingly deformed such that the time series begins to resemble a series of intermittent spikes rather than a smooth oscillation. A one-parameter bifurcation analysis in B (see Figure 2) shows that this behaviour is due to the stable limit cycle meeting the limit point of the high stable equilibrium. This transition is known as a saddle-node on

invariant circle (SNIC) bifurcation. SNIC bifurcations result in a deformation of the vector field in such a way as to permit high amplitude and infinitely long periodic orbits, exactly as is seen in the solutions of the model in this region of parameter space. This behaviour type corresponds to “sporadic spikes” using the terminology of Wendling [91] and colleagues. The sporadic spiking is explained by the decrease in frequency as the SNIC bifurcation is approached.

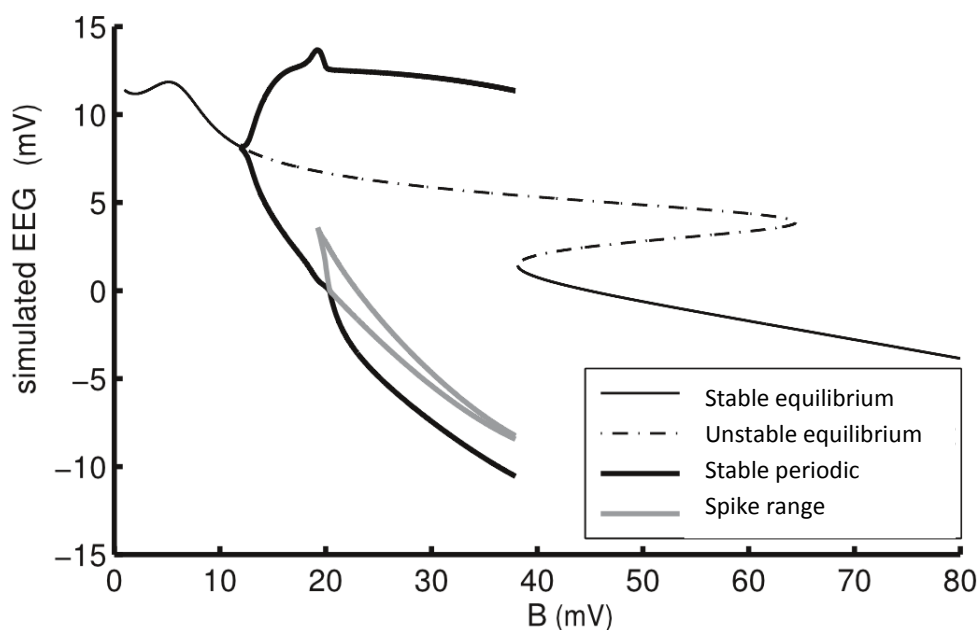


Figure 3.4. A co-dimension 1 bifurcation diagram in parameter B . Thick black lines show maximum and minimum of the simulated EEG potential of each limit cycle. Additional maximum and minimum (where they exist) for each limit cycle is shown in grey. Stable steady state undergoes a supercritical Hopf bifurcation at approximately $B=11\text{mV}$, after which simple “pseudo-sinusoidal” oscillations appear with a single maxima per oscillation. Further increasing parameter B increases the amplitude of oscillations. At approximately $B=20\text{mV}$, the system undergoes a false bifurcation, adding an extra maxima and minima per cycle (shown in grey). At $B=38\text{mV}$ the limit cycle meets the saddle node which is the limit point of the fold. This is a SNIC bifurcation and results in a deformation of the vector field such that, before the bifurcation, high amplitude oscillations exist with an arbitrarily long period. System solutions for values of B above the SNIC are steady states.

The presence of Hopf, false and SNIC bifurcations in the A - B parameter subspace explains many of the qualitative features of the oscillatory solutions. The equilibrium states of this model are now considered. For regions of parameter space, within which the dynamics are at equilibrium, different transient behaviours can be observed when the system is perturbed from this state. These transient behaviours are important since noise continuously disturbs a system from equilibrium. The leading pair of

eigenvalues (the pair with largest real part) of the dynamical system governs the path by which the system returns to its steady state and a transition in this eigenstructure can explain the boundary between the two regions identified in [91], as “low-voltage rapid” and “slow rhythmic” activities (See Figure 3.7 reproduced from [91], for example time series of these behaviours. See Figure 3.8 reproduced from [91] to see the transition between behaviour types in the noise driven model). Low-voltage rapid activity is displayed by the model in regions of parameter space for which the leading eigenvalues are real and negative, whilst slow rhythmic activity is characterised by the leading eigenvalues being a complex conjugate pair with negative real part. The system, when perturbed away from its equilibrium in this region of parameter space will return to steady state via a damped oscillation. When this oscillation is superimposed on the noise (which is the perturbing force) the behaviour seen is that which Wendling [91] describes as “slow rhythmic”. The boundary between these two types of equilibria is defined by the birth or annihilation of a complex conjugate pair of eigenvalues.

Figure 3.5(a) shows the output of numerical continuation software for which all of these transitions in structure for regions of B and G [0mV,50mV] and [0mV,30mV] respectively have been continued. In a recent study, [106] conducted a bifurcation analysis on a dimensionally reduced version of the Wendling model [91] (with similar bifurcation parameters) and identified regions of *normal activity* and *rhythmic spikes* which are in agreement with the results presented in Figure 3.5.

It is important to note that the hard transition lines corresponding to bifurcations and eigenstructure transitions become blurred when considering the noise-driven solutions of the generative model. This makes detecting the actual location of deterministic oscillation-onset (as opposed to noise driven oscillations) impossible when simulating the model. For example, the Hopf bifurcation is supercritical and the stable equilibrium preceding the Hopf is a stable focus-node. A supercritical Hopf bifurcation has the property that oscillations have arbitrarily small amplitudes at the bifurcation point. Crossing a supercritical-Hopf by varying the bifurcation parameter results in oscillations that gradually increase in amplitude from zero. In contrast, when a subcritical-Hopf is crossed, oscillations of a finite amplitude appear suddenly. The stable focus-node means that, although the equilibrium state is stable, when perturbed from equilibrium the system takes a spiral path through phase space on its return to equilibrium. This is transient oscillatory behaviour. This means that when the system is constantly buffeted by noise a succession of oscillatory transients is seen. Ultimately this results in a subjective decision regarding the location of transition points when numerically simulating the noise-driven model (see eg. Figure 3.8, $A=5\text{mV}$ (original location: [91] figure 4, $A=5\text{mV}$)). Figure 3.5(b) shows a two-parameter continuation in the B-A plane which captures the transitions represented in the other panels of, Figure 3.8 (original location: figure 4, [91]).

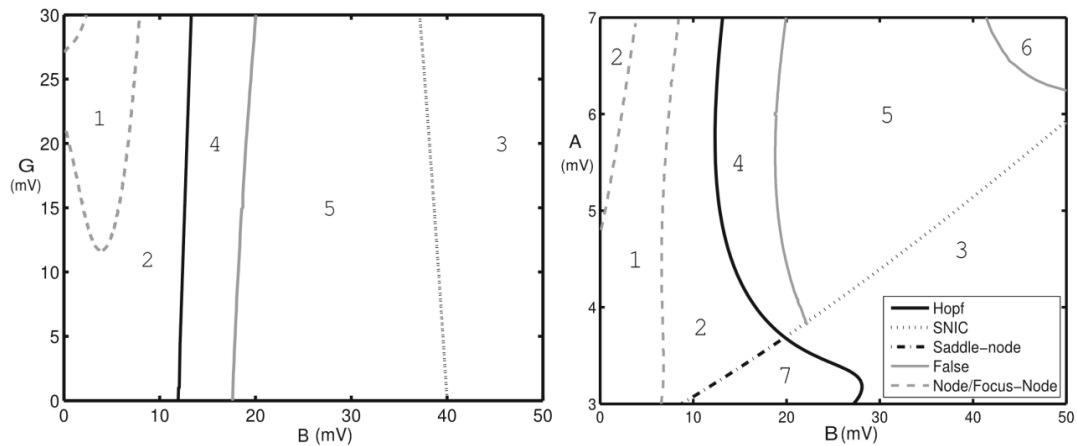


Figure 3.5. Two-parameter numerical continuation diagrams.

Presenting two-parameter numerical continuation plots of the model for the parameter range considered in the studies of Wendling *et al.* [91]. Compare this figure with Figure 3.8 taken from [91]. Region 1: Steady state with leading eigenvalue real and negative (node). Region 2: Steady state with complex conjugate eigenvalues with negative real part (focus-node). Region 3: Steady state. Region 4: Simple “pseudo-sinusoidal” solution-type with a single maxima per cycle. Region 5: Spike and wave solution with two maxima per cycle. Region 6: Characteristic waveform but without the spike. Region 7: Steady state. **Left:** Parameter subspace B-G with $A=5$. Figure can be compared directly with Wendling *et al.* [91] figure 4, middle panel, in which the red region labelled “low voltage rapid activity” corresponds with region 1 in this figure. Region 5 is virtually identical to the green region in the Wendling study [91], in which it was called “sustained discharge of spikes”. A discrepancy exists between region 4 and the comparable “pseudo-sinusoidal” white area identified by Wendling *et al.* [91] See text for an explanation. System solutions close to the SNIC bifurcation are consistent with the behaviour identified by Wendling *et al.* [91] as “sporadic spiking”. **Right:** Parameter subspace A-B plane with $G=20$. Exploring the effect of varying parameter A on overall system dynamics. For high A the oscillatory region in B expands, eventually leading to the appearance of a waveform (region 6) that lacks the additional maxima of region 5. Note that region 1 (the so-called “low voltage rapid activity” in Wendling [91]) extends to high A, with a new region 2 appearing above $A=5$ mV. See Figure 3.6 for examples of waveform profiles from each of these regions

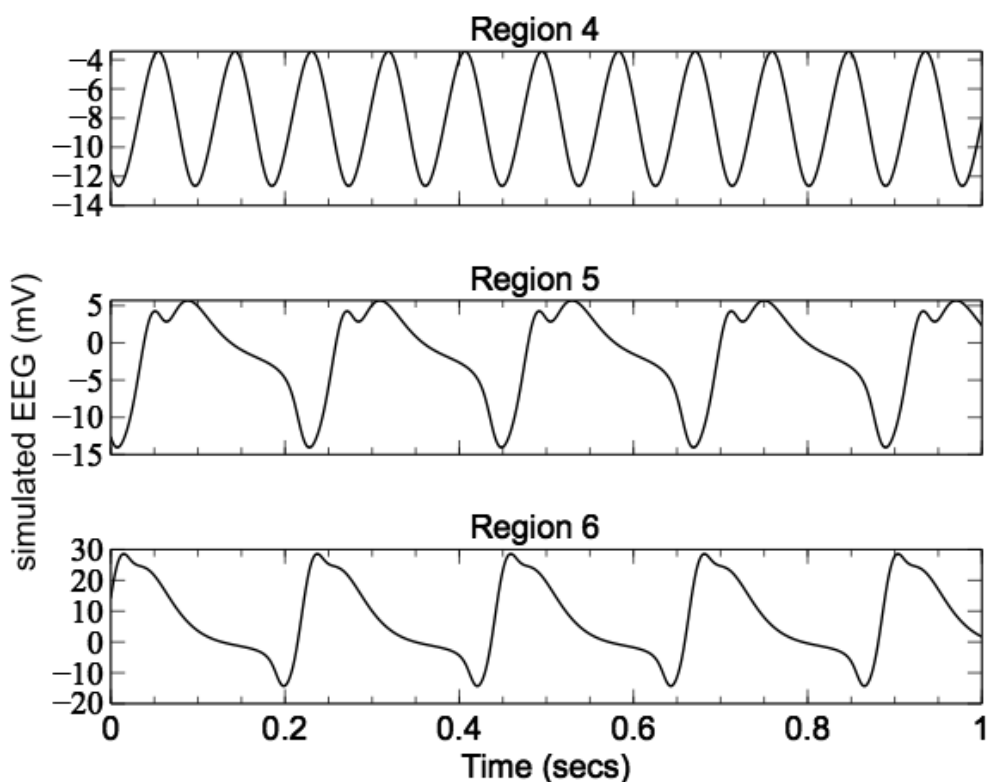


Figure 3.6. Examples of waveforms from regions numbered in Figure 3.5. **Regions 1, 2, 3 and 7** are all steady states and are therefore not shown. **Region 4:** $A=5$, $B=15$, $G=10$. Shown as *white* in Figure 3.7 and Figure 3.8 [91]. **Region 5:** $A=5$, $B=25$, $G=10$. Shown as *green* in Figure 3.7 and Figure 3.8 [91]. **Region 6:** $A=7$, $B=50$, $G=20$. Likely indistinguishable to Region 5 in the noise driven model, and is therefore shown as *green* in Figure 3.8 [91].

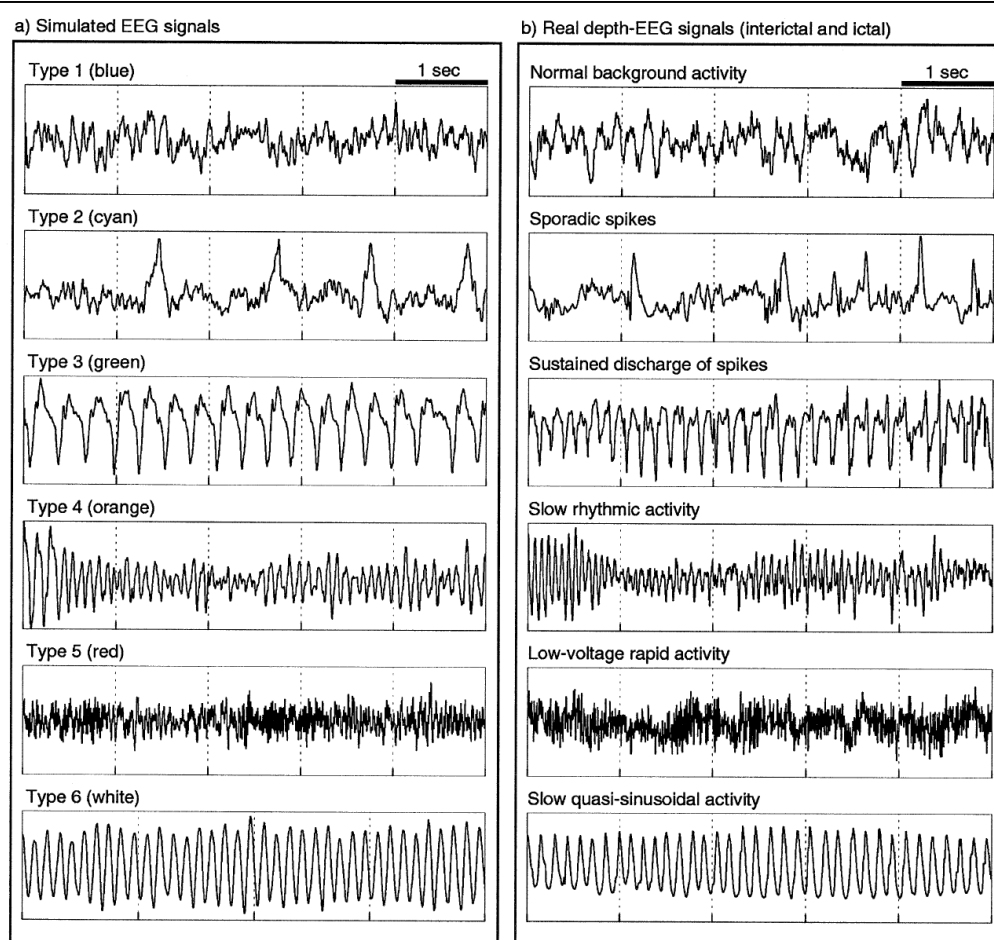


Figure 3.7. Hypocampal EEG behaviour-types in noise driven model and data. Figure reproduced from [91]. Classifications of waveforms seen in the EEG of human TLE sufferers. **Left:** Wendling model outputs. **Right:** Data recorded from human EEGs. Type 6 behaviour is reproduced in the current work in region 4 of Figure 3.5. Type 3 behaviour is reproduced in the current work in region 5 of Figure 3.5. The dynamics of the remaining behaviour-types are a consequence of the noise driven model of [91] being perturbed away from its equilibria. See text for a full discussion.

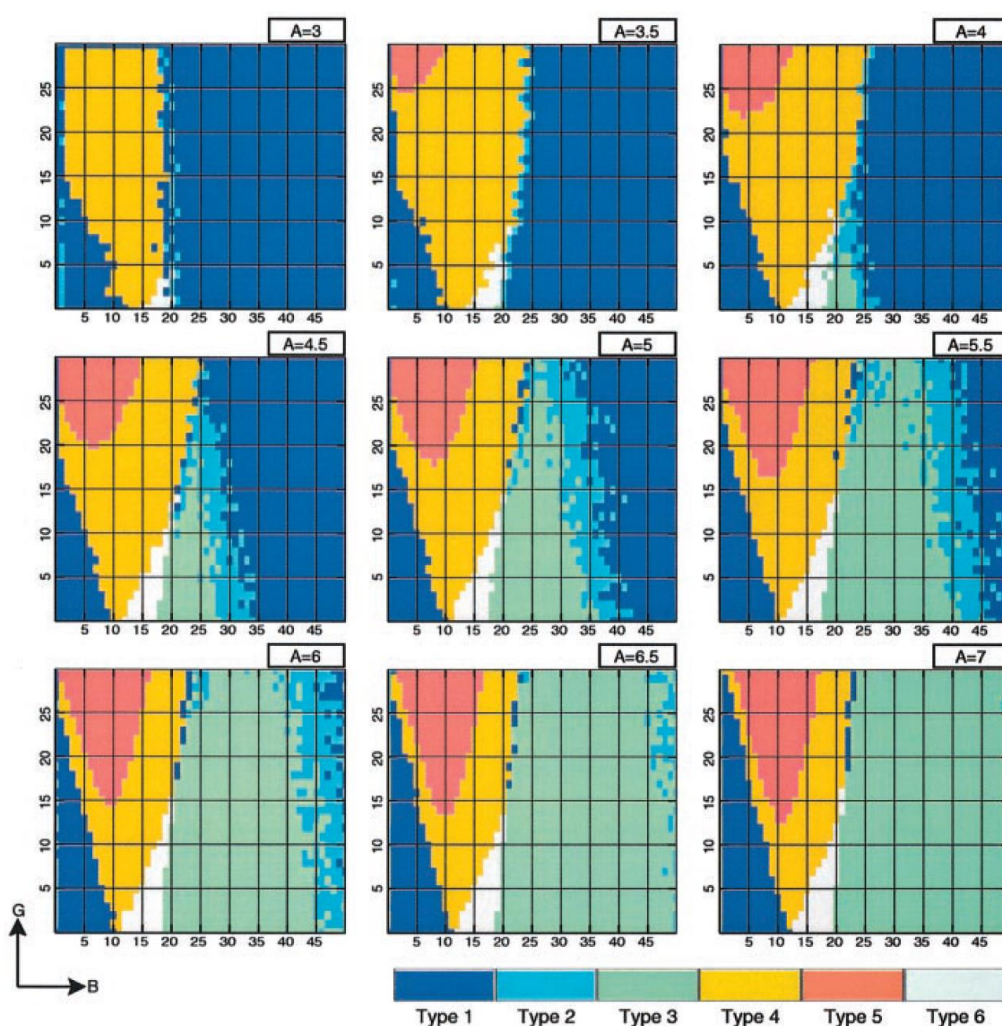


Figure 3.8. Solution-types as a function of synaptic gain parameters (A , B & G) in noise driven model [91].

Figure reproduced directly from [91]. Wendling's noise driven model was simulated at each of the pixels in the above plots. Behaviour-type was classified by hand. This figure is included for direct comparison to Figure 3.5. The current work demonstrates that the solution-types identified in [91] as types 1-6 are explainable in terms of the bifurcation structure and eigenstructure of the system.

3.3.2: Bifurcation analysis: Part II

We now proceed to explore the behaviour of the model upon larger variation of model parameters (B and G) corresponding to the different timescales of inhibitory action of $GABA_A$ projections. This part of the study is motivated in

part by the works of [117], [151], [152] who all explored experimentally how the levels of tonic GABA_A inhibition governed the onset of epileptiform activity in different animal models of epilepsy. Extending the B-G parameter subspace (B[0mV,70mV] and G[0mV,260mV]) it was found that the model supports spike and wave, polyspike complexes, period doubling cascades, and further complex solutions that qualitatively replicate many of the waveforms commonly observed in the EEG of TLE sufferers (see Figure 3.9).

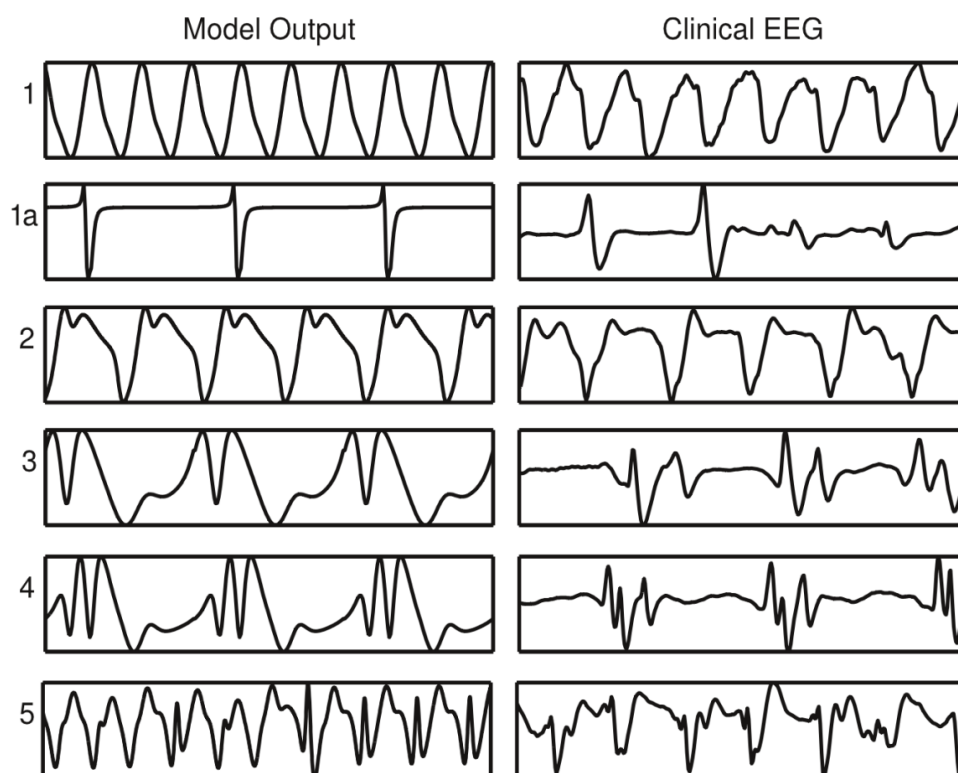


Figure 3.9. Comparison of model with clinical data.

Comparisons of waveform profiles of model output and stationary segments (see results section) of real clinical iEEG recordings of TLE. Examples of waveforms with 1-4 maxima per cycle are shown along with an example of complex chaos-like behaviour (last row). Y axis labels correspond to regions defined subsequently in Figure 3.10. Model outputs are computed using the following $[B, G]$ parameters. 1:[19,60], 1a:[62,40], 2:[23,16], 3:[22,49], 4:[24,149], 5:[24,225].

When the synaptic gain of the fast inhibitory feedback loop (parameter G) is allowed to increase it can be seen that the SNIC bifurcation, which bounds the periodic behaviour, occurs at lower and lower values of the parameter B (synaptic gain of the slow inhibitory feedback loop). The SNIC eventually crosses the Hopf bifurcation creating a bounded region of oscillatory activity (see Figure 3.10). The SNIC-Hopf crossing point occurs at larger values of G as the synaptic gain of the excitatory feedback loop (parameter A) increases.

Hereafter the analysis is restricted to the region of the B-G plane which is bounded by the SNIC curve at $A = 7\text{mV}$.

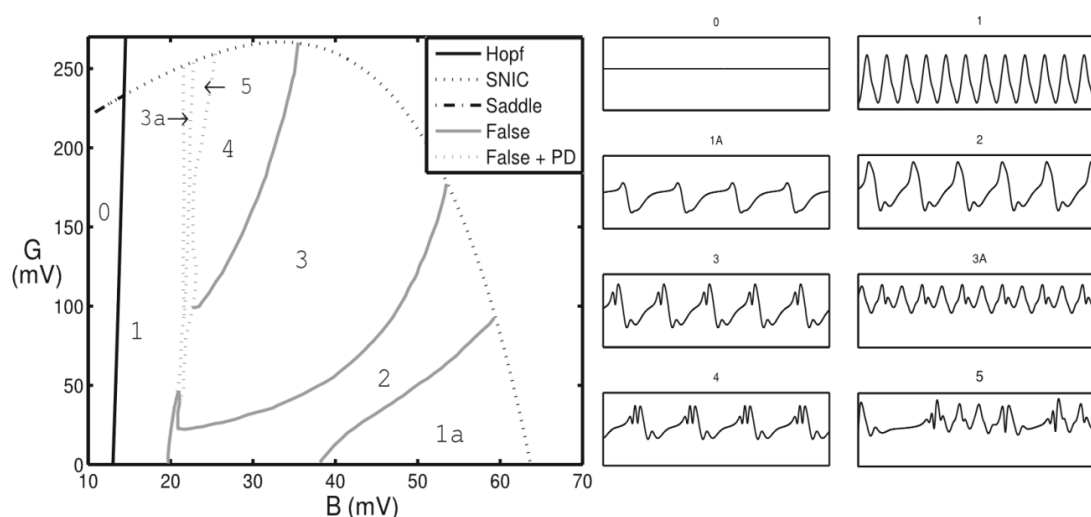


Figure 3.10. Two parameter continuation plot of B and G with associated waveforms.

Main plot shows a two-parameter continuation plot in parameters B (slow GABA_A inhibitory dendritic projection strength) and G (fast GABA_A inhibitory soma projection strength). Only parameter sets bounded by the SNIC bifurcation are considered. Regions are numbered according to the number of maxima per cycle, except region 5, in which more complex chaos-like solutions exist. Panels show exemplars of the expected waveform within each region.

In the present study, solution types are characterised by the number of maxima per oscillation. There are two ways that the number of maxima per oscillation can increase; either through an inflection point in the vector field (the so-called false bifurcation described in the previous subsection) or through a period doubling bifurcation. The Hopf bifurcation occurs at roughly the same value of B for any combination of A and G. Further, the pseudo-sinusoidal solution-type persists alongside it with the first false bifurcation occurring at a roughly constant value of B for all A and G values. Regions of extremely complex behaviour are seen at the boundary between simple pseudo-sinusoidal solutions and solutions with relatively high

numbers of maxima in each period. Approaching these complex regions (by increasing the gain in the slow inhibitory loop, parameter B) the solution undergoes virtually simultaneous false bifurcations and period doublings (see Figure 3.11).

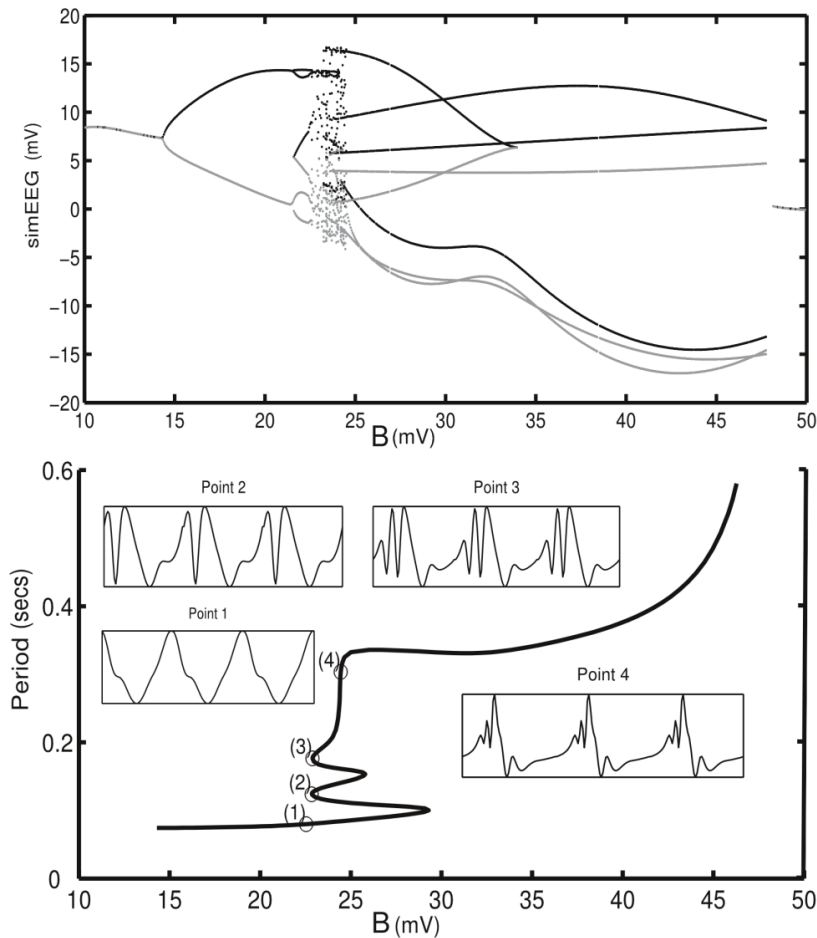


Figure 3.11. Illustrating the deformation of waveform upon increasing parameter B .

Both plots show the same slice through BG plane of $A=7\text{mV}$ at $G=226\text{mV}$. Top: Maximas (minimas) for each orbit of the limit cycle are plotted in black (grey) for varying values of parameter B . Steady states are observed, as expected before the Hopf (at $B=14\text{mV}$) and after the SNIC (at $B=46\text{mV}$). Pseudo-sinusoidal solution emerges at the Hopf and persists until a virtually simultaneous period doubling (PD) and false bifurcations (at $B=22\text{mV}$). Further PDs quickly give way to extremely complex behaviour. A 4-maxima solution exists up to $B=34\text{mV}$, when a false bifurcation annihilates a maxima and minima. A 3-maxima solution then dominates up to the SNIC. Bottom: DDE-BifTool was used to continue a branch of periodic orbits in parameter B . At around $B=24\text{mV}$ the PD can be seen. This region (region 5 in Figure 3.10) is of particular interest since it demonstrates how a high diversity of solutions can exist in a very small region of parameter space. The period tends to infinity as parameter B approaches the SNIC. Each inset shows three periods of the waveform at each of the marked locations on the branch.

When parameters B and G are close to region 5 (the narrow band of apparently chaotic solutions), many different stable solution-types exist in close proximity to each other. This is of particular relevance when studying clinical EEGs as small variations in the connectivity strength of slow GABA_A dendritic projections to pyramidal cells can give rise to sudden and dramatic changes in the shape and period of the waveforms. The solution time series in region 5 of Figure 3.10 appears chaotic, which would be consistent with the period doubling cascade observed numerically.

For values of B above this region of complex behaviour, solutions exist with varying numbers of maxima per period. Transitions between these regions are due solely to false bifurcations, evidenced by the fact that the number of maxima per oscillation changes but no discontinuity exists in the period as one of these boundaries is crossed (see Figure 3.11, B = 34mV).

3.3.3: Consistency of seizure evolution in clinical recordings

The results contained within this section were obtained from intracranial EEG data from three patients, containing thirteen seizures (four from two patients and five from one) in total. For each seizure the channel of the iEEG spatially closest to the clinically determined seizure focus was chosen for analysis. Essentially, this was the channel with the highest amplitude ictal oscillations and the earliest moment of seizure onset. Seizures from each patient are assigned a lower case letter and are referred to as such hereafter.

The presented bifurcation analysis explored regions of parameter space for which the dynamic transitions between solution types of the model were characterised. From initial visual observations of the seizure recordings it can be seen that some seizure evolutions appear qualitatively consistent with parameter variation of the generative model. In patient 3 for example, low amplitude, sinusoidal waveforms can be seen at seizure onset, consistent with crossing a supercritical Hopf bifurcation. Likewise, iEEG at the point of seizure termination in patient 3 displays lower frequency, high amplitude oscillations consistent with approaching and passing through a SNIC bifurcation. The iEEG of all three patients show that early-ictal oscillations have relatively simple waveforms, with extra maxima being added as the seizures evolve. They also show regions which resemble chaotic behaviour at periods during each seizure.

To explore this relationship more quantitatively each seizure recording is subdivided into epochs of data for which the time-series is approximately stationary using the algorithm described in the methods. An example of the output of this algorithm is presented in Figure 3.12. Observable features of dominant waveform within each epoch are identified and these are mapped into the BG parameter plane, labelling them 0-5 according to their dynamic form as presented within Figure 3.10, noting that a five is assigned to segments displaying chaotic-like behaviour. It should be noted that, due to the noise nature of iEEG data it can be difficult to distinguish noisy high-period solutions from chaos.

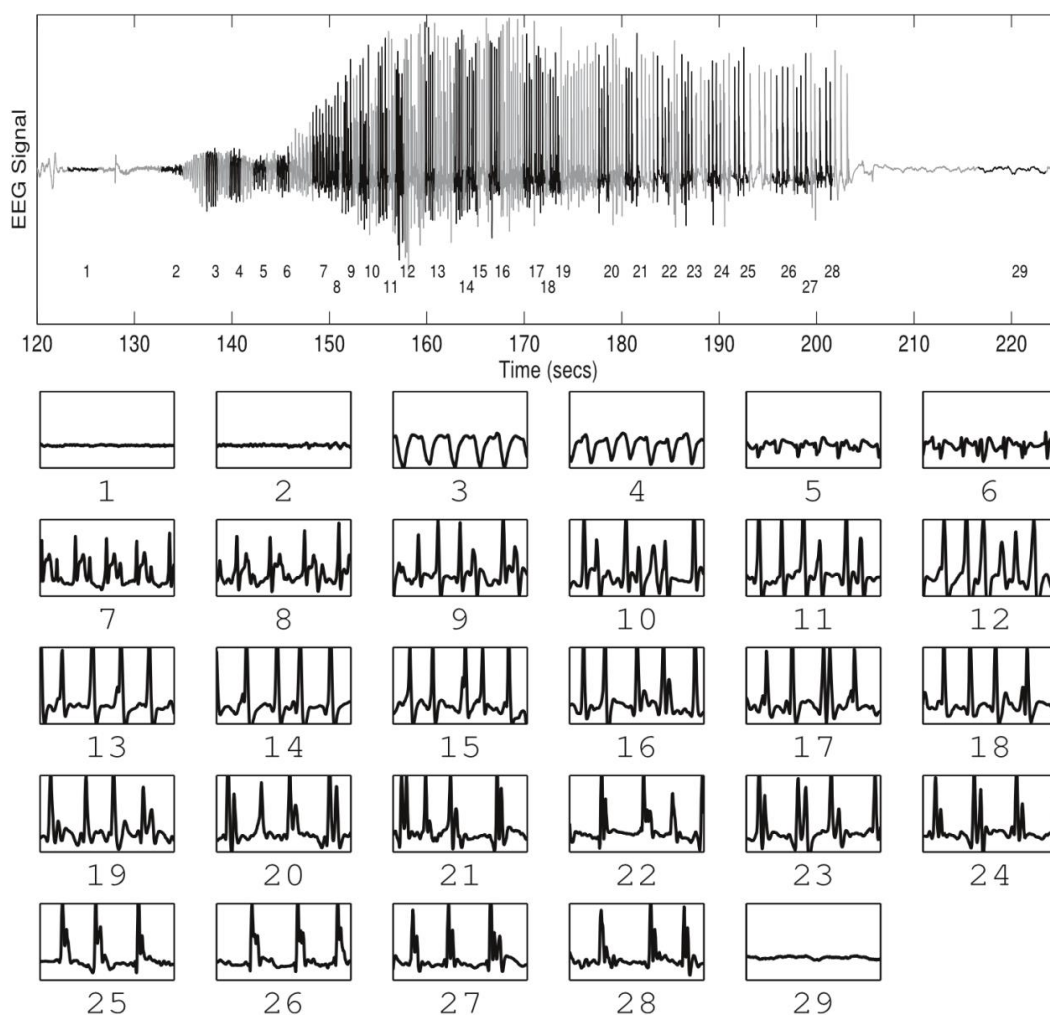


Figure 3.12. Output of stationarity algorithm.

Illustrating the output of the stationarity algorithm used to epoch the clinical data. **Top:** Time series of a discharge, in arbitrary units, shown in grey.

Segments selected by the algorithm shown in black and numbered below.

Bottom: Detailed view of each of the selected stationary segments. In order to classify waveform-types or to fit model parameters to the data sections of the data are found for which the underlying system is approximately stationary.

Each ictal epoch is classified in this way and a vector is created corresponding to all epochs for each seizure. The similarity between these evolutions is then compared by interpolating each vector to a length of 100 corresponding to the time period of the ictal discharge (as the number of epochs identified for each seizure by the segmentation algorithm varies according to how stationary epochs appear). These trend lines are shown in

Figure 3.13. Cross-correlation is used to determine the lag time to maximum correlation of each pair of vectors. This lag time is used to align the vectors so a common point from which ictal evolution is considered. The evolution of each seizure is then truncated to the length of the shortest seizure (to enable the consistency of evolution across seizures to be evaluated). From here, we used two separate measures to quantify the similarity between pairs of seizures; correlation and the Euclidean distance between paths. Euclidean distance, in this context, means the sum of the magnitudes of the element-wise differences between the two vectors.

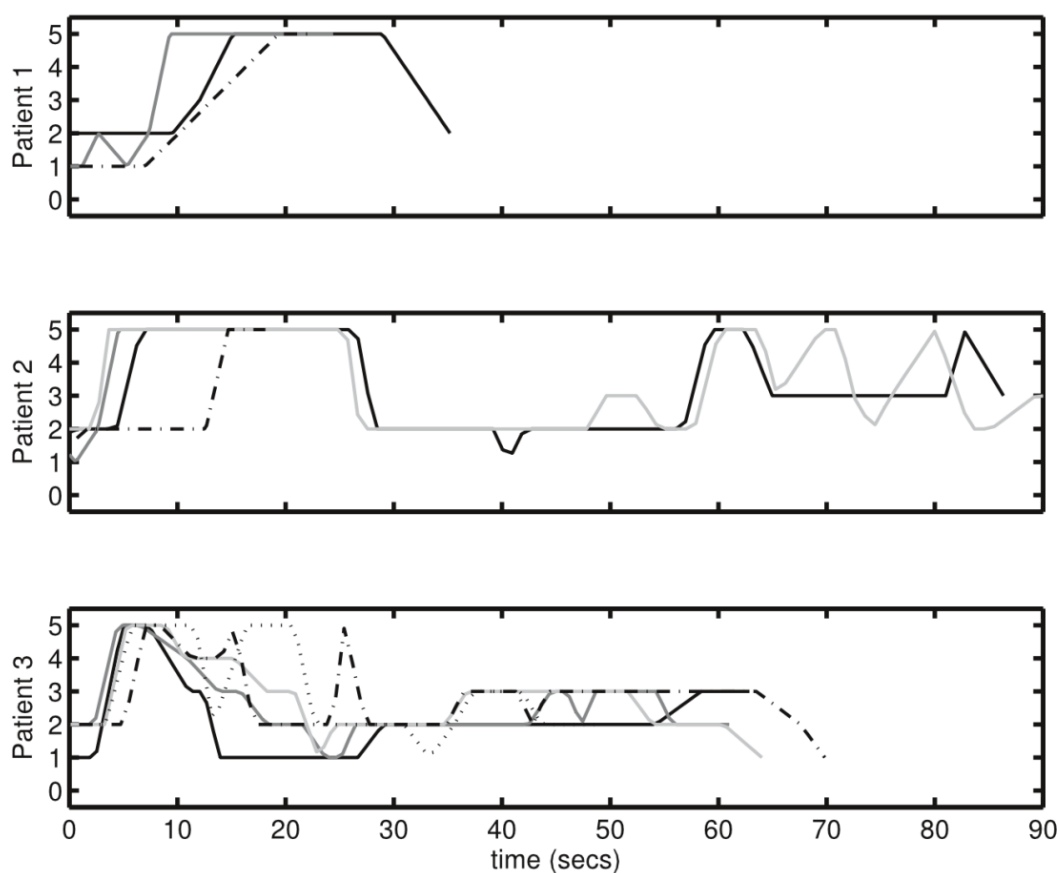


Figure 3.13. Temporal evolution of multiple seizures from three TLE patients. Selected 'stationary' epochs are classified by the number of maxima per cycle, with apparently chaotic segments assigned a five (y-axes on above plots). Segments are re-normalised in time and aligned with each other according to the approximate start of the discharge seizure. Vectors are then interpolated and then truncated to the time window of the shortest seizure. For each patient the same channel was used for analysis each time, with the exception of one seizure from patient 1, where a discharge (seizure *d*) occurred in the opposite hemisphere relative to all others and is therefore omitted from the plot.

To test whether pairs of seizures are statistically similar, correlations and Euclidean distances were compared to the Euclidean distances and correlations between randomly generated vectors. Vectors of the same length as those given by the number of ictal segments were filled with digits 0-5, with equal probability. As with the real data, each vector was

interpolated to 100, aligned with each other by maximum correlation, truncated and re-interpolated to 100. Correlations and Euclidean distances between pairs of vectors were calculated and used to generate two distributions (see Figure 3.14). Statistical significance was assessed by evaluating the 5% and 1% values of these distributions of random trends.

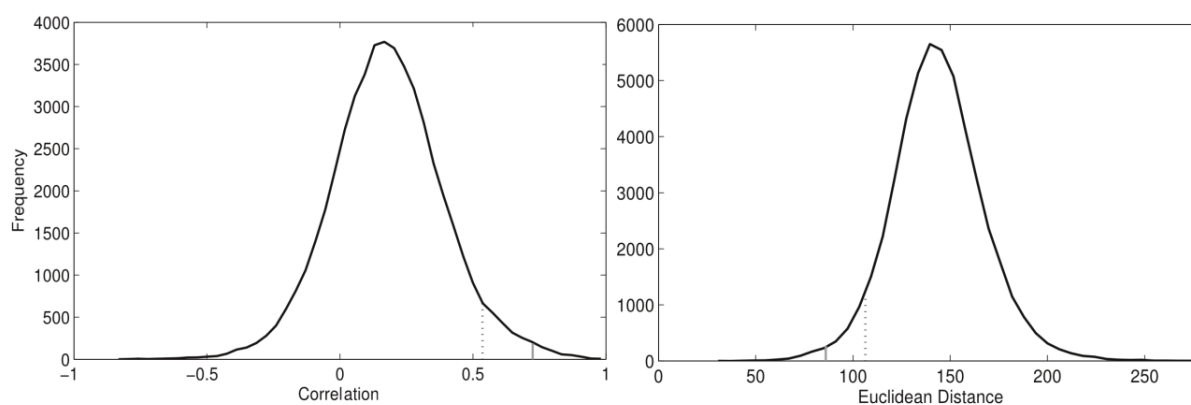


Figure 3.14. Distributions of random vectors for statistical tests.

10,000 random vectors, with entries 0-5, of varying lengths corresponding to those of the original seizure recordings were calculated. Random pairs of vectors were then compared. As with the real data the two vectors were aligned by maximum cross-correlation and the longer vector cropped to the length of the shorter (in the same manner used to compare the seizure evolutions). The distributions of these random trends for either the correlation (Left panel) or Euclidean distance (Right panel) was then calculated. 5% confidence level are shown by the dotted lines (0.536 correlation, 106.4 Euclidean distance). 1% confidence level given by the solid grey lines (0.725 correlation, 86.0 Euclidean distance).

Using either measure, the calculated evolutions were found to be strongly statistically significant across many of the considered pairs for all three patients (see

However, given the nature of EEG recordings and the different length of seizures (for example discharge 'b' and 'c' in patient 2 were of short duration compared to the other discharges), not all pairs display significance and this

Results and Statistical Analyses

should not be considered surprising. Further, it should be noted that the seizure focus for discharge ‘d’ of patient 1 was clinically determined to occur in the opposite hemisphere to all other recorded discharges for this patient. Again, it should not be expected that significant correlations would be observed between this discharge and others from the same patient.

Patient 1			Patient 2			Patient 3		
Pair	Corrltn.	Euc. Dist	Pair	Corrltn.	Euc. Dist	Pair	Corrltn.	Euc. Dist
a,b**	0.8574 (0.0018)	53.3 (0.0003)	a,b	0.1894 (0.4724)	159.4 (0.7691)	a,b	0.7416 (0.0080)	62.0 (0.0007)
a,c**	0.8051 (0.0036)	124.0 (0.1833)	a,c**	0.7299 (0.0095)	56.6 (0.0004)	a,c	0.4489 (0.0965)	96.8 (0.0230)
a,d	-0.3990 (0.9950)	194.9 (0.9778)	a,d	0.0580 (0.7276)	138.1 (0.4059)	a,d	0.6239 (0.0251)	98.0 (0.0256)
b,c	0.7102 (0.0117)	126.7 (0.2184)	b,c	-0.2602 (0.9814)	189.3 (0.9677)	a,e	-0.2789 (0.9843)	139.9 (0.4405)
b,d	-0.0151 (0.8357)	192.3 (0.9736)	b,d	0.5097 (0.0614)	138.2 (0.4077)	b,c	0.7452 (0.0077)	53.4 (0.0003)
c,d	-0.3927 (0.9946)	181.6 (0.9443)	c,d	0.1757 (0.5001)	129.5 (0.2601)	b,d	0.3890 (0.1493)	70.6 (0.0020)
						c,d	0.3867 (0.1520)	58.5 (0.0005)
						c,e*	0.6080 (0.0283)	69.6 (0.0018)
						d,e	0.3979 (0.1410)	81.3 (0.0066)

Table 3.3. Correlations between seizures for each patient. Seizures are labelled *a-d* for each patient (*a-e* for patient 3). Stationary segments from each seizure were classified according to solution-type (See Figure 3.10). Correlations and Euclidean distances between different seizures from each patient were calculated and compared against a distribution constructed from a similar pairwise comparison between 10,000 randomly generated vectors. P-values shown in brackets below each result. All seizures are recorded from the same channel for each patient with the exception of seizure “d” from patient 1, which was recorded from a seizure whose focus was in the opposite hemisphere from the others.

These findings show that significant similarities exist in the evolution of temporal features of different seizures from the same patient. Whilst our characterisation of time-evolution is crude in many respects, that such strong

significances are observed is suggestive that a method to fit parameters of the underlying generative model based on temporal-features of the clinical data (following a similar approach to Nevado-Holgado et al., 2012 will provide additional information. There are many challenges that must be overcome to allow such an approach to work in this more complex setting.

3.4: Discussion

In this chapter, the relationship between the dynamics of a generative model of intracranial EEG recordings introduced by Wendling [91] and clinical recordings from patients with temporal lobe epilepsy has been explored. A combination of bifurcation theory and numerical continuation has been used to explore how combinations of Hopf bifurcations, false bifurcations, SNICs and eigenstructure changes in the noise free model, give rise to dynamics that are strongly reminiscent of clinically observed waveforms and those of the noisy model as characterised by [91]. Extending these findings to larger parameter planes, it was found that more complex transitions including period doublings and multiple false bifurcations, which give rise to polyspike complexes that are frequently observed in clinical recordings. Using an algorithm for determining approximately stationary epochs of data from intracranial EEG recordings a path through parameter space was mapped out by matching temporal features of each identified epoch to regions of parameter space identified from numerical continuation, observing consistencies across several seizures from each patient.

The Wendling model is closely related to the model of the EEG developed by Jansen & Rit [138] in which a population of cortical pyramidal neurons is connected to two feedback loops of interneuron populations, one excitatory and one inhibitory. The Wendling model includes an additional inhibitory feedback loop that has a shorter timescale to represent what is known of the connectivity of hippocampal cortex. The analysis in this chapter shows that the inclusion of two timescale of inhibition allows the model to capture time domain features that cannot be created by the Jansen & Rit formulation. The Wendling model is therefore an improvement over the Jansen & Rit model for the modelling of hippocampal tissue. However, any future work that attempts to model spatial evolution of seizures across the cortex should note that the Wendling formulation is a model of mass action in the hippocampus and not a model of the EEG. Spatial dependencies would therefore have to be modelled using formulations such as [34], [63], [90] using the output of the Wendling model as inputs.

It is important to note that subtle changes in parameters of the generative model give rise to a wide-variety of complex waveforms. Of particular importance is that changes in different model parameters (in our case reflected changes in fast and slow inhibitory mechanisms) result in near-identical waveforms that would be indistinguishable using standard clinical methodologies. Given that subtle changes in different mechanisms would most likely warrant different treatment strategies, an additional

computerised analysis of EEG may ultimately enable more robust decisions regarding treatment strategy at the point of first diagnosis.

To enable this would require two important steps. The first is for greater validation studies of neural mass models that are currently used to study clinical data. The need for this is to establish the precise relationships between parameter variation of the generative model and the neurophysiological changes that underpin the observation data. Experimental models provide a route towards model validation (although care must be taken with linking between animal models of epilepsy and their clinical equivalents) and studies such as [117], [151], [152] are all suggestive of changes to GABA_A dynamics in different epilepsy models that may be captured by varying inhibitory mechanisms of neural mass models. Such animal models may provide the environment to systematically explore the conditions that favour, or prevent, particular types of dynamic transitions. A similar approach has been used by [90] to characterise transition to epileptiform dynamics by modelling the effect of general anaesthetic agents.

The second step is to develop more robust methods for fitting parameters of an underlying generative model to the diversity of clinical waveforms observed during focal discharges. For example, the work of Fabrice Wendling et al., 2005 and our current study both suggest consistency of underlying mechanisms during seizures. However these methods are likely too crude to capture the subtle changes in parameters that may underpin the dynamic evolution recorded clinically. The recent study of [92] used a multi-objective

genetic algorithm (MOGA) to fit parameters of a neural mass model from scalp EEG that was clinically recorded from patients with idiopathic generalized epilepsies. Extending this work to enable the MOGA to fit the wider variety of waveforms observed from iEEG may represent an initial step towards the patient specific modelling of epilepsy.

3.5: Summary

- The relationship between the eigenstructure of a generative model of the EEG and clinical recordings has been illuminated. Eigenstructure changes in the model give rise to waveform profiles that have a strong resemblance to clinically recorded iEEGs.
- Small changes in certain parameter values give rise to dramatic and obvious changes in the profiles of simulated waveforms. Of particular importance is the relative strength of the two inhibitory feedback loops of interneurons that have different characteristic timescales.
- Bifurcation analysis of the model allows the waveform profiles to be characterised across the parameter space. Clinically recorded EEGs were temporally segmented using a novel algorithm and these segments were categorised according to which region of the parameter space of the model they most closely resembled. This analysis demonstrated that there exist statistically significant similarities between different seizures from the same patient. Thus it can be concluded that the evolution of focal onset TLE seizures is likely to follow a characteristic pattern for each sufferer.

Chapter 4: Bayesian estimation of connection strengths between neural populations using SMC-ABC

4.1: Introduction

The increase in computational power over recent years, combined with the increase in understanding of neural systems has led to an explosion in neural modelling studies. A serious issue at the heart of modelling is how to find the values of parameters that are inherently undiscoverable by purely experimental methods. The connection strength between two populations of neurons is the main example of this kind of parameter with which subsequent chapters will be concerned.

The value of the connection strength is a function of multiple physiological elements, for example; number of receptors per synapse; number of synapses; location of the synapses on the dendrites; and many more. Measuring each of these variables experimentally and calculating a value is impossible, hence the need to use available experimental evidence to infer values.

The Bayesian paradigm provides a natural choice for the inference of parameter values, since it is inherent in the Bayesian framework that

parameters are learned through evidence rather than assumed, as is the case in frequentist frameworks. The Bayesian approach also has the advantage that distributions of parameter values are inferred rather than a single *best* or *adequate* value. Having access to the full distribution of parameter values that explain the observed data gives the modeller much more information about the robustness of the system to small changes in parameters and therefore the means to assess the validity of conclusions drawn from the model.

However, Bayesian techniques have not been widely used in neural modelling due to the difficulty in calculating the *likelihood function*, the probability of observing the experimental data given a particular set of parameter values. In instances where compute-time of a single simulation is relatively large, the computational overhead of doing sufficient simulations to calculate the likelihood is often too large to be tractable. All but the simplest toy neural models fall into this category. There have, over the last decade or so, been advances in so called *likelihood free* inference techniques in which the likelihood is approximated by sampling from the posterior. For a full review of these techniques see [102]. Outlined in this chapter is a simple and effective method for finding the parameters of high dimensional systems, called *sequential Monte-Carlo approximate Bayesian computation* (SMC-ABC) [100].

4.2: Description of the method

4.2.1: Introduction to likelihood free Bayesian inference

Bayesian computation in general requires the modeller to estimate a conditional probability density that describes the probability of any parameter vector, θ , given the observed data, x . This is known as the posterior distribution and is given by Bayes rule,

$$p(\theta|x) = \frac{p(x|\theta)\pi(\theta)}{p(x)}. \quad (4.1)$$

This is very often hard to compute owing to the difficulty of calculating the marginal likelihood $P(x)$, which can be stated as the *probability of the data* and is often a high dimensional integral:

$$p(x) = \int p(x|\theta).\pi(\theta)d\theta \quad (4.2)$$

This problem can be avoided by noting that $p(x)$ can be evaluated to a normalising constant, yielding a relative measure of the posterior probability of parameter vectors rather than an absolute measure, which in most cases is sufficient. However, as models become more complex, the definition and calculation of the *likelihood*, $p(x|\theta)$, becomes difficult. It becomes easier to generate data, x , by simulating the model with parameter vector θ . If the data being modelled are discrete and of low dimension, one can use this to generate the posterior distribution without having to calculate the likelihood

using the following algorithm from [153], in which $\pi(\theta)$ is the prior distribution of θ .

For an observed data point, y . Repeat the following until N parameter vectors are found.

Draw $\theta_i \sim \pi(\theta)$

Simulate $x_i \sim p(x|\theta_i)$

Reject θ_i **if** $x_i \neq y$

This simple case can be generalised to models in which the system variables are continuous by comparing some measure of the *distance*, φ , between the data y and the simulated data, x_i , to a threshold ε . Performing this operation means the result is an approximation to the posterior rather than posterior itself.

Reject θ_i **if** $\varphi(x_i, y) > \varepsilon$

This can be further generalised to more complex systems by using some summary statistic, S , to reduce the number of dimensions, yielding a complete *approximate Bayesian computation* algorithm [154]:

For an observed data point, y . Repeat the following until N parameter vectors are found.

Draw $\theta_i \sim \pi(\theta)$

Simulate $x_i \sim p(x|\theta_i)$

Reject θ_i **if** $\varphi(S(x_i), S(y)) > \varepsilon$

Values are assigned to the unknown parameters from a prior distribution which is informed by pre-existing knowledge of the system. The simulation is run using these values and the model output is then used to compute an *error statistic*. The error statistic is compared to a threshold; if it is below

threshold then the random values constitute an acceptable parameter set and the values are stored; if the error statistic is above threshold then the values are rejected. This process continues until N acceptable parameter-sets are found. This process is approximate Bayesian computation [101]. However, in cases where the data is highly informative and the dimensionality of the parameter space is high, this algorithm is still unable to find a good approximation to the posterior in acceptable compute times. A solution to this issue is to use *sequential* sampling. This is the method that is employed in the modelling work of the following chapters as is therefore described in detail.

4.2.2: SMC-ABC method

When dealing with high dimensional parameter spaces where the data is highly constraining to the values being sought, the above method alone is inefficient. An improved algorithm has been suggested [100], in which the rejection threshold is initially set to be very large such that it is relatively easy for the values drawn from the prior to be accepted. Each of the N parameter sets is assigned a weight and the threshold decreased. A parameter set is chosen from the N sets of the previous iteration using a weighted random selection. All the parameter values in this set are perturbed to create a new parameter-set by adding a noise term drawn from a zero mean Gaussian kernel with a variance of twice the variance of that parameter across all N values [102]. As before, the simulation is then run using the new parameter values and the error statistic computed. The error

statistic is then compared to the new lower threshold and the parameter-set is accepted or rejected. This process continues until we once again have N acceptable sets. The threshold is decreased further still and the whole process is repeated. The effect of the algorithm could be visualised as using a loose threshold to “capture” parameter-sets and then shrinking the threshold to shepherd the sets into the region of parameter space that is acceptable according to the final (strict) rejection threshold. See Figure 4.1 for a graphical description of the algorithm.

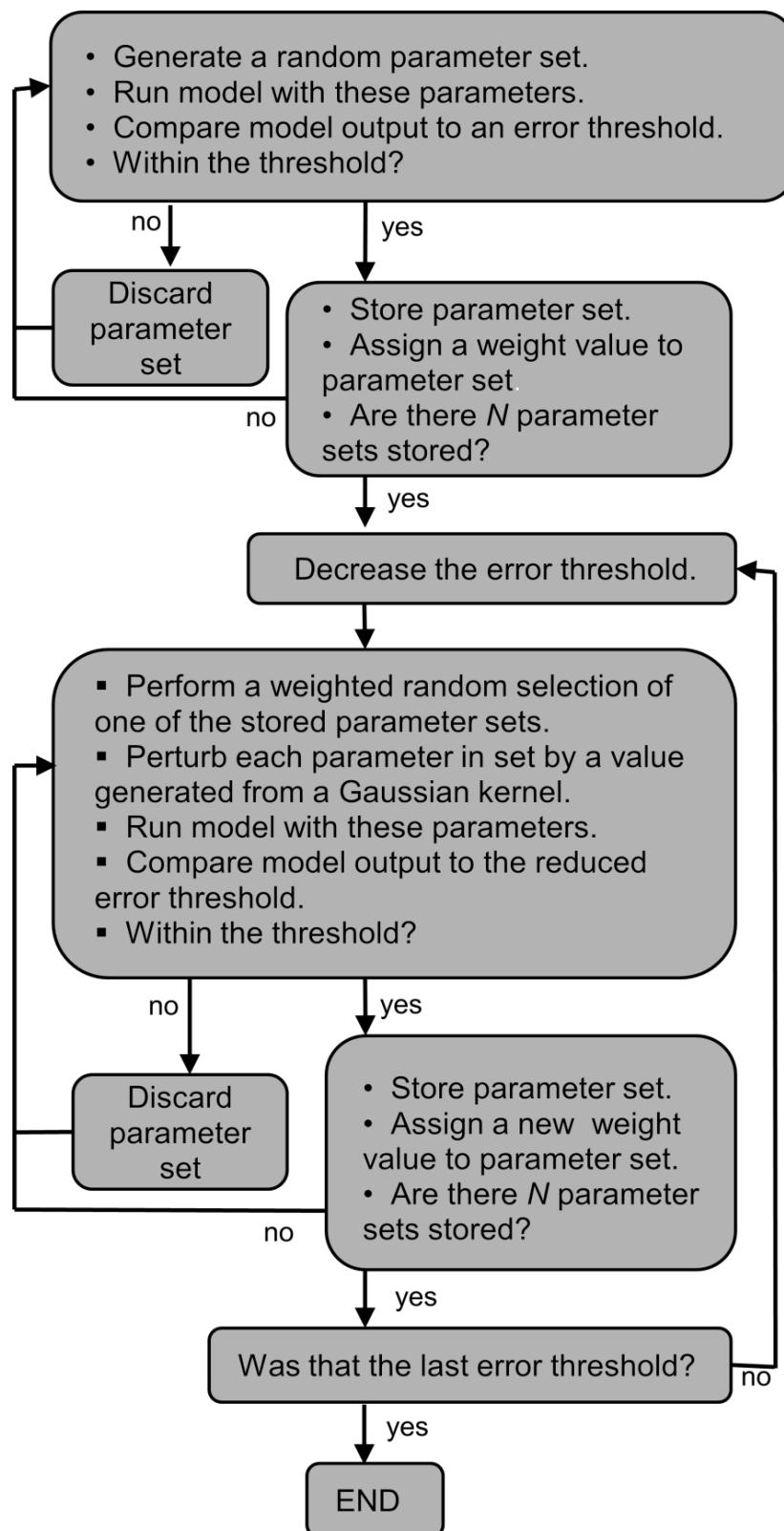


Figure 4.1. Flow chart describing the SMC-ABC algorithm.

4.2.3: SMC-ABC Algorithm

The following algorithm was formulated by Beaumont [155] but is very similar to the algorithms of Toni [99] and Sisson [100]. In the following pseudo-code $\theta_i^{(t)}$ is the i^{th} parameter-set in the t^{th} iteration. It is a column vector with length equal to the number of free parameters. $\theta^{(t)}$ refers to all N parameter-sets found in the t^{th} iteration. $\pi(\theta)$ is the prior distribution of θ , and $\pi(\theta_i^{(t)})$ is the value of the prior distribution evaluated at $\theta_i^{(t)}$. N is the number of parameter-sets to be found. $\varepsilon_1, \varepsilon_2, \varepsilon_3, \dots, \varepsilon_t, \dots, \varepsilon_T$ is a series of incrementally decreasing rejection thresholds. f is the model that generates the simulated data, y , using the parameter-set $\theta_i^{(t)}$. D is the function that generates the error statistic from the simulated data. K is a Gaussian kernel.

for iteration $t = 1$

Set index, $i = 1$

while $i < N$

Sample $\theta_i^{(t)}$ from $\pi(\theta)$

Use $\theta_i^{(t)}$ to generate simulated data y . $y \sim f(y | \theta_i^{(t)})$

Generate error statistic $D_i(y)$.

if $D_i \leq \varepsilon_t$

set weight, $w_i^{(t)} = \frac{1}{N}$

set index, $i = i + 1$

end if

Description of the method

end while

Set $\tau^2 = 2 \text{var}(\theta^{(t)})$

Normalise weights

end for

for iteration $2 \leq t \leq T$

Set index, $i = 1$

while $i < N$

Sample θ_i^* from $\theta^{(t-1)}$ with probabilities $w^{(t-1)}$

Create $\theta_i^{(t)}$ by perturbing θ_i^* . $\theta_i^{(t)} \sim K(\theta | \theta_i^*; \tau^2)$

Use $\theta_i^{(t)}$ to generate simulated data y . $y \sim f(y | \theta_i^{(t)})$

Generate error statistic $D_i(y)$.

if $D_i \leq \varepsilon_i$

set weight, $w_i^{(t)} = \frac{\pi(\theta_i^{(t)})}{\sum_{j=1}^N w_j^{(t-1)} K(\theta_i^{(t)} | \theta_j^{(t-1)}; \tau^2)}$

set index, $i = i + 1$

end if

end while

Set $\tau^2 = 2 \text{var}(\theta^{(t)})$

Normalise weights

end for

4.2.4: Validating the use of SMC-ABC

Since SMC-ABC has not previously been used in the field of neural modelling its use is evaluated and validated for the first time here for neural modelling by replicating an earlier study by Nevado Holgado [50]. The Nevado Holgado (NH) model is a first order firing rate model of the STN-GPe feedback loop. The model is defined by the following pair of first order delay differential equations representing the dynamics of the feedback loop between the STN and the GPe under constant inputs from cortex and striatum.

$$\begin{aligned}\tau_S \dot{Y}_S &= F_S \left(W_{G-S} Y_{GP}^{(t-\Delta T_{GS})} + W_{Ctx-S} Ctx \right) - Y_S \\ \tau_G \dot{Y}_G &= F_G \left(W_{S-G} Y_{STN}^{(t-\Delta T_{SG})} - W_{G-G} Y_G^{(t-\Delta T_{GG})} + W_{Str-G} Str \right) - Y_G\end{aligned}\tag{4.3}$$

Function dependencies are shown in superscript for clarity. τ is the membrane time constant of either GPe (G) or STN (S) neurons; Y is the firing rate of each nucleus; W_{m-n} is the connection strength between the m^{th} and the n^{th} nuclei; Ctx and Str are the inputs to the system from cortex and striatum respectively; ΔT_{mn} is the axonal transmission delay between nuclei m and n . F is a function that transforms each nucleus's summed inputs into the firing rate of the nucleus. It is given by

$$F = \frac{M_n}{\left(1 + \frac{(M_n - B_n)}{B_n} \exp\left(\frac{-4k_n}{M_n}\right) \right)}\tag{4.4}$$

Model parameters are given in Table 4.1

Description of the method

Table 4.1. Parameter values and sources for the Nevado-Holgado model [50].
Table reproduced from [50]

Parameter	Value	Source
Δt_{SG}	6 ms	Kita et al. (2005)
Δt_{GS}	6 ms	Extrapolation to monkeys based on Fujimoto and Kita (1993) and Δt_{SG}
Δt_{GG}	4 ms	Based on proximity between cells
τ_S	6 ms	Kita et al. (1983); Nakanishi et al. (1987a); Paz et al. (2005)
τ_G	14 ms	Kita and Kitai (1991)
Ctx	27 spk/s	Lebedev and Wise (2000)
Str	2 spk/s	Schultz and Romo (1988)
M_S	300 spk/s	Hallworth et al. (2003)
B_S	17 spk/s	Hallworth et al. (2003)
M_G	400 spk/s	Kita et al. (2005); Kita (2007)
B_G	75 spk/s	Kita et al. (2004); Kita (2007)

Equilibrium firing rates of this network have been recorded *in vivo* under a number of experimental conditions (muscimol blockade of STN for example). Similar conditions were replicated in the model (by setting all efferent STN connection strengths to zero, for the above example) and the equilibrium firing rates were recorded (See [50], table 2). In the NH study this data was used to constrain a genetic algorithm whose task it was to find the connection strengths, W , between each of the nuclei. The NH study used another set of experimental results to constrain their parameter search: the network response to a single or burst stimulation of the STN. However, the dynamics displayed by the first order NH model depend on the duration of the stimulus. Since this is physiologically unrealistic these constraints were omitted from this validation study. It is of no consequence to the present analysis since all that this chapter is attempting to do is to demonstrate that the single parameter values found using the genetic algorithm in the NH

study are contained within the distributions found using SMC-ABC. For full details of the NH model see the original paper [50].

Table 4.2. Experimental data used to constrain free parameter in NH model [50]

Number	Experimental measure	Nucleus	Firing rate (spk/s)	n	Source
1	Control	STN	19 ± 10 (SD)	220	Bergman et al. (1994)
2	Control	GPe	62.6 ± 25.8 (SD)	35	Kita et al. (2004, 2005)
3	$w_{SG} = 0$ Glutamate blocker into GPe	GPe	17.3 ± 8.5 (SD)	6	Kita et al. (2004)
4	$w_{SG} = 0, w_{GG} = 0, w_{XG} = 0$ Glutamate blocker into GPe GABA _A blocker into GPe	GPe	68.4 ± 28.5 (SD)	5	Kita et al. (2004)
5	$w_{GS} = 0$ GABA _A blocker into STN	GPe	96.8 ± 35.0 (SD)	6	Kita et al. (2004)
6	$w_{GG} = 0, w_{XG} = 0$ GABA _A blocker into GPe	GPe	135.1 ± 107.3 (SD)	11	Kita et al. (2004)

In some of the experimental conditions shown, neurotransmitter blockers were injected into different nuclei, which corresponds in our model to the suppression of the related network weights, as indicated in the second column. n = Number of sample measurements.

SMC-ABC was used to find the full distribution of parameter values satisfying the same equilibrium constraints as were used in the NH study. The priors were uniform distributions bounded below by zero and above at 100. Equilibrium firing rates of the model were recorded under each experimental manipulation. To calculate the ABC error statistic the standard deviation of the equilibrium firing rates as reported in the experimental studies was used. The “distance” between the model firing rates and the experimental firing rates is calculated in terms of the number of standard deviations. This measure ensures that the ABC algorithm is not striving to exactly replicate a value whose variance in the original data was extremely high. The error statistic, E , is given by

$$E = \max_{i \in K} \left(\frac{|y_i - \bar{y}_i|}{\sigma_i} \right) \quad (4.5)$$

where i indexes which of the K experimental manipulations are being considered ($K=6$ in this case). y_i is the model's equilibrium firing rate of whichever nucleus is recorded during the i^{th} experimental manipulation. \bar{Y} and σ are the mean and standard deviation of the real firing rates recorded from the i^{th} experiment (see Table 4.2). This formulation of the error statistic was chosen to simplify the definition of the vector of error thresholds. The error statistic is the maximum difference between the mean of the real experimental data in multiples of the standard deviation of the experimental data, across all eight experimental conditions. Thus if a model yields an error statistic, E , of 1.8, this means that none of the six experimental manipulations cause the model to be more than 1.8 standard deviations away from the true experimental mean.

The ABC algorithm was run with the number-of-parameter-sets-to-be-calculated, N , set to 400. The first iteration's threshold was set to 4 standard deviations from the mean. Thus if the maximum deviation of the model from the data was less than 4 standard deviations, the parameter set was accepted. 30 thresholds were linearly spaced from 4 to 0.2. The algorithm is not permitted to attempt to fit the model with zero error since this makes it very inefficient [156]. It would also be counterproductive since the variance in the original experimental data is high.

4.2.4.1: Validation results

The results demonstrate the advantage of the Bayesian approach to parameter estimation in that, not only can parameter sets be found that

enable a good fit between model and data, but also it gives information on the distribution of possible parameter sets (see Figure 4.2). Knowing the distribution of possible values rather than simply a single “best” parameter set is useful in assessing the significance of conclusions drawn from the data. The histograms show that the experimental data is highly constraining to STN afferent connections. However, the same data is an extremely weak constraint of the connection from striatum to GPe, with the posterior distribution spanning nearly the full range of possible values. The fact that the parameters found by the NH study are within the distribution is demonstrates that the SMC-ABC algorithm produces results consistent with the genetic algorithm used in the Nevado Holgado study [50]. It is therefore an effective tool for finding parameters in this kind of system.

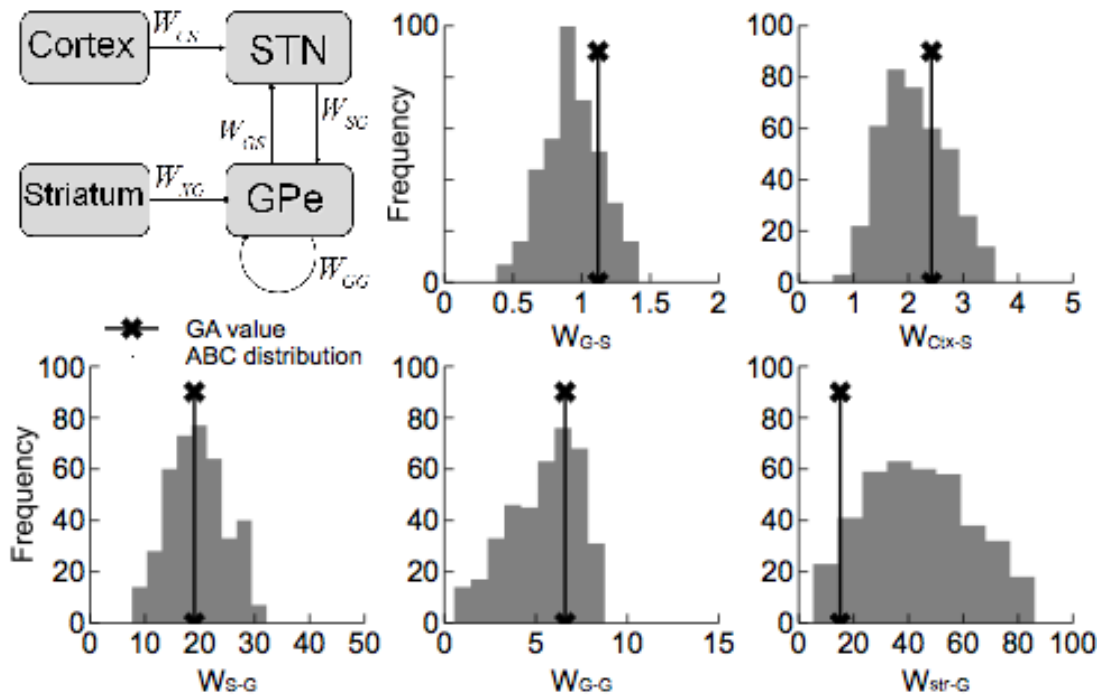


Figure 4.2. Nevado Holgado model and parameter distributions.

Top left) Schematic diagram of the connectivity of the model of the GPe-STN feedback loop as formulated in [50]. Connectors terminating in arrows indicate excitatory connections. Connectors terminating in dots indicate inhibitory connections. **Histograms)** The distributions of parameter values found using the SMC-ABC algorithm are shown in the grey histograms. Connection strengths of the model found in [50] using a genetic algorithm are shown as black stems. The fact that the parameters found using the GA lie within the posterior distributions validates the use of SMC-ABC for finding parameters of firing rate models. The benefit is clear of the Bayesian approach in that the full distribution of values that can explain the data is available. The data is shown to be a strong constraint of the GPe-STN connection strength, W_{G-S} , but a very weak constraint of the striatum –GPe connection strength, W_{XG} .

4.3: Discussion

The use of SMC-ABC has been demonstrated in the context of neural modelling and it has been shown it to be very well suited to the task of finding the parameters of highly nonlinear neural models. The application of SMC-ABC to neural modelling is a novel contribution of this thesis, as the method has hitherto been mainly used in the context of population genetics.

There is a high likelihood that SMC-ABC could become much more widely used in the neural modelling community. Indeed, the method has been described (though not applied) for a biological modelling audience in a recent journal article in the PLoS Computational Biology journal [156].

It is extremely easy to parallelise. Since it is purely a sampling and simulation based approach, the algorithm does not require reformulating for use in different contexts and it can be used to find parameters of arbitrarily complex nonlinear systems. These are advantages that are lacked by DCM. Like DCM, SMC-ABC can also be used for model selection [99].

SMC-ABC is conceptually easy to understand and relatively simple to implement. Unlike genetic and evolutionary algorithms, SMC-ABC has very few parameters that need to be set to allow the method to function correctly. The only parameters that are required are the number of parameter sets to be found and the number and spacing of the sequence of the rejection thresholds.

ABC has some similarities to stochastic optimisation methods (SOMs). SOMs contain random variables in the formulation of the optimisation problem. They can be used in cases in which there is random error in the input data, as is often the case in neural modelling. Stochastic approximation [157] or the method of finite difference [158] are examples of algorithms used to solve problems of this kind, in which the true values of the functions parameter have to be inferred from uncertain data. Random variables can also be introduced to deterministic models to increase compute times and

robustness in the optimisation. Genetic algorithms [159], stochastic hill climbing [160] or swarm optimisation [161] are examples of algorithms of this kind.

The algorithms of ABC and GAs have significant elements in common; both use random sampling to attempt to identify global minima of some predefined cost function. In both ABC and GAs an initial search space is defined which is necessarily informed by prior beliefs about the system before any optimisation is done. The difference between ABC and GAs is that ABC defines this formally as a *prior distribution*. In GAs there is no formal definition of prior belief distributions but rather the prior knowledge is implicit in choice of bounds of the search space. This could be interpreted in a Bayesian framework as a uniform prior and therefore, in this respect, a GA is a special case of likelihood free Bayesian inference. In both GAs and ABC some large number of parameter vectors are found during the course of the procedure. The difference between the two classes of methods is that ABC seeks explicitly to find a posterior distribution whereas GAs seek to find the global minimum of the cost function; the posterior distribution could be approximated using the other data points found by the stochastic optimisation algorithm, but this is not its primary purpose. Thus the differences between GAs and ABC are largely philosophical, with the only significant difference between them being the formal inclusion of probability distributions of prior knowledge that bias the sampling in the case of ABC. This makes ABC well suited to parameter estimation in neural modelling,

since we typically have a reasonably good estimate of parameter ranges but a high dimensional parameter search space. A uniform prior over all unknown parameters, as would be used in GAs, would make the search prohibitively slow.

The model examined in this chapter, and the models of the following chapters are all deterministic. That is to say, there is no noise in the models and thus any given parameter vector will give rise to a single simulated data-set. The likelihood distribution of the models is therefore a delta function. However, this is not to say that the posterior is also just a single point. Uncertainty arises in the model parameters due to the fact that the observed data is noisy. Further uncertainty is added when comparing the model simulation to data, since the model is not capable of fitting the complex and noisy data perfectly. The fact that the model is deterministic does not therefore preclude the use of ABC. Nor does it mean that standard Bayesian inference would be better suited to the task. The current model, and the models that follow, are all coupled delay differential equations that are nonlinear in their unknown parameters, so no closed-form solution exists. It would be necessary to use numerical optimisation techniques to find the parameters of the posterior distribution. This makes it much more computationally intensive and it is likely to be more efficient to approximate the posterior using Monte-Carlo methods such as ABC. Furthermore, a deterministic estimation is a useful first step to a full stochastic treatment because it avoids having to both model and simulate the noise, both of which may be nontrivial tasks involving

modelling neural noise and numerical integration methods for stochastic differential equations.

The validation study in this chapter demonstrates the value of this approach. Broad distributions indicate that the system is likely to be robust to changes in that particular parameter value. Narrow distributions show that the system is likely to be very sensitive to small changes in the value of that parameter.

In what follows, SMC-ABC will be used to constrain the parameters of a novel, physiologically accurate, firing rate model of the whole basal ganglia.

4.4: Summary

- This thesis is the first time that SMC-ABC has been used in a neural modelling context. It has the potential to be much more widely used than it is currently.
- SMC-ABC has been shown to be well suited to the task of finding the parameters of neural models.
- It is an easy method to understand and relatively simple to implement.
- As a Bayesian method it has the advantage that it yields parameter distributions rather than a single best value.
- Since it is a likelihood free method, it can be used to find parameters of arbitrarily complex nonlinear systems.

Chapter 5: A novel firing rate model of the basal ganglia

5.1: Introduction

The basal ganglia (BG) are a set of subcortical nuclei that takes inputs from most areas of cortex and many subcortical structures via the thalamus. Their output is a tonic inhibition of the same structures that provide their inputs. This has led to the hypothesis that one of the primary functions of the basal ganglia is to select between competing inputs [52]–[56]: selection meaning the focused disinhibition of one particular input channel and the maintenance of inhibition of all other channels. If this is the case then the motor symptoms of PD can be viewed as a dysfunction of selection ability of the BG.

The fact that the BG includes a feedback loop between the inhibitory globus pallidus external segment (GPe) and the excitatory subthalamic nucleus (STN) has led many to believe that this loop may be the origin of the pathological beta frequency oscillations that are often coexistent with the tremor of PD [46], [50]. Given that the BG may be the locus of selection as well as the pathological oscillations of PD there is a need for a model that can capture both these phenomena in a way that enables a numerical analysis to be conducted. Gillies et al. [46] conducted a study of the GPe-STN feedback

loop and found that increasing the strength of the cortex-STN connection increases oscillations. However transmission delays have been shown to be crucial to the presence and frequency of oscillatory solutions, and these were neglected in their study. Their conclusions rely on the assumption of the presence of self-excitatory connections within the STN, but experimental evidence for these connections is not strong enough to justify this assumption [47], [48].

The work of Nevado Holgado et al. [50] used a first order firing rate model of the GPe-STN feedback loop to analytically generate conditions for the generation of beta oscillations in the network. Their work showed that STN self-excitation is not necessary so long as transmission delays are included. However, their analysis is compromised by the fact the cortical input was modelled as a constant of 27Hz, a rate which would only be present when the cortical inputs are active. However, the oscillations of PD are present only when the sufferer is inactive. It is therefore much more likely that the cortical input to the model would be nearer to a 4Hz background firing rate.

The action selection functionality of the BG has been modelled many times [53]–[56]. However, the only model to quantitatively represent BG firing rates and capture oscillatory phenomena is [55]. This model is composed of leaky integrate and fire neurons and contains a great deal of physiological detail. The model is therefore unsuitable for analytical or numerical analysis. It also does not address the changes that occur in the BG network with the advance of PD. In this chapter we set out new methodologies that enable

firing rate dynamics to be captured in physiologically realistic, yet efficient way. This is in preparation for chapter 6 in which an analysis is conducted of functionality and oscillatory phenomena in the healthy and Parkinsonian conditions.

The modelling framework that was used to model the hippocampal cortex in chapter 3 is less suitable for the modelling of the whole basal ganglia. The higher number of connections in the basal ganglia as compared to the cortical model greatly increases the dimensionality of the parameter space necessitating that the system be captured in a simpler model. In this chapter a novel firing rate model of the basal ganglia is created in order that the oscillatory phenomena that occur with the advance of Parkinson's disease can be studied alongside the selection functionality of the network.

We firstly set out to independently test the hypothesis that the BG is a selection mechanism and then go on to analyse how the network changes observed in PD affect BG functionality. While there have been many computational models of action selection in BG [53]–[56] they tend to find the free parameters of the model such that the network performs the hypothesised function. We here outline a novel paradigm for the testing of hypotheses of neural function:

1. Construct the connectivity of a model according to what is known of the anatomy of the system.

-
2. Infer the full distribution of the model's free parameters (in this case using SMC ABC) from experimental data in order that we gain a full picture of the diversity of models that can explain the known data.
 3. Test this suite of models for a correlation between the fit to data and ability to perform the function. A positive correlation is taken as evidence in favour of the hypothesis.

In this paradigm, modelling is used to provide actual evidence for or against hypotheses of function, rather than using modelling to demonstrate that a particular function is possible.

The BG consists of at least five neural populations. In order to understand the dynamics of the network a model is constructed in which the firing rate of each nucleus can be represented by a single differential equation. Firing rate models have the advantage that they are simple enough that large systems can be modelled but they have been severely limited by their ability to accurately represent observed response latencies. Firing rate models are often first order approximations and often use the membrane time constant as the characteristic time constant of the system. This makes response latencies of the models much slower than is observed in reality. The complex relationships between the input and output firing rates of the nuclei necessitate that a new way to capture these dynamics is created. A new methodology is outlined whereby the firing rates of the nuclei are approximated by a second order transfer function, the time constant of which is dependent on the firing rates of the pre-synaptic nuclei relative to their

tonic rates. This method increases the physiological realism that can be captured in a firing rate model. It also negates the need to assume that there is no processing occurring between synapse and soma of neurons, as is the case in neural mass formulations. By modelling firing rate interactions directly we greatly reduce the number of parameters that need to be found.

In order to find the distributions of parameter values in the nonlinear neural models a Bayesian sampling technique called *sequential Monte-Carlo approximate Bayesian computation* (SMC-ABC) is used. Due to the intractability of calculating what is known in Bayesian inference as the *likelihood function*, Bayesian methods have not been widely used in neural modelling. However, SMC-ABC has the advantage that the likelihood function does not need to be explicitly calculated. It has gained popularity in population genetics and may also be well suited to neural modelling. Its implementation is outlined in this context in the methods section.

5.2: Materials and Methods

5.2.1: Model architecture

We created a model of the whole basal ganglia for the study of healthy BG function and the pathological network dynamics of conditions such as PD. Our model includes the striatum and the GPi as well as the well-studied STN-GPe feedback loop. The model remains relatively simple in that it consists of only five delay differential equations each of which governs the firing rate of

one of the basal ganglia nuclei. See Figure 5.7 for a graphical illustration of model connectivity. Connections are as in [162]

An identical excitatory cortical input drives the striatum and the STN [39], [43], [45], [163]. Since more than 90% of striatal neurons are medium spiny neurons (MSNs), the striatum of the model is assumed to consist only of MSNs [164]. No attempt is made to simulate the striatal microcircuit. The striatum is split into two distinct populations which represent MSNs expressing mostly D1 receptors and MSNs with mostly D2 receptors [165]. A normalised parameter governs the average dopamine receptor occupancy and modulates the firing rate of both the striatal populations. Increasing the dopamine parameter modulates the firing rate of the D1 striatal population upwards [166] and the firing rate of the striatal D2 population downwards [167].

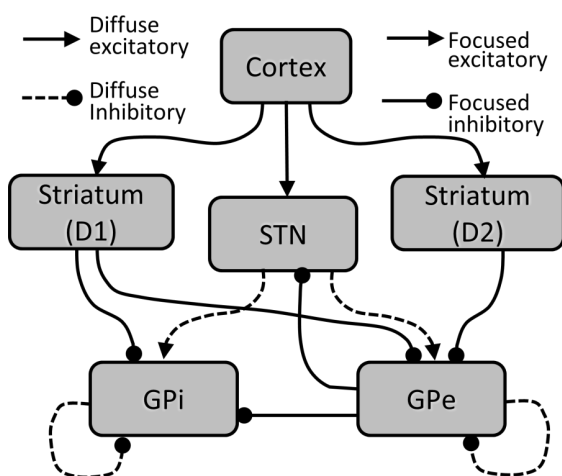


Figure 5.1. Basal Ganglia connectivity

The D1 striatum projects to GPi (the *direct* pathway) and the D2 striatum projects to the GPe [167]. The D1 striatum projects to the GPe with a connection strength of roughly the same as that of the D2 striatum-GPe connection [168]–[170]. The GPe is connected to the GPi both by direct GABAergic projections [171] and also via the STN [45]. In turn the STN has projections back to the GPe, creating a feedback loop [172]–[174]. Neurons in GPe are connected to their local neighbours [175]. While direct evidence of intrinsic collaterals in GPi is sparse it should be noted that studies have focused on the GPi’s extrinsic connections. There is strong evidence for collateral connections in the basal ganglia’s output nuclei in the rodent, the substantia nigra pars reticulata [176] and the entopeduncular nucleus [177]. These pallidum collaterals are implemented in the model as self-inhibitory connections. See Figure 5.1 for BG connectivity.

5.2.2: Initial attempts to model the basal ganglia using a first order model

Initially, attempts were made to model the whole BG using a first order firing rate model [86], [87], in which the firing rate, y , of each nucleus, n , is given by

$$\tau_n \frac{dy_n}{dt} = F(g) - y_n \quad (5.1)$$

Where τ is the time constant, F is a sigmoidal input to firing-rate operator and g is a weighted linear sum of inputs to the nucleus.

$$g_n = \sum_m W_{mn} y_m(t - \Delta T_{mn}) \quad (5.2)$$

Where m is the index of every nuclei that has afferent connections to the current nucleus, n . W_{mn} is the connection strength between the pre-synaptic nucleus, m , and the postsynaptic nucleus, n . y_m is the firing rate of the m^{th} pre-synaptic nucleus. ΔT_{mn} is the axonal transmission delay between nuclei m and n (parameter values given in Table 5.1). Attempts were made to infer the distributions of the unknown parameters using equilibrium firing rate data from eight different experimental manipulations.

1. Firing rate of the GPe under normal conditions
2. Firing rate of STN under normal conditions
3. Firing rate of GPi under normal conditions
4. Firing rate of GPi following the administration of a glutamate antagonist in GPi. Modelled by setting $W_{\text{STN-GPi}}$ equal to zero.

5. Firing rate of GPe following the administration of a GABA antagonist in GPe. Modelled by setting $W_{\text{str-GPe}}$ and $W_{\text{GPe-GPe}}$ equal to zero.
6. Firing rate of GPi following the administration of the GABA agonist muscimol into STN. Modelled by setting $W_{\text{STN-GPi}}$ and $W_{\text{STN-GPe}}$ equal to zero.
7. Firing rate of GPi following the administration of the GABA agonist muscimol into GPe. Modelled by setting $W_{\text{GPe-GPi}}$ and $W_{\text{GPe-GPe}}$ and $W_{\text{GPe-STN}}$ equal to zero.
8. Firing rate of GPi following administration of GABA_A and GABA_B blockers in GPi. Modelled by setting $W_{\text{GPe-GPi}}$ and $W_{\text{str-GPi}}$ equal to zero.

In the interests of creating the most parsimonious description of the system possible, a variety of different model connectivities had their parameters fit to the experimental data. The model has the connectivity set out in [53].

The error statistic is defined as

$$E = \max_{i \in K} \left(\frac{|y_i - \bar{y}_i|}{\sigma_i} \right), \quad (5.3)$$

where i indexes which of the K experimental manipulations are being considered. y_i is the model's equilibrium firing rate of whichever nucleus is recorded during the i^{th} experimental manipulation. \bar{y} and σ are the mean and standard deviation of the real firing rates recorded from the i^{th} experiment. This formulation of the error statistic was chosen to simplify the definition of the vector of error thresholds. The error statistic is the

maximum difference between the mean of the real experimental data in multiples of the standard deviation of the experimental data, across all eight experimental conditions. Thus if a model yields an error statistic, E , of 1.8, this means that none of the eight experimental manipulations cause the model to be more than 1.8 standard deviations away from the true experimental mean. The error thresholds used were 46 linearly spaced values between 5 and 0.5, each threshold being 0.1 lower than the previous one.

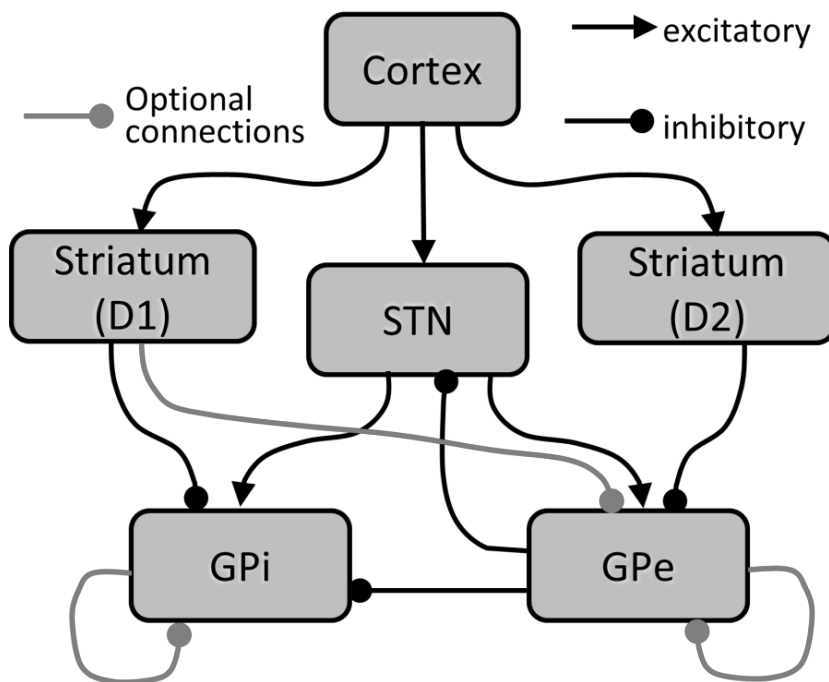


Figure 5.2. Connectivity schematic of first order BG model. Connections of the basic basal ganglia model are shown as black connectors. Every combination of the three *optional* connections (shown in grey) were added to the basic connections to create eight different models.

Parameters were fitted to the experimental data using SMC-ABC. Since the model is the same as the model of Nevado Holgado [50] with extra nuclei

added, the range of connection strengths found in that study were taken as a guide for setting the range of the uniform priors. Priors were uniform distributions bounded below at zero and above at 40. 800 parameter sets were found in each iteration of the algorithm. The series of rejection thresholds were defined using the means and standard deviations of the firing rates found experimentally under the eight manipulations listed above. The initial rejection threshold was defined as the mean firing rate plus or minus four times the standard deviation. Subsequent rejection thresholds were 25 linearly spaced increments between the initial threshold and the mean plus or minus 0.5 times the standard deviation. Parameters were fit using the basic model's connections plus every combination of three additional pathways; strD1-GPe; GPe-GPe recurrent connections and GPi-GPi recurrent connections.

It was found that the model composed of the basic connections plus the GPe recurrent and the strD1-GPe connections yielded firing rates with the smallest deviation from the experimentally observed values (see Figure 5.4). While the distribution of firing rates in all experimental conditions were found to agree well with the data (see Figure 5.5) it was found that the estimation algorithm preferentially found parameters such that the most direct pathways through the network were used, minimising almost to zero the connection strength of the GPe-STN pathway (see Figure 5.6). This effectively eliminates information flow through the indirect pathway. This is known to be physiologically implausible.

For the model to be a useful tool for the study of the BG it should be able to replicate the dynamics of the BG under stimulation experiments. In order to test this, the model was tested against data recorded from:

- 1) The STN from [178] figure 3A.
- 2) The GPe from [178] figure 4A.
- 3) The GPi from [84] figure 4A.
- 4) The GPi with a muscimol blockade of the STN [84] figure 4B.

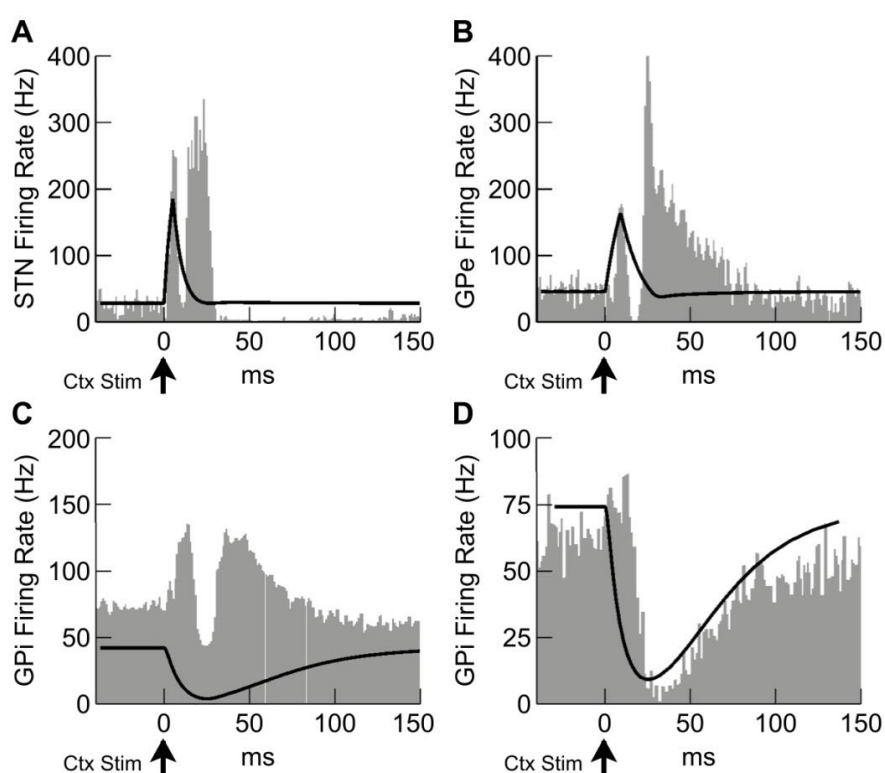


Figure 5.3. Response of the 1st order model to a brief cortical stimulation. Model parameters were trained using SMC-ABC on equilibrium firing rate data. The parameter set with the smallest error statistic was used to simulate the network's response to cortical stimulation. Black lines show model response to a cortical stimulation (22Hz, 0.3ms) at $t=0$. Grey histograms show experimental data. A is from [178] figure 3A. B is from [178] figure 4A. C is from [84] figure 4A. D is from [84] figure 4B.

As can clearly be seen from Figure 5.3 the model fails to capture the dynamics following cortical stimulation. It was therefore concluded that the equilibrium data was insufficient to accurately constrain the search of parameter space.

The 800 parameter sets were also tested for their ability to function as selection mechanisms (see chapter 6 for details). While some of the parameter sets allowed this simple first order model to perform action

selection, the majority did not. This is likely due to the lack of information flow through the indirect pathway.

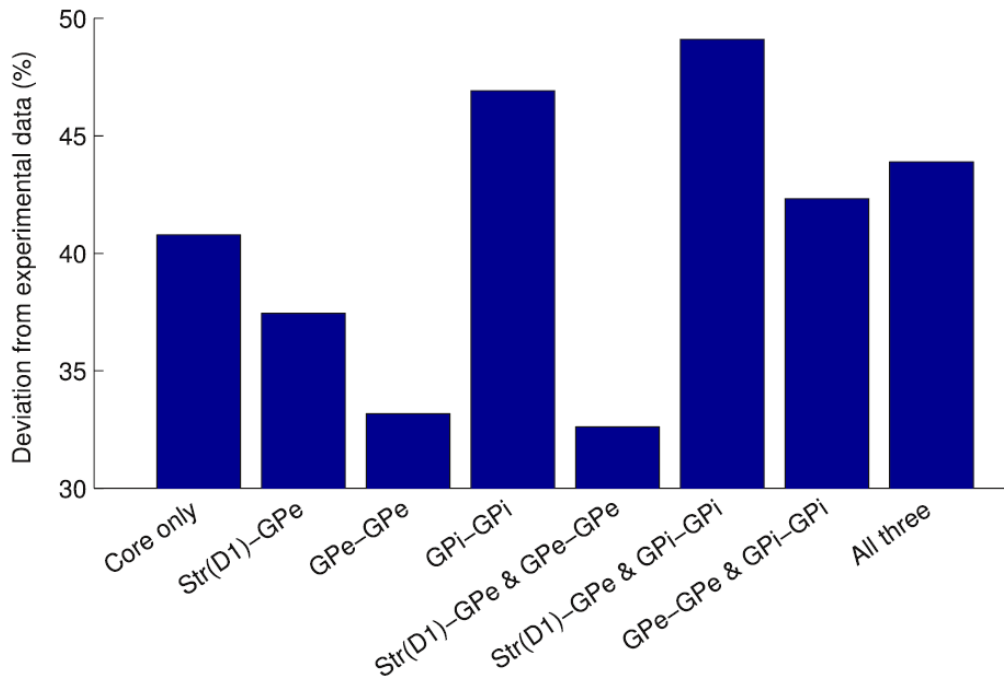


Figure 5.4. Deviation from observed firing rates for different model connectivities.

For each model connectivity the firing rates of specific nuclei were recorded under 8 conditions. 800 parameter sets were found that matched observed rates as closely as possible. The root mean squared percentage error, averaged across all 8 conditions for each model connectivity is shown. Core connections are those described in [53]. The model with the smallest deviation from the data is composed of the core connections plus strD1-GPe and GPe recurrent connections.

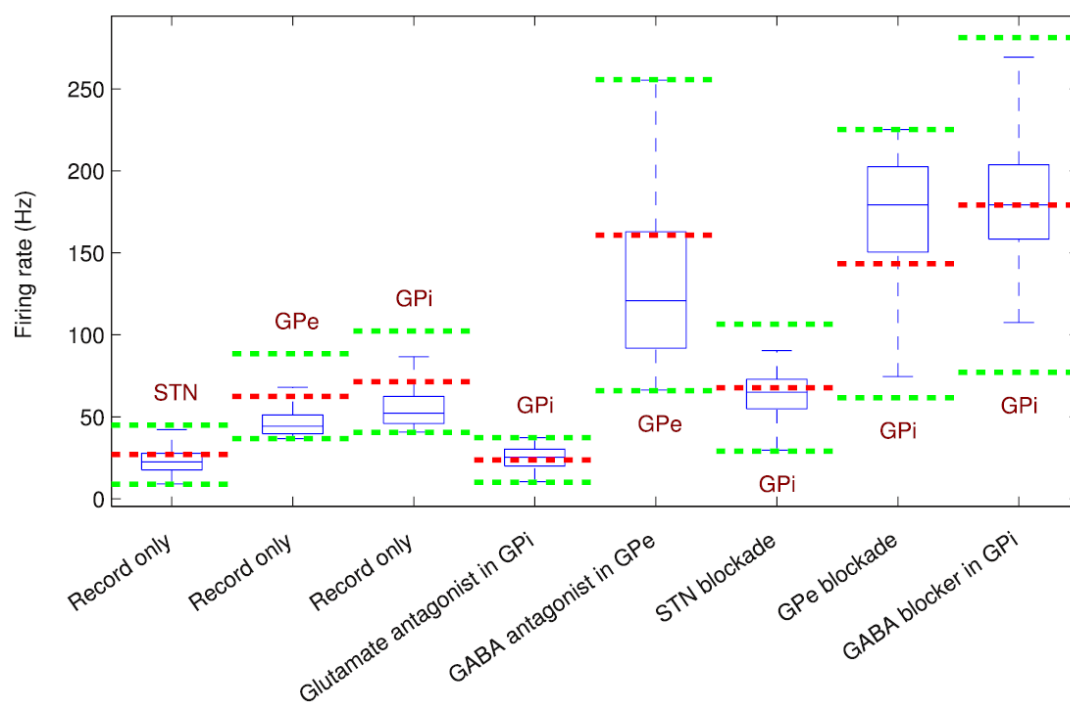


Figure 5.5. Performance of best model under the 8 experimental conditions. Distribution of the best model's firing rates under the 8 experimental manipulations (blue). Details of experimental manipulation given on x axis. Mean (red) and standard deviation (green) of experimental data shown by dotted lines. Nucleus from which the firing rate is recorded is shown in red text. Model connectivity can be parametrised such that there is good agreement between equilibrium states of the model and tonic firing rates recorded in vivo.

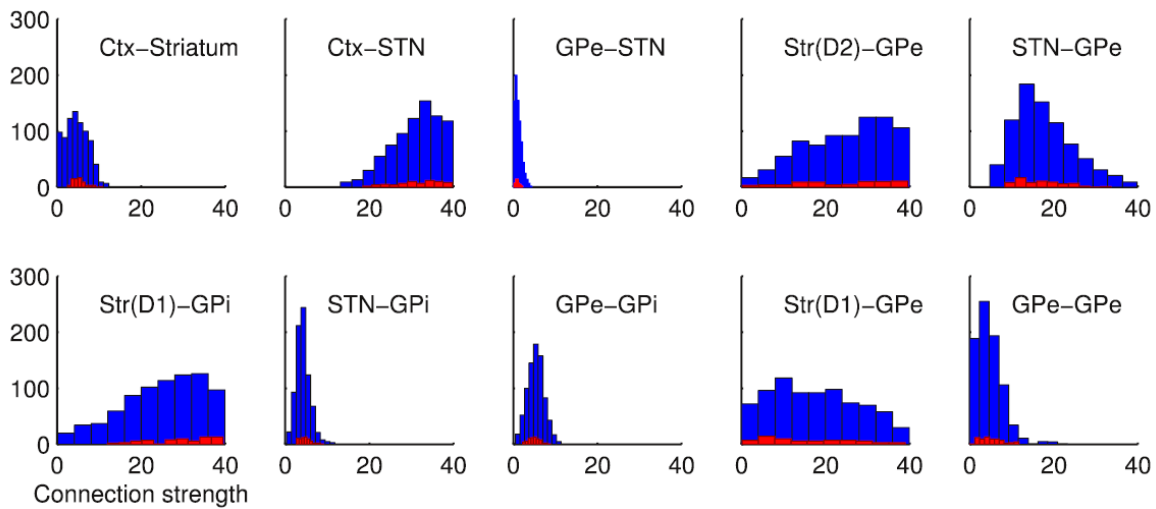


Figure 5.6. Distributions of connection strength parameters in first order model. The connection strength parameter distributions of the best model are shown in blue. Distributions were found using SMC-ABC. Priors were uniform distributions bounded below at zero and above at 40. Shown in red is the subset of parameter sets that also function as good action selectors (see chapter 6).

Dynamical data is far more informative than equilibrium data and stimulation studies of BG nuclei are common. However, first order models are not capable of capturing the dynamics with sufficient accuracy. In first order approximations increases in firing rate depend on the duration of the stimulus. The response of a first order model to an extremely short duration but high amplitude input cannot be physiologically accurate. The dynamics can only be captured accurately by using a second order formulation.

5.2.3: Second order firing rate model of the basal ganglia

The model was rebuilt using the methodology described below. All three of the optional connections were included in this formulation. See Figure 5.7 for connectivity schematic.

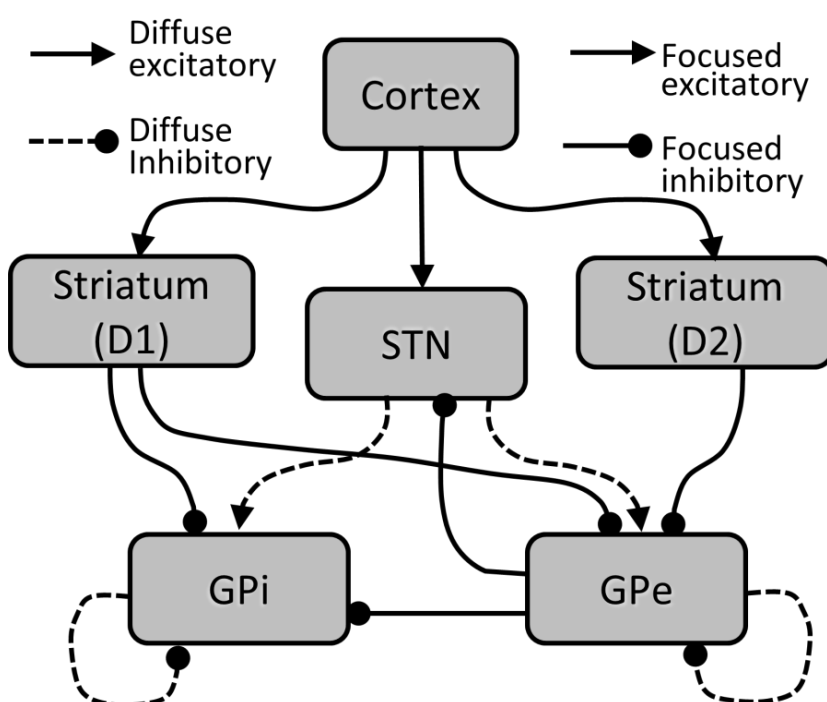


Figure 5.7. Connectivity schematic of full model of basal ganglia. Schematic diagram of the basal ganglia as modelled in this paper. Both striatal nuclei and the STN are assumed to receive identical inputs from cortex. Medium spiny neuron populations expressing mostly D1 or D2 receptors are modulated differently by dopamine and as such are modelled separately. Focused/diffuse connections are only of relevance when modelling action selection. No distinction is made between them when finding parameters using the SMC-ABC algorithm.

The model was rebuilt using an alpha function to model the firing rate impulse response of each nucleus. The impulse response of the n^{th} nucleus is given by

$$y_n = \frac{t}{\tau_n} \exp\left(\frac{-t}{\tau_n}\right) \quad (5.4)$$

Where τ_n is the time constant of the n^{th} nucleus and t is continuous time.

Differentiating twice with respect to time yields

$$\frac{d^2 y_n}{dt^2} = \frac{t}{\tau_n^3} \exp\left(\frac{-t}{\tau_n}\right) - \frac{2}{\tau_n^2} \exp\left(\frac{-t}{\tau_n}\right) \quad (5.6)$$

which can be written as an homogeneous ODE

$$\tau_n^2 \frac{d^2 y_n}{dt^2} + 2\tau_n \frac{dy_n}{dt} + y_n = 0 \quad (5.7)$$

The second order delay differential equation (DDE) governing the firing rate of each nucleus is defined by setting the left hand side of the homogeneous equation equal to the input to the nucleus, yielding

$$\tau_n^2 \frac{d^2 y_n}{dt^2} + 2\tau_n \frac{dy_n}{dt} + y_n = F\{k_n(t - \overline{\Delta T})\} \quad (5.8)$$

where k_n is the weighted linear sum of all afferent firing rates at their respective axonal transmission delays, ΔT . F is a function that relates the inputs of each nucleus to its output firing rate and is given by [50].

$$F = \frac{M_n}{\left(1 + \frac{(M_n - B_n)}{B_n} \exp\left(\frac{-4k_n}{M_n}\right)\right)} \quad (5.9)$$

Where M_n is the maximum firing rate of the n^{th} nucleus, and B_n is the firing rate of the nucleus when all inputs are blocked, hereafter referred to as the *baseline* firing rate. This function is a sigmoid with a maximum firing rate of M_n . The denominator is written such that the maximum slope of the sigmoid is always one, regardless of the values of maximum and baseline firing rates. The total firing rate input, k_n , is given by

$$k_n = \sum_m W_{mn} y_m (t - \Delta T_{mn}) \quad (5.10)$$

Where m is the index of every nuclei that has afferent connections to the current nucleus, n . W_{mn} is the connection strength between the pre-synaptic nucleus, m , and the postsynaptic nucleus, n . y_m is the firing rate of the m^{th} pre-synaptic nucleus. ΔT_{mn} is the axonal transmission delay between nuclei m and n . In the case of the D1 and D2 striatal populations the weight is multiplied by a factor of $(1+DA)$ for the D1 population and $(1-DA)$ for the D2 population, where DA is a normalised parameter describing the proportion of dopamine receptors that are occupied. This has the effect of increasing the firing rate of the striatal D1 population and decreasing the firing rate of the D2 striatum when dopamine is present (see Figure 5.10). Other model parameters are given in Table 5.1. Table of model parameters.

The error statistic is defined as a root mean square error (RMSE). Both the experimental data and the relevant model outputs are interpolated to a length of 600 linearly spaced time points. The time series of the four

stimulation experiments (Figure 5.3) are concatenated and the following RMSE applied to calculate the error statistic, E .

$$E = \sqrt{\frac{1}{600} \sum_{i=1}^{i=600} (s_i - y_i)^2} \quad (5.11)$$

Where s is the interpolated vector of experimental firing rates, length 600, and y is the interpolated vector of model firing rates, also length 600. Initial error threshold was set to 5.3, decreasing linearly in steps of 0.067.

5.2.3.1: Second order model results

The SMC-ABC algorithm failed to converge further at iteration 20; an error value of 3.73. In Figure 5.8 the time series of the model with the smallest error is plotted with the real experimental data. It is clear that, even with the second order formulation, the model is still not capable of reproducing the dynamics that are seen in the BG in vivo. The GP nuclei are not capable of producing dynamics at an appropriately short time scale. The following section examines the membrane time constant and its role in population level neural responses.

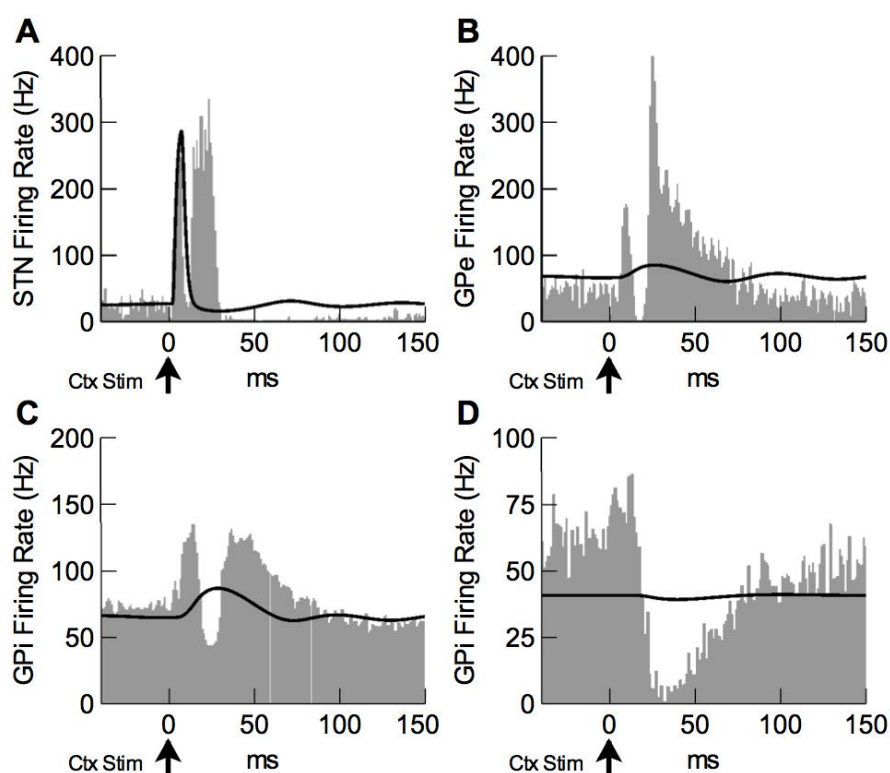


Figure 5.8. Second order model comparison to experimental data. Model parameters were trained using SMC-ABC on the data shown in grey histograms. A is from [178] figure 3A. B is from [178] figure 4A. C is from [84] figure 4A. D is from [84] figure 4B. The network's response to cortical stimulation (22Hz, 0.3ms, $t=0$) (using the parameter set with the smallest error statistic) is shown in black. The second order model, like the first order model, is not capable of replicating the dynamics seen in vivo.

5.2.4: Second order model with variable time constants

In previous firing rate models the characteristic time constant of each nucleus is assumed to be constant. However, it has been found that this assumption cannot be justified when attempting to fit models to dynamical data [82]. As an exemplar see Figure 5.11,D [84], which shows the firing rate of the GPi decreasing quickly in response to inhibition from the striatum but returning to its tonic firing rate at a much slower rate. A review is now

conducted of the evidence that neural processing occurs at different time scales within the same population, and that the characteristic time constants can vary rapidly according to their afferent populations' activities.

Large populations of neurons are able to react extremely quickly to changes in firing rates of pre-synaptic populations. The model represents the averaged activity of an extremely large number of cells. The sub-threshold membrane time constant, which is often used in firing rate models, yields response latencies that are far too large to be physiologically realistic [82]. The response latency of a population to its inputs can be divided into three components; firstly, the axonal transmission delay of the pre-synaptic cell, which is modelled as the delays in the delay differential equations; secondly, the rise-time of the post-synaptic currents (PSCs); thirdly, the membrane time constant, which governs the signal propagation between the synapse and the soma. Critically, the membrane time constant has been shown to change by up to a factor of ten when dendritic synapses are active [179].

In the absence of inputs that are significantly different from the pre-synaptic nucleus's tonic firing rates, the fast time scales of the PSCs do not affect changes in firing rate. When afferent nuclei are firing close to their tonic levels, it is assumed that the firing rate of each nucleus returns to its tonic rate according to its sub-threshold membrane time constant. Two distinct regimes in which populations operate have therefore been effectively delineated; firstly the *active* regime, when response latencies are governed by the rise time of synaptic currents; and secondly the *passive* regime in

which the dynamics are governed by the slower intrinsic cellular membrane processes.

The second order model is now augmented to represent what is known about neuronal physiology [179] is increased by allowing this time constant to vary depending on the firing rates of the nucleus itself and the nucleus's upstream connections. It is required that high excitatory inputs create fast positive changes in firing rate, and high inhibitory inputs create fast negative changes in firing rate. As such, equations are developed that have the effect of allowing high excitatory inputs to induce a reduction in the time constant of a nucleus only if the gradient of the firing rate is positive. Likewise, high inhibitory afferents must only induce a change to a short time constant if the gradient of the firing rate is negative. Thus the time constant of the n^{th} nucleus, τ_n is defined by the following equation. Equation 5.12 is a sum of two sigmoid functions, each of which is multiplied a Heaviside function. The Heaviside functions act as a switching term: when the gradient of the firing rate, y , is positive, the first sigmoid is multiplied by one and the second sigmoid is multiplied by zero and therefore has no effect on the value of the time constant. When the gradient of the firing rate is negative, the first sigmoid is multiplied by zero and the second sigmoid is multiplied by one. The input to the first sigmoid is the weighted sum of all excitatory inputs. The input to the second sigmoid is the weighted sum of all inhibitory inputs (see equation 5.13). Equation 5.12 therefore allows high excitatory inputs to induce a reduction in the time constant of a nucleus only if the gradient of the

firing rate is positive. Likewise, high inhibitory afferents only induce a change to a short time constant if the gradient of the firing rate is negative.

$$\tau_n = H(\dot{y}_n) \left(\tau_{Sn} + \frac{(\tau_{Ln} - \tau_{Sn})}{1 + e^{s(Pe-q)}} \right) + (1 - H(\dot{y}_n)) \left(\tau_{Sn} + \frac{(\tau_{Ln} - \tau_{Sn})}{1 + e^{s(Pi-q)}} \right) \quad (5.12)$$

See Figure 5.9 for a graphical description of this function. H is the Heaviside step function and \dot{y}_n is the rate of change of firing rate of the n^{th} nucleus. τ_{Ln} (τ_{Sn}) is the longest (shortest) time constant of the n^{th} nucleus. s and q are parameters governing the nature of the transition between the two time constants. s is the slope of the sigmoid; a large value of s means that the switching is hard; a small value means the shift between the time constants is more gradual. q is a normalised parameter governing how much activation of the upstream nuclei is required to produce a change in time constant. q and s can be altered according to what is known about the input-output characteristics of each neuronal population. P_e (P_i) are weighted and normalised averages of the total excitatory (inhibitory) input to the nuclei, given by

$$P_e = \frac{1}{M} \sum_m \frac{w_{mn} (y_m - y_m^{tonic})}{\sum_m w_{mn} (M_m - y_m^{tonic})} \quad (5.13)$$

The nucleus n has M excitatory (inhibitory) afferents. y_m^{tonic} is the equilibrium value of y_m and represents the tonic firing rate of the m^{th} nucleus. Thus P_e (P_i) is the average of the firing rates of all excitatory (inhibitory) afferents relative to their tonic rate, weighted by its relative

connection strength. All y_m^{tonic} values are found by running the model using only the short time constants and recording the equilibrium firing rates.

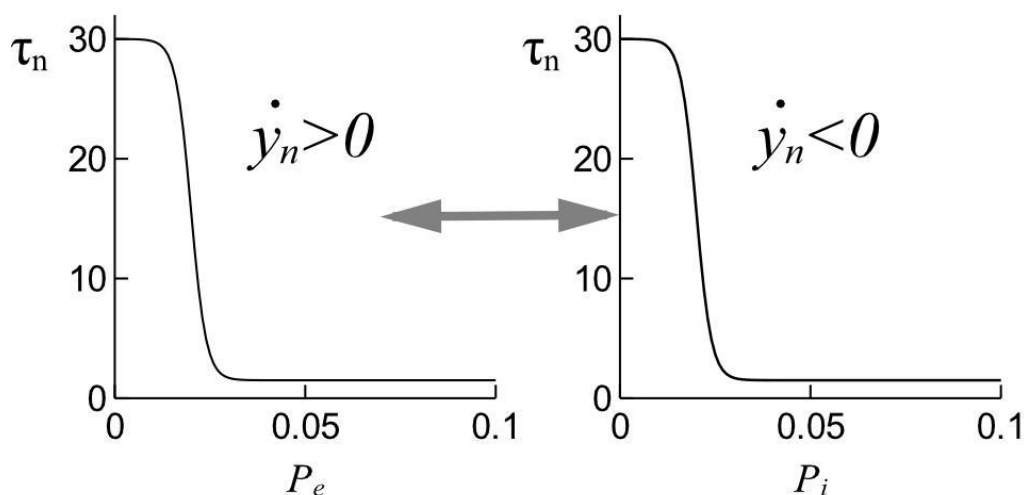


Figure 5.9. Dependency of time constants on rate of change of firing rate and inputs P_e (P_i) is normalised weighted average of all excitatory (inhibitory) afferent firing rates. If the rate of change of firing rate \dot{y}_n is positive (negative) the time constant τ_n is defined by P_e (P_i). Average deviations of afferent firing rate of more than 2% from tonic levels result in a change in time constant.

5.2.4.1: Model parameters defined from experimental data

Information from the literature is used to set as many of the parameters of the model as possible (see Table 5.1). Tonic firing rates and axonal transmission delays are found from experimental recording studies using awake but inactive Japanese monkeys, *macaca fuscata*. Peak firing rates are easily estimated from PSTHs. Baseline firing rates for STN and GPi of this species are unavailable so are included in the search algorithm. The time constants of the PSCs are different for different neurotransmitters and receptor types and sub-types. The two main neurotransmitters with which

this model is concerned are glutamate and GABA. The rise time of PSCs generated from the activation of receptors operate on an extremely fast time scale (~ 1 ms) [180]. Therefore when a neural population is being driven by its pre-synaptic populations its response latency should be of the order of 1 or 2 milliseconds (not including pre-synaptic axonal transmission delays). As such, time constants of striatal and pallidum nuclei are set to 1.5ms. Evidence exists that the response latency of the cortico-subthalamic pathway is smaller than that of the cortico-striatal pathway [84], [181]. The time constant of the STN is therefore set to 0.5ms shorter than the other BG nuclei at 1ms. It should be noted at this point that that constants of 1-2ms that we refer to here are not the first order decay time constants of postsynaptic currents. Rather they are the time constants of the second order alpha function and reflect the time-to-peak-response of the firing rate. If this second order function were to be approximated by a first order system with an instantaneous rise followed by an exponential decay, the equivalent decay time constant would be about 4ms. This is approximately the decay time constant of AMPA EPSCs which dominates the response latency of these neurons.

Noting that both the striatal nuclei have membrane time constants that are similar in magnitude to the short time constant governing the response latency (2-5ms, [182]), we make the approximation that the striatum acts on its short time scale at all times. While recent work has shown that the membrane time constant of the STN may be extremely high, the same work also shows that the probability of an STN neuron firing following a high stimulus is reduced. So the decrease in the firing rate of an STN cell following the withdrawal of a stimulus can be as rapid as the increase in firing rate following the onset of a stimulus [183]. For the purposes of creating our firing rate model it is only the input/output firing rate relationships that are of interest. Thus it is assumed that the STN is acutely sensitive to inputs and reacts at its short (~ 1 ms) timescale at all times. And so the model is left with only the two GP nuclei having variable time constants.

The set of 5 second order DDEs is split into 10 first order DDEs and solved using MatLab DDE solver, dde23.

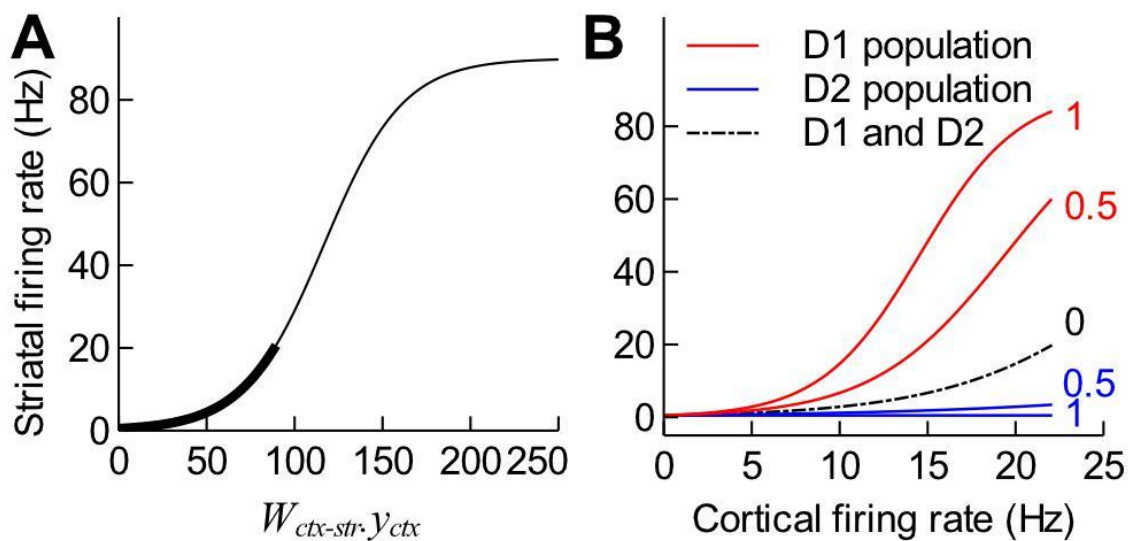


Figure 5.10. FF curve for the model striatum

A) Weighted input against output firing rate for the striatum with dopamine parameter set to zero. Realistic firing rates and dopaminergic modulation can be attained by restricting the available portion of the curve to section shown in bold. This is done by setting the value of the cortico-striatal connection strength to 4. This allows the maximum striatal firing rate to be attained only by D1 MSNs in the high dopamine condition. **B)** Firing rate input/firing rate output curve for the striatum with $W_{ctx-str} = 4$, for both D1 (red) and D2 (blue) MSN populations. Dopamine level is shown on the right. In the absence of dopamine both populations are identical. Dopamine modulates the firing rate of D1 MSNs upwards and D2 MSNs downwards as required.

5.2.4.2: Estimation of unknown model parameters using SMC-ABC

There are a large number of pathways of information transfer through the network (see Figure 5.7) so the data used to constrain the unknown connection strength parameters has to be informative. SMC-ABC functions at its best when low dimensional but highly informative data are used to generate the error statistic [156]. Time series of firing rates are a good example of this kind of data. Dynamical data recorded from the STN, GPe and GPi were used. The time-series of the response of GPi to a single short duration M1 stimulation is taken from [84] (figure 4, A & B), as is the GPi's

response to the same stimulation with a muscimol blockade of the STN. The time series of the response of the GPe and the STN to the same cortical stimulation is taken from [184] (figure 4, A1 and figure 3, A respectively). The error function used in the SMC-ABC algorithm is created by comparing data from these studies with model output. The parameter fitting was done using data in the temporal range beginning 40ms before the cortical stimulation and ending 150ms after the stimulation. Thus the SMC-ABC algorithm is compelled to fit the equilibrium firing rates observed before the stimulus as well as the dynamical behaviour post-stimulus. Each time series was interpolated to create a vector of firing rates at 500 evenly spaced sampling times. The simulation was run using the parameter values generated by SMC-ABC. The resulting vector of firing rates was truncated to the temporal range of the experimental data and then interpolated to the same 500 sampling times. To generate the value of the error statistic from this vector a simple root-mean-squared function was applied in an identical way to Equation 5.11.

Priors of connection weight parameters are Gaussian distributions. Mean connection strengths are set such that when multiplied by the maximum afferent firing rate the resulting value spans the output range of the nuclei. Since the slope of the f-f sigmoids is set to one, this value is approximately double the ratio between the maximum firing rate of the downstream nucleus to the max firing rate of the pre-synaptic nucleus. For example if the maximum cortical firing rate is 22Hz and the maximum STN firing rate is 300

Hz then to calculate the mean of the prior it was assumed that the maximum cortical firing rate will give rise to the maximum firing rate in STN. The sigmoid of the Ctx-STN's ff-curve is at 99% of its maximum value when the STN's inputs total 600. Therefore the Ctx-STN weight multiplied by the maximum cortical firing rate must equal 600. Thus the mean of the prior of $W_{Ctx-STN} = 600 / 22$. This is obviously quite uncertain so the variances of the Gaussian priors are set to twice the mean value. Search space is bounded below at zero for all parameters and above at 80 times the mean of the prior, though it is not to be expected that this high upper bound would be needed.

Information about the inputs and outputs of MSNs is used to set the connection strength between the cortex and the striatum. In this model, striatum takes its inputs solely from cortex. It is known that a baseline cortical input of ~4Hz [185] should give rise to a striatal firing rate of no more than about 0.5 Hz [182] and that the maximum possible firing rate of an MSN is about 90Hz [186]. It is also known that both D1 and D2 populations of MSNs should be firing at roughly 20Hz when dopamine is low [182]. Therefore the cortex-striatum connection strength is fixed such that a cortical firing rate of 22Hz [185] induces a striatal firing rate of 20Hz. This firing rate can be modulated up to 80Hz or down to zero by the action of dopamine on the D1 and D2 MSNs respectively. This information allows the cortex to D1 striatum and cortex to D2 striatum connection strengths to be set to 4 (see Figure 5.10).

5.2.5: Model summary

In summary of the above, the complete model is defined by the following five delay differential equations.

$$\begin{aligned} \frac{d^2 y_{sD1}}{dt^2} &= \frac{1}{\tau_{sD1}^2} F \{ (1 + da) W_{clx-str} in_{clx} \} - \frac{2}{\tau_{sD1}} \frac{dy_{sD1}}{dt} - \frac{y_{sD1}}{\tau_{sD1}^2} \\ \frac{d^2 y_{sD2}}{dt^2} &= \frac{1}{\tau_{sD2}^2} F \{ (1 - da) W_{clx-str} in_{clx} \} - \frac{2}{\tau_{sD2}} \frac{dy_{sD2}}{dt} - \frac{y_{sD2}}{\tau_{sD2}^2} \\ \frac{d^2 y_{STN}}{dt^2} &= \frac{1}{\tau_{STN}^2} F \{ W_{GPe-STN} y_{GPe}^{(t-\Delta T_{GPe-STN})} + W_{clx-STN} in_{clx} \} - \frac{2}{\tau_{STN}} \frac{dy_{STN}}{dt} - \frac{y_{STN}}{\tau_{STN}^2} \\ \frac{d^2 y_{GPe}}{dt^2} &= \frac{1}{\tau_{GPe}^2} F \{ W_{STN-GPe} y_{STN}^{(t-\Delta T_{STN-GPe})} - W_{sD2-GPe} y_{sD2}^{(t-\Delta T_{sD2-GPe})} - W_{sD1-GPe} y_{sD1}^{(t-\Delta T_{sD1-GPe})} - W_{GPe-GPe} y_{GPe}^{(t-\Delta T_{GPe-GPe})} \} - \frac{2}{\tau_{GPe}} \frac{dy_{GPe}}{dt} - \frac{y_{GPe}}{\tau_{GPe}^2} \\ \frac{d^2 y_{GPI}}{dt^2} &= \frac{1}{\tau_{GPI}^2} F \{ W_{STN-GPI} y_{STN}^{(t-\Delta T_{STN-GPI})} - W_{GPe-GPI} y_{GPe}^{(t-\Delta T_{GPe-GPI})} - W_{sD1-GPI} y_{sD1}^{(t-\Delta T_{sD1-GPI})} - W_{GPI-GPI} y_{GPI}^{(t-\Delta T_{GPI-GPI})} \} - \frac{2}{\tau_{GPI}} \frac{dy_{GPI}}{dt} - \frac{y_{GPI}}{\tau_{GPI}^2} \end{aligned}$$

Functional dependencies are written in superscript to aid legibility. da is the normalised dopamine level and is varied. F is the sigmoid function that relates the summed inputs of the nucleus to its firing rate and is defined by Equation 5.9 [50]

$$F = \frac{M_n}{\left(1 + \frac{(M_n - B_n)}{B_n} \exp\left(\frac{-4k_n}{M_n}\right) \right)}$$

Where k_n is given in {...}.

τ_n is varies with the activity of each nucleus as well as its afferents, and is defined by Equation 5.12

$$\tau_n = H(\dot{y}_n) \left(\tau_{Sn} + \frac{(\tau_{Ln} - \tau_{Sn})}{1 + e^{s(Pe-q)}} \right) + (1 - H(\dot{y}_n)) \left(\tau_{Sn} + \frac{(\tau_{Ln} - \tau_{Sn})}{1 + e^{s(Pi-q)}} \right)$$

Where P is given by Equation 5.13

$$P_e = \frac{1}{M} \sum_m \frac{w_{mn}}{\sum_m w_{mn}} \frac{(y_m - y_m^{tonic})}{(M_m - y_m^{tonic})}$$

Where w_{mn} is the connection strength between the m^{th} and n^{th} nuclei.

All parameter values are given in Table 5.1. Connection strength parameters are found using SMC-ABC with an error statistic given by

$$E = \sqrt{\frac{1}{600} \sum_{i=1}^{i=600} (s_i - y_i)^2}$$

Where s is the model generated data interpolated to a length of 600 and y is the experimental data, also interpolated to a length of 600.

Table 5.1. Table of model parameters.

Parameter	Meaning & reference	Value
$\Delta T_{\text{ctx-str}}$	Axonal transmission delay [187]	2.5 ms
$\Delta T_{\text{ctx-STN}}$	Axonal transmission delay [187]	2.5 ms
$\Delta T_{\text{STN-GPe}}$	Axonal transmission delay [187]	2.5 ms
$\Delta T_{\text{STN-GPi}}$	Axonal transmission delay [187]	2.5 ms
$\Delta T_{\text{GPe-STN}}$	Axonal transmission delay [187]	1 ms
$\Delta T_{\text{str-GPe}}$	Axonal transmission delay [187]	7 ms
$\Delta T_{\text{str-GPi}}$	Axonal transmission delay [187]	12 ms
$\Delta T_{\text{GPe-GPe}}$	Axonal transmission delay [187]	1 ms
$\Delta T_{\text{GPi-GPi}}$	Axonal transmission delay **	1 ms
τ_{str}	Time constant of striatum [180]	1.5 ms
τ_{STN}	Time constant of STN [183]	1 ms
τ_{GPeS}	Short <i>active</i> time constant of GPe [188]	1.5 ms
τ_{GPeL}	Upper bound of time constant of GPe [184]	30 ms
τ_{GPiS}	Short <i>active</i> time constant of GPi [180]	1.5 ms
τ_{GPiL}	Upper bound of time constant of GPi *	30 ms
M_{str}	Max firing rate of striatum [189]	90 Hz
B_{str}	Baseline firing rate of striatum [190]	0.5 Hz
M_{STN}	Max firing rate of STN [178]	300 Hz
M_{GPe}	Max firing rate of GPe [191]	300 Hz
B_{GPe}	Baseline firing rate of GPe [188]	100 Hz
M_{GPi}	Max firing rate of GPi [84]	300 Hz
$W_{\text{ctx-str}}$	Connection strength between cortex and striatum *	4
$W_{\text{D1str-GPe}}$	Connection strength between D1 striatum and GPe [192]	$W_{\text{strD2-GPe}}$
s	Slope of sigmoid governing time constants *	500
q	Fraction of deviation from tonic firing required to induce a change in time constant	0.02

* Set in this paper

** Based on proximity of cells

5.3: Results

5.3.1: Parameter estimation using ABC gives an accurate description of BG dynamics

It was discussed at the start of this chapter that equilibrium data alone is not sufficiently informative to constrain the search of the large parameter space of the full BG model and that dynamical data is far more informative. The four peristimulus time histograms (PSTHs) shown in Figure 5.11 (hereafter referred to as the *fitting data*) are the dynamical data that were used to constrain the search of the parameter space.

Results

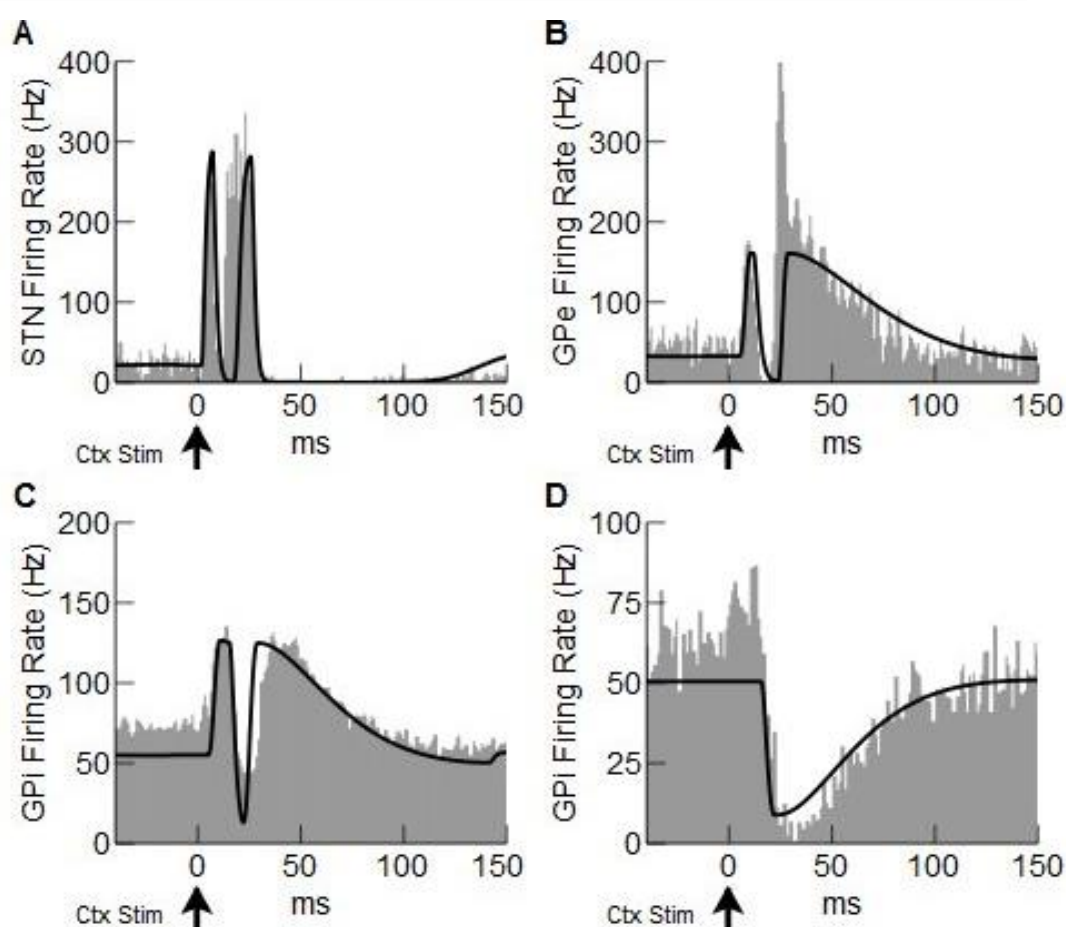


Figure 5.11. Fit of *second order variable time constants* model to data. The distributions of the model's free parameters (9 inter-population connection strengths and 2 baseline firing rates) were found using SMC-ABC. Solid black lines are the simulations produced from running the model using the parameter set which gave the smallest deviation from the data $W_{\text{ctx-str}} = 4.0$, $W_{\text{ctx-STN}} = 77$, $W_{\text{GPe-STN}} = 13.6$, $W_{\text{strD2-GPe}} = 41.6$, $W_{\text{STN-GPe}} = 1.1$, $W_{\text{strD1-GPi}} = 20.6$, $W_{\text{STN-GPi}} = 0.54$, $W_{\text{GPe-GPi}} = 0.08$, $W_{\text{GPe-GPe}} = 1.4$, $W_{\text{GPi-GPi}} = 0.75$, $B_{\text{STN}} = 96\text{Hz}$, $B_{\text{GPi}} = 98\text{Hz}$. In grey are the PSTHs of the experimental data used for parameter estimation. (A is from [178] figure 3A. B is from [178] figure 4A. C is from [84] figure 4A. D is from [84] figure 4B). All plots show the response of each nucleus to a brief ($300\mu\text{s}$) cortical stimulus at $t=0$. **A)** Time series of STN firing rate following the cortical stimulus. **B & C)** Time series of the GPe and GPi respectively following the same stimulus. **D)** Time series of the GPi following the same cortical stimulation but with STN afferent pathways blocked (In the experimental data: by administration into STN of the GABA agonist *muscimol*. In the model: by multiplying every instance of STN firing rate by zero.)

The free parameters (inter-nuclei connection strengths and the GPi and STN baseline firing rates) of the model were found such that the resulting

simulation matched the fitting data as closely as possible. All PSTHs in Figure 5.11 are a single BG nucleus's response to a single brief cortical stimulation (300 μ s duration, 200-700 μ A current in [84], [178]). A single time series was used for STN and another for GPe [178]. The GPi response to the cortical stimulation was recorded twice; once under normal conditions and once under a simulated blockade of STN using the GABA agonist *muscimol* [84]. This condition was replicated in the model by multiplying all STN firing rates by zero. The SMC-ABC algorithm yielded 100 parameter sets, all of which satisfy the constraints of the available experimental data. Plotted in Figure 5.11 in black is the model solution that is closest to the fitting data.

Initial observations of the model solutions indicate that the model is capable of representing the dynamics of the BG network to a single cortical stimulus. The fact that the model can be fit to the data indicates that the connectivity structure is plausible and that the modelling framework is sound. The solutions of the GPe and GPi nuclei to the impulse from cortex demonstrate that the model is capable of acting on two distinct timescales depending on the firing rates of the upstream populations.

The close match between the data and the model solutions indicate that separately modelling active and passive population responses is a successful way to increase the biological detail that can be included in a high level firing rate model without having to model in detail the membrane processes involved in shaping the firing rate behaviour. Observations of model behaviour indicate that this difference between the rates of active and

passive mechanism is essential in preventing high amplitude oscillations in the gamma band driven by fast feedback between the STN and GPe. The long timescale of the passive cellular processes of the GP nuclei may exist, at least in part, to strongly dampen the high frequency oscillations that would occur in the STN-GPe feedback loop if the GP were to always react at its short *active* time scales.

5.3.2: Parameter distributions

The distributions of the parameter values found by SMC-ABC that satisfy the constraints of the fitting data are shown in Figure 5.12. The posterior distribution relative to the prior is informative. Priors, shown in dotted lines, are Gaussian distributions with a mean given by twice the maximum firing rate of the post-synaptic population divided by the maximum firing rate of the pre-synaptic population. The maximum firing rate of the afferent nucleus is therefore capable of maximising the firing rate in the population that it targets (see section 5.2.4.2: for details). Therefore, in instances in which the mean of the posterior is higher than the mean of the prior, the pre-synaptic population has a greater influence over its target nucleus than would be necessary to maximise the efferent nucleus's firing rate. The GPe-STN connection strength is much higher than one would expect if the simple relationship on which the prior was based were true. The baseline firing rate of the STN (~100Hz, Figure 5.12 J) is much higher than its tonic firing rate (~35Hz, Figure 5.11 A). This indicates that the GPe-STN connection strength is higher than expected because it is serving to reduce the STN rate from its

high baseline down to its tonic level. The GPe may be able to exert this strong influence due to the fact that GPe projection neurons possess large terminal boutons at the soma or on the proximal dendrites of efferent populations [192], [193]. This strong tonic inhibition of STN may serve to make the STN very sensitive to changes in GPe firing rate. Small reductions in GPe firing rate may lead to dramatic increases in the STN.

The Cortex-STN connection is also a little higher than the prior. The tonic inhibition from GPe must therefore be providing more inhibition than it takes to reduce the activity of the STN to its tonic level. It can be concluded from this analysis that the feedback loop between STN and GPe is held in a balanced state in which each nucleus relies on its inputs from the other to maintain their tonic activity levels.

The mean of the STN-GPi connection (~ 0.5) is relatively weak in comparison to the mean of the prior of 2. The GPi's baseline firing rate of roughly 100Hz is higher than its tonic firing rate of 50-80Hz. The GPi is therefore under tonic inhibition from its inhibitory afferents [84]. Thus it takes comparatively little excitation from the STN to have a relatively large effect on GPi firing rate.

Results

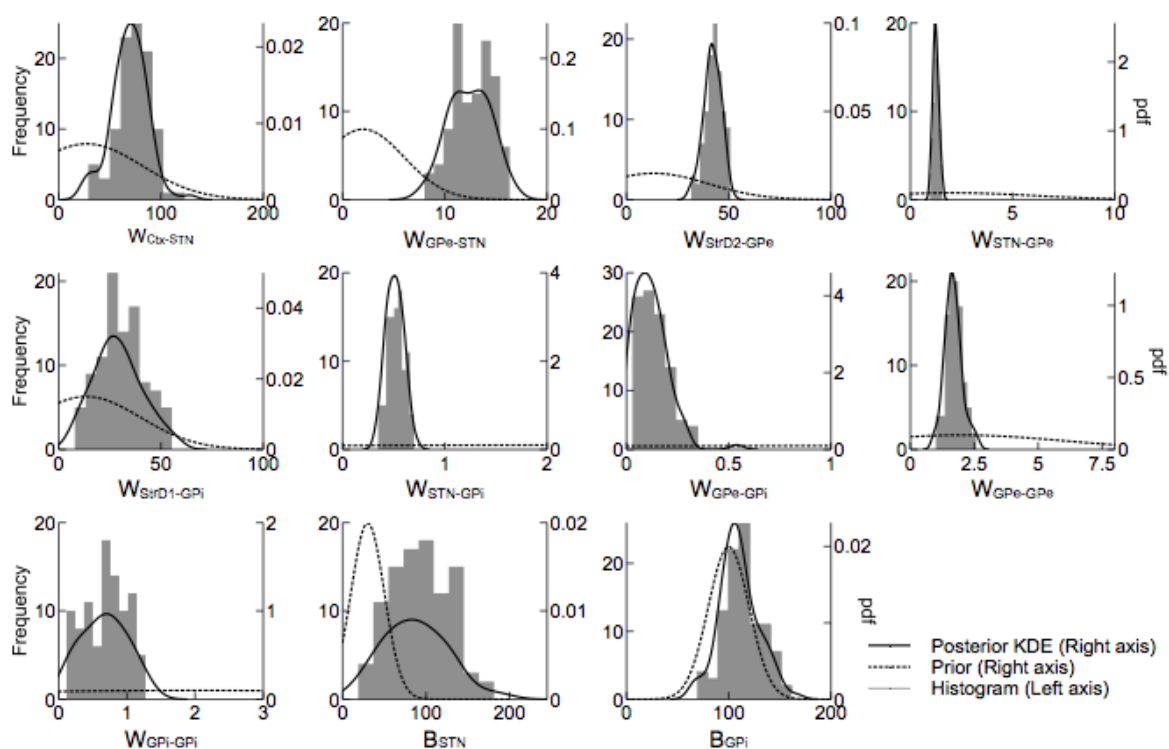


Figure 5.12. Distributions of free parameter values.

Distributions of the free parameters as found by the SMC-ABC algorithm. Histograms are shown in grey (left axis). Prior distributions are shown in dotted lines. For comparison a kernel density estimate of the posterior distributions are shown in solid black lines. Panels in which the prior appears to be at a constant low value are actually instances where the prior distribution is very much broader than the posterior. Graphs of the prior distributions are truncated where appropriate to allow the posterior to be plotted at a suitable scale.

5.3.3: The identified model accurately predicts an independent validation data set of BG dynamics.

It was confirmed that the model not only represents the experimental manipulations on which it was fitted, but also has predictive power. The model was validated by replicating the results of stimulation experiments against which the free parameters of the model were not fitted. In a study conducted by [191] the striatum of Japanese macaque monkeys was

stimulated and single unit recordings were taken from multiple GPe and GPi neurons. The stimulation protocols were simulated by adding brief ($300\mu\text{s}$) pulses of high firing rate input to both the D1 and D2 striatal populations (Figure 5.13 A-F). It was assumed that the $300\mu\text{s}$ $200\text{-}700\mu\text{A}$ stimulation currents were sufficient to maximise the responses in the stimulated nuclei. Thus, in our second-order model the magnitude of the firing rate input that is given to the stimulated nucleus is immaterial, so long as it is high enough to enable the nucleus to reach the maximum firing rate that can be gained from a $300\mu\text{s}$ stimulation. The stimulation was in addition to the 4Hz cortical background rate. The direct input to the STN was the cortical background firing rate only. Stimulations were either a single stimulation or a 0.2 second burst of 50Hz stimulation. Results are shown in Figure 5.13. The fact that the model solutions are similar in qualitative form as well as approximate magnitude is taken as good evidence that the model accurately reflects the average network activity of the basal ganglia of the macaque in vivo. The model output resembles a low pass filtered version of the experimental PSTHs. This is a good validation of the usefulness of the model.

The response of the network to the cortical stimulus is now analysed. Initial increases in firing rate of the GP occur at a very short latency and with a very short time constant since they are both receiving excitatory inputs from the STN. For evidence of this see Figure 5.11D in which all afferent STN connections are set to zero. The early excitation is abolished. The subsequent decrease in firing rate of both GP nuclei also occurs with short latency. This

is due to the arrival in the GP of the rapid onset, high firing rate inhibition from the striatum. (Blocking most of the inhibition from all inhibitory nuclei to the GP diminishes this early inhibition in GPe and almost completely abolishes it in GPi (see Figure 5.13 E,F)). The resulting depression below the tonic level of the firing rate of the GPe releases the tonic inhibition from the STN. There is, therefore, a second sharp increase in the firing rate of the STN (see Figure 5.11A). Evidence of this is shown in Figure 5.13 A & B, in which the late excitation is a direct consequence of the disinhibition of the STN by the GPe. Also when STN afferent connections are set to zero the late excitation is abolished (see Figure 5.11D). Since the firing rate of the cortex has, by this point long since returned to its background level, there is no excitation on the STN or the striatum. As such none of the GP's afferents are firing significantly above their tonic levels, so the firing rates of the GP nuclei return to their tonic levels according to their long passive time constant. Our theoretical analysis of the propagation of the cortical impulse through BG is supported by many experimental studies [178], [192], [194], [84]. A careful analysis of the experimental observations surrounding these impulse response dynamics can be found in [195].

The only instance in which the model does not accurately predict the equivalent experimental manipulation is in the GPe's response to striatal stimulation following local administration of gabazine (Figure 5.13 E). It was found that the model solution will never include an increase in firing rate if the totality of inhibitory connections is set to zero. Working on the

assumption that gabazine will not perfectly block all GABA_A, the strength of the striatum-GPe connection was reduced to one quarter of its original strength. This allows the firing rate of the GPe to fall sufficiently that the STN is disinhibited and so passes excitation back to the GP. Presuming that this is indeed the mechanism by which the GP excitation is elicited in the experiments, it shows that the STN is more sensitive to changes in GPe firing rate than the model: so much so that the short latency decrease in GPe firing rate from the striatal stimulation is barely visible on the PSTH (Figure 5.13 E inset).

Another slight deviation between the model and the observed data is the long latency decrease in spike count following the initial inhibition in Figure 5.13 G (GPi response to cortical stimulation with a muscimol blockade of GPe). The source of the long latency inhibition is likely to be the slow action of GABA mediated by metabotropic GABA_B receptors from striatum. GABA_B was not included in this model. A similar explanation could be applied to Figure 5.13 F.

Results

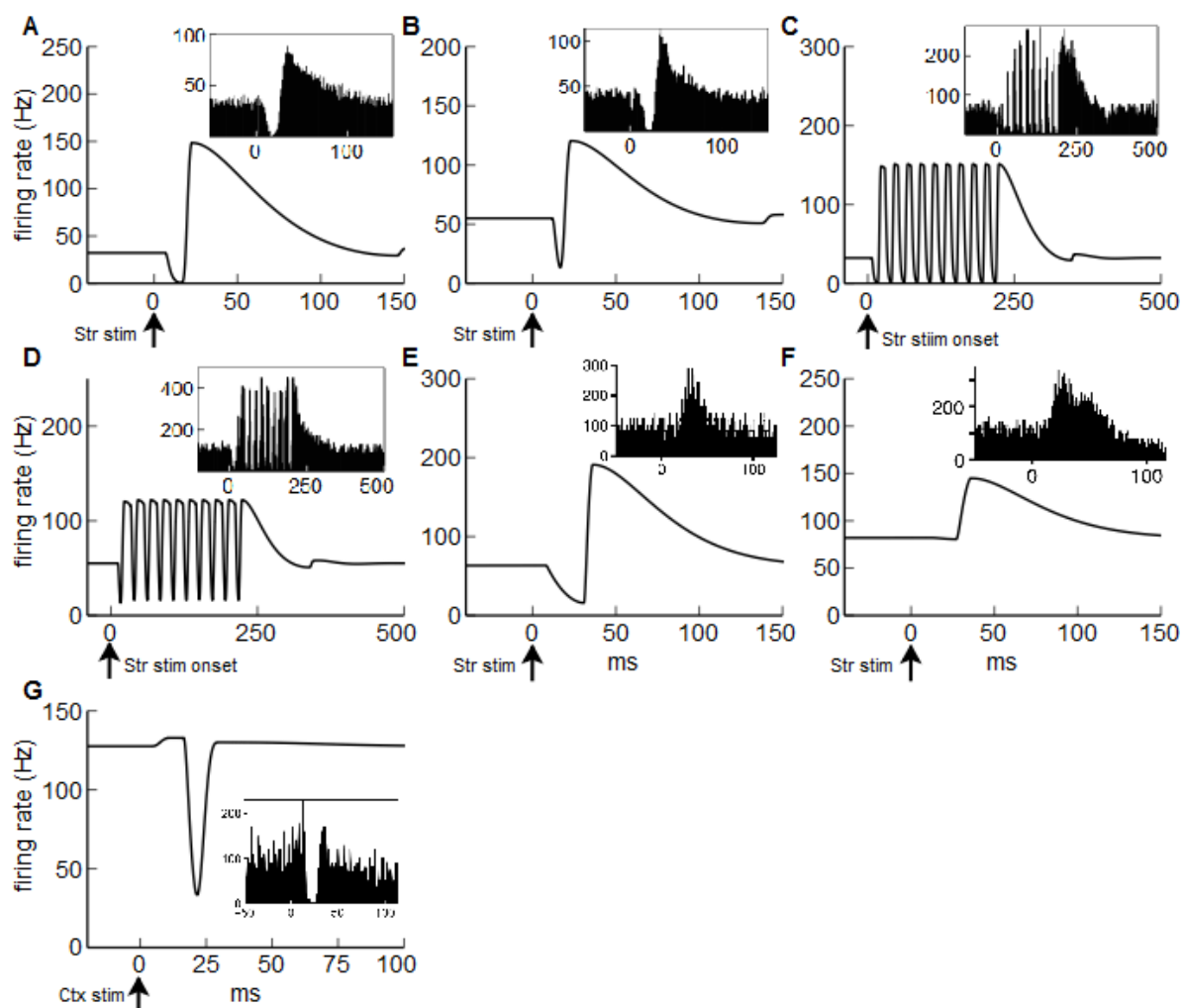


Figure 5.13. Model validation time series.

Figure to show the model's responses to experimental manipulations on which the free parameters were not fitted. Simulations are run using the parameter set with the smallest deviation from the data on which the model was fitted (see Figure 5.11). Main figures show model solutions and inset figures show the PSTHs of the experimental data. Insets A-F are from [191]. Inset G is from [84]. **A)** GPe response to a single brief stimulation of striatum at $t=0$. **B)** GPi response to the same stimulus as A. **C)** GPe response to 50Hz BHFS stimulation beginning at $t=0$. **D)** GPi response to the same stimulus as C. **E)** GPe response to a single stimulation of the striatum with inhibitory afferents reduced to 24% of their original value (see text). Inset: GPe response to striatal stimulation after local application of the GABA_A antagonist *gabazine*. **F)** GPi response to same stimulation as E. **G)** GPi response to single cortical stimulation with all GPe afferent connections set to 2% of their original value. Inset: PSTH of GPi response to cortical stimulus following application of the GABA agonist *muscimol* into GPe.

5.4: Discussion

It has been demonstrated that it is possible to model the dynamics of the whole basal ganglia using a firing rate model with a single delay differential equation for each nucleus. The model is physiologically accurate in that it can predict both equilibrium firing rates and temporal dynamics under a wide range of experimental manipulations. Furthermore, the connection strength parameters that were found using SMC-ABC have illuminated the relative dependencies of each nucleus on their afferent populations.

SMC-ABC has been shown to be capable of finding the parameters of nonlinear and high dimensional neural models. SMC-ABC is well suited to neural modelling since it functions at its best when the error statistic can be calculated from low dimensional but highly informative data. Time series of membrane potentials, local field potentials or firing rate PSTHs are good examples of this and are common in the experimental neuroscience literature. However, it is not without complications. For a full discussion of potential issues see [156]. The number of parameter sets that need to be computed in order that one can be sufficiently confident that the whole parameter space has been explored is unknown. In the current model it was ensured that using the small number of parameter sets (100) was sufficient by initially running the algorithm with 10,000 parameter sets. It was found that the small sample size was merely a uniform subsample of the larger distribution, indicating that the small population is adequate.

The modelling framework that is set out in this chapter has the potential to be generalised to other systems. By focusing solely on the input-output relationships between neural populations the number of variables in the system has been reduced. It has therefore become possible to model much larger systems of interaction populations. While this is true of all firing rate models, their scope has been extended by modelling active and passive cellular mechanisms separately. This has made it possible to accurately model the dynamics of multiple channels of all the neural populations of the basal ganglia.

5.5: Summary

- A new physiologically realistic firing rate model of the BG has been created that parsimoniously describes firing rates in all BG nuclei under dynamical as well as steady state conditions.
- A novel firing rate modelling framework has been described. The membrane time constant is allowed to vary with the activity of each nucleus's afferent connections as required by physiology. This modelling framework has the potential to be applied in to firing rate models of other systems.
- SMC-ABC has been shown to be a useful and effective tool for finding the parameters of nonlinear neural models.

Chapter 6: Computational analysis of basal ganglia function

6.1: Introduction

In the previous chapter a firing rate model of the BG was obtained. Sequential Monte-Carlo approximate Bayesian computation was used to find the posterior distributions of the unknown parameters of the model. In this chapter the model is used to firstly find independent theoretical corroboration that the healthy BG network is tuned to perform action selection, and secondly to explore the network dynamics associated with PD. A principled approach to using computational models to test hypotheses is outlined and employed. Having already used what is known of the physiology of the BG to construct the model, the full distribution of parameters that can explain the experimental data is identified. To test the hypothesis that the BG functions as a selection mechanism, all models found by the SMC-ABC algorithm are tested for their ability to select between inputs. A positive correlation between fit-to-data and ability-to-select is taken as evidence that the network is tuned to perform that function.

The model is then used to analyse network dynamics when the dopaminergic input is reduced to zero, simulating the onset of PD. The network changes that are observed experimentally in advanced PD are then applied to model.

Our analysis suggests possible mechanisms of action of some treatments that are currently in use but whose reasons for their efficacy are unknown.

6.2: Function and pathologies of the basal ganglia

The hypothesis that the basal ganglia acts as a selection mechanism has gathered much support [52], [56], [196]–[198]. That the BG can, in principle, act as a selector has been demonstrated in numerous computational models [54], [199]–[201]. The deficits in selection ability and motor function that are seen in disorders of the BG demonstrate the importance of the BG in both motor control and cognition.

Pathologies of the BG are responsible for the symptoms of many neurological disorders. Since the BG is thought to be responsible for the suppression of motor commands, disorders of the BG network can lead to a variety of motor and cognitive deficits. Inadequate inhibition of competing actions gives rise to an inability to suppress unwanted actions (*hyperkinseasia*), which is the case in Huntingdon's disease. Huntingdon's disease results in sudden involuntary jerky movements [202]. While BG disorders are most commonly associated with movement deficits there is now a growing realisation that BG malfunction is also responsible for cognitive impairments. Indeed the first symptoms of Huntingdon's disease are changes in mood and cognition and precede the more obvious motor deficits. The involuntary ticks of Tourette syndrome, obsessive compulsive disorder and attention deficit hyper-activity

disorder have also recently been found to be caused by malfunctions of the BG [203].

BG disorders can also result in difficulty in initiating voluntary actions, called *hypokinesia*. This is a common symptom of Parkinson's disease. Parkinson's disease (PD) is a neurodegenerative condition in which the dopaminergic neurons of the substantia nigra pars compacta die. The primary targets of the dopamine neurons are neural populations in the basal ganglia (BG), primarily but not exclusively the striatum. It is widely accepted that the loss of dopamine in the basal ganglia results in the most obvious outward motor symptoms of PD; rigidity; slowed movements; and tremor. This is evidenced by the effectiveness of dopamine replacement drug treatments such as *levodopa*.

6.3: Emergence of action selection in the model of basal ganglia

To test the ability of the model to select between competing inputs the model is replicated three times and all three models were connected as described below. Each parallel instantiation of the model is hereafter referred to as a *channel*. Each channel is driven by a different cortical input to simulate a time varying pattern of competing actions. In keeping with what is known of BG physiology the efferent connections of the STN are diffuse [193]. Since it has been observed that the somatotopic organisation of cells within BG nuclei is conserved from striatum through to the output nuclei of SNr and GPi [204],

it is assumed that the diffuse efferents of STN connect across different channels. Wherever an STN input appeared in the one-channel model, in the three-channel model the STN input is now the sum of STN firing rates on all three channels. Similarly it is also assumed that GP recurrent connections also connect between different channels. The model running in *selection mode* is thus composed of 15 second order coupled DDEs. See Figure 6.1.

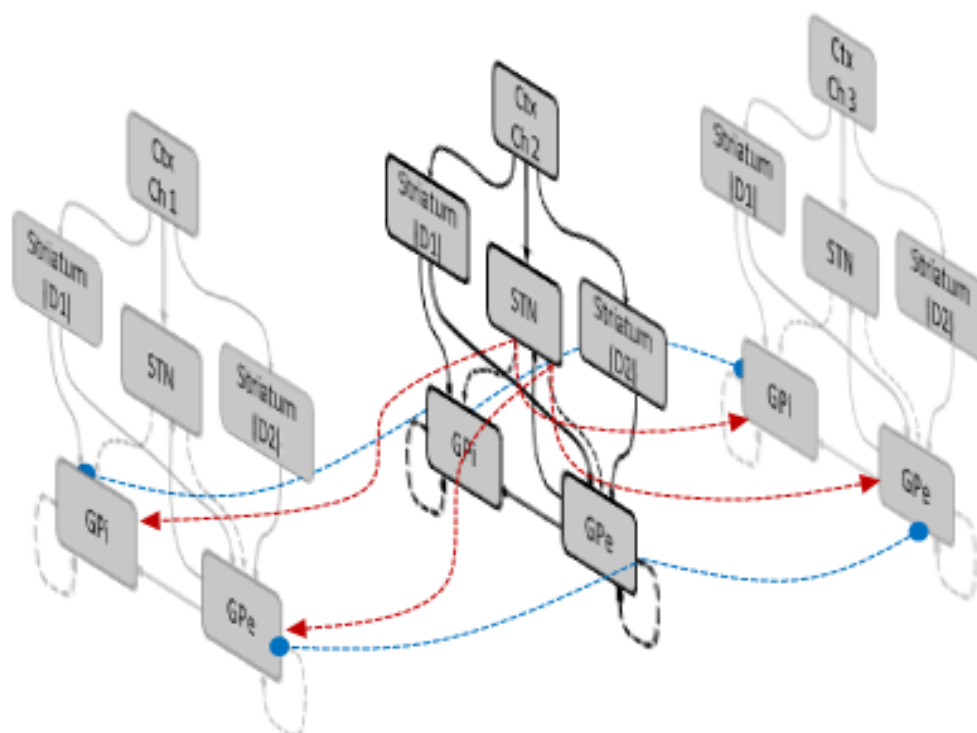


Figure 6.1. Three channel BG model schematic.

To create the three channel model, three BG models are implemented in parallel. Each channel's striatum and STN receive different cortical inputs to represent three distinct action choices. Each channel's STN projects not only to its efferent nuclei in its own channel but also to the same nuclei in all other channels. The recurrent connections of the GPe and GPi are similarly constructed. For clarity, only channel 2's cross channel connections are shown. Blue dotted lines indicate inhibitory cross channel connections. Red dotted lines indicate excitatory cross-channel connections.

The three-channel model was run for a period of 2 simulated seconds (see Figure 6.3 top). All three channels spent the first 0.5 seconds with only the cortical background firing rate of 4Hz as an input. Channel 3's input to the BG model was a constant background level of 4Hz for the full 2 seconds of the simulation. Cortical inputs on channels 1 and 2 were arranged such that different channels should be selected at different times during the simulation. Every half-second of the 2 second simulation sees a change in the relative strength of cortical inputs between the three channels. 0.25 seconds is

allowed for transient dynamics to decay and the network's equilibrium to be found. The first 0.5 seconds is disregarded during which all three channels are at rest. This leaves three epochs of interest; epoch 1, from 0.75 – 1 second; epoch 2, from 1.25 – 1.5 seconds; and epoch 3, from 1.75 - 2 seconds. See Figure 6.2.

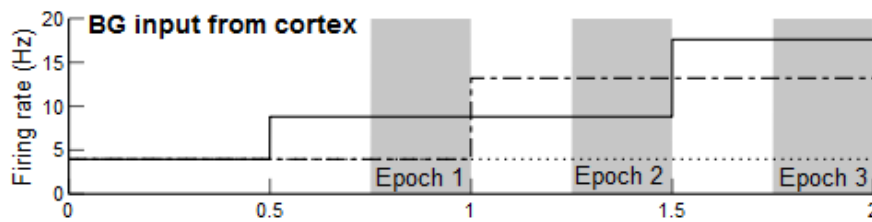


Figure 6.2. Three channel cortical inputs. Solid line – channel 1. Dot dashed line – Channel 2. Dotted line – Channel 3. Cortical firing rate input for each of the three channels as a function of time. Epochs are positioned in such a way as to avoid any transients that may occur following changes to inputs.

The output of GPi is a tonic inhibition of the same populations that supply inputs to the BG [41]. The action selection hypothesis requires that the BG mechanism selects one or more of the channels, and that the tonic inhibition of those channels is released. The selection of a channel therefore appears as a drop in GPi firing rate below some threshold for the duration of that particular cortical input configuration. A channel is counted as selected if the firing rate in the relevant epoch is below 75% of the tonic firing rate.

All parameter sets found in one in every five iterations of the SMC-ABC algorithm were tested for selection properties. It has been proposed that dopamine aids selection [162]. The higher the levels of dopamine in the striatum, the greater should be the likelihood that GPi drops to below a

threshold releasing the inhibition of its cortical targets thus selecting an action. When dopamine is high it is expected that multiple active channels would be simultaneously selected. Similarly, in the low dopamine condition, it should not be expected that more than one channel at a time could be selected, even if both channels' cortical inputs are high. Each parameter set was tested in each of the three epochs in both a high dopamine ($DA = 1$) and a low dopamine ($DA = 0.2$) condition. (Dopamine is not set to zero as it is envisaged that this would constitute the pathological condition of advanced Parkinson's disease and therefore not a healthy condition.) This yields a suite of six selection tests. A parameter set was classed as a *good selector* if it passed all six tests.

6.3.1: Selection tests

Low dopamine ($DA = 0.2$)

1. In epoch 1 channels 2 and 3 should not be selected.
2. In epoch 2 channel 2 should be selected and channels 1 and 3 should not be selected.
3. In epoch 3 channel 1 should be selected and channels 2 and 3 should not be selected.

High dopamine ($DA = 1$)

4. In epoch 1 channels 2 and 3 should not be selected.
5. In epoch 2 channel 2 should be selected and channel 3 should not be selected.

6. In epoch 3 channel 1 and 2 should both be selected and channel 3 should not be selected.

6.3.2: Selection properties

In order to test the hypothesis that one of the functions of the basal ganglia is to select between competing inputs, the parameter sets found by SMC-ABC are tested for their ability to function in this way. If the hypothesis is correct then the closer the simulations get to the fitting data the better they should function as selection mechanisms. As such a test was conducted for a negative correlation between deviation-from-data and ability-of-the-network-to-select. The model was run in *selection mode* (fully described above) in which three channels are simulated. Each channel is given a different time-varying cortical input and the relative GPi firing rate for each of the three channels is recorded (see Figure 6.3).

Emergence of action selection in the model of basal ganglia

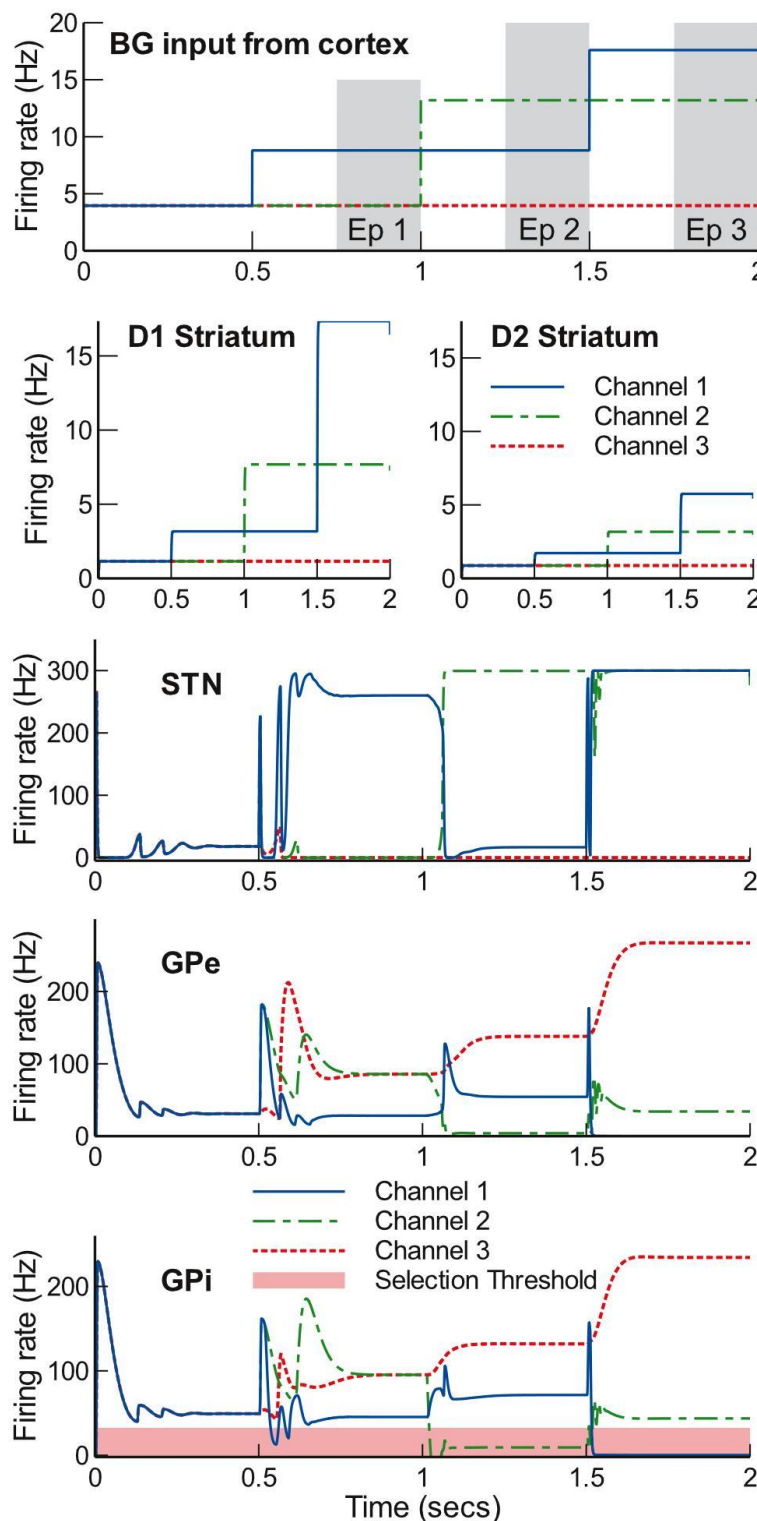


Figure 6.3. Time series of the model basal ganglia network selecting between inputs.

Multi-channel BG dynamics under time-varying cortical inputs. Simulation is run using low dopaminergic input ($DA = 0.2$) and with the cortical inputs showed in the top plot. Tests for selection ability of the model are done on mean GPi firing rates in each of the three temporal epochs shaded in grey. **Striatum)**

Both D1 and D2 striatal populations receive identical inputs from cortex. D1 striatal activity is modulated upwards by the effects of dopamine while the D2 population is modulated downwards.

GPi) A channel is defined as selected if its activity in the relevant epoch is below 75% of the tonic GPi firing rate. This corresponds to a release of the tonic inhibition of the GPi's target structures, permitting the execution of the action.

Firing rates above the 75% threshold indicate that the channel is not selected.

Accordingly, in the example displayed above, in epoch 1 no channel is selected; in epoch 2 only channel 2 is selected; and in epoch 3 only channel 1 is selected.

When a similar simulation

is run using a high level of dopamine ($DA = 1$) it is required that both channels 1 and 2 be selected in epoch 3. See *selection tests* for full details.

In order to check that selection ability improves as the model solutions get closer to the fitting data, not only the parameter sets in the final iteration were tested but also the parameter sets from earlier iterations in which the deviation from the fitting data was much higher. The process of using SMC-ABC to find the free parameters yielded 100 parameter sets for each of the 45 completed iterations of the algorithm: a total of 4500 parameter sets. Since it is reasonably computationally intensive to test for action selection all the parameter sets in only every fifth iteration of the SMC-ABC algorithm were tested. In the early iterations of SMC-ABC the error threshold is extremely high meaning that the parameter sets that are found yield system solutions that have a large deviation from the experimental data. As the algorithm progresses into latter iterations the error threshold is much closer to the experimental data. The iteration number can therefore be thought of as a proxy for *goodness-of-fit-to-data*.

For each of the selected iterations the percentage of parameter sets passing different numbers of tests was recorded (see Figure 6.4). It was found that simulations run using parameter sets from early iterations (i.e. poor fit to data) passed far fewer of the tests for selection functionality than later iterations. The early iterations have less than 10% of parameter sets passing all six selection tests. By the final iteration over 55% of parameter sets pass all six tests. During the SMC-ABC algorithm the root mean squared error (RMSE) for every accepted parameter set was stored. This error value was plotted against the number of selection tests that were passed when the

model was run in *selection mode* (see Figure 6.4B). The clear negative correlation between the two is evidence that the closer the model gets to physiological accuracy the better the network functions as a mechanism for selecting between competing inputs. This is a novel result that has not been demonstrated before, lending further support to the suggestion that the BG functions as an action selection mechanism. In part, this analysis was enabled by the novel application of SMC-ABC estimation to BG network parameters.

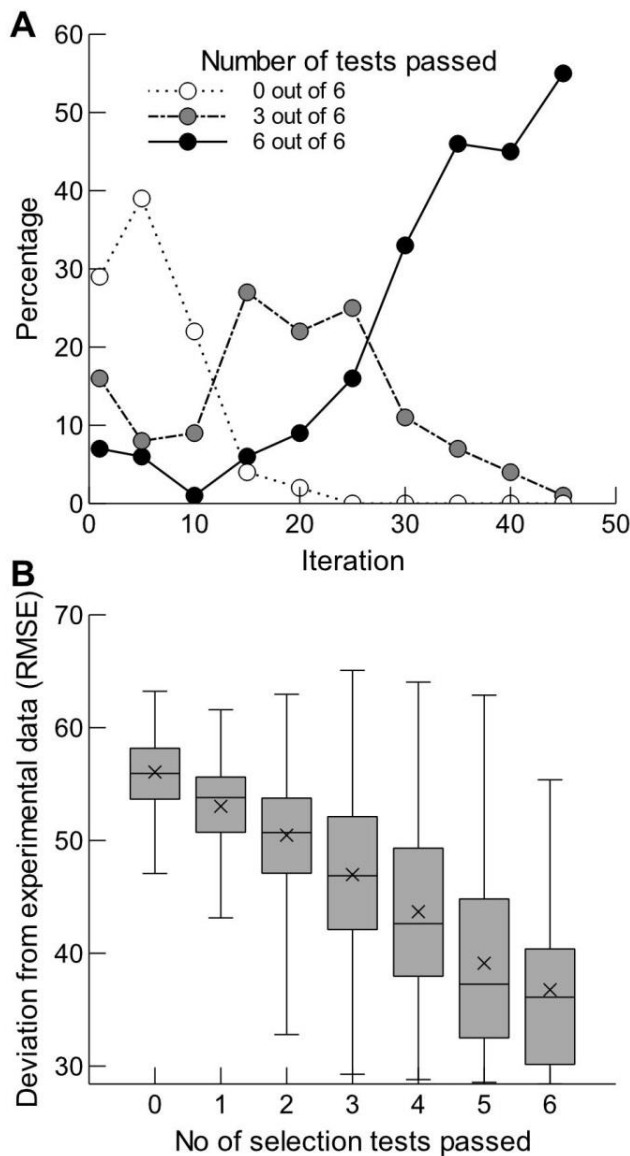


Figure 6.4. As the model approaches the data, selection functionality improves.

One in every five of the iterations of the SMC-ABC algorithm had all 100 of their accepted parameter sets tested for their ability to permit the model BG network to function as a selection mechanism. Selection ability was tested by the application of six tests (see *selection tests* section). The number of tests that were passed by each parameter set was recorded. **A)** Early iterations of the SMC-ABC algorithm, where the fit to data is poor have a high percentage of the parameter sets not passing any of the selection tests, and a very small percentage passing all six tests. Later iterations, where the fit to the data is much better, show a much higher percentage (over 55%) passing all six tests for selection ability. **B)** Boxes:

1st & 3rd quartiles. Whiskers: 1.5 inter-quartile range. Crosses mark mean values. For every parameter set in every iteration in which selection ability was tested, the root mean squared deviation from the experimental data is plotted against the number of selection tests that were passed. The high negative correlation (correlation of means: $r = -0.997$, $p < 10^{-5}$) between the two variables shows that the closer the model network gets to the experimental data the better the network functions as a selection mechanism.

6.4: Consequences of network changes in Parkinson's disease

Attempts were made to use SMC-ABC to find the connection strength parameters in the case of advanced Parkinson's disease. This would have enabled a quantitative description of how connection strengths change from the healthy state to the pathological state. This information has hitherto only been qualitatively assessed using experimental studies on animal models (see [50] for a review of these experimental results). The search was constrained using two pieces of information; the fact that STN, GPe and GPi should all oscillate in the beta frequency range; and the mean firing rates of the GPe and STN. There is little other reliable information on firing rates in macaque models of PD. However, this data alone is insufficient to constrain the parameter space. There is a wide range of parameter values that induce beta oscillations in the network, mostly found when the connection strength parameters are higher than in the healthy model. This is in keeping with what is known about the changes that occur with the advance of PD (see [50] for a full review of this evidence). Rather than attempting to fit the model parameters using these weak constraints it is more informative to use experimental studies to work out which connection strengths in the network are changed in the advance of PD as described below. The model connection strengths were then changed in the same way and the effects on the action selection capabilities of the network were observed (see Figure 6.5).

A distinction is drawn between two kinds of experimental evidence; those that demonstrate changes in firing rate as an immediate consequence of dopamine loss; and those that demonstrate long term changes in connection strengths as the network adapts to the loss of dopamine. For the purposes of changing network weights only the later is of interest: the former occurs naturally in the model by setting the DA parameter to zero. Setting the dopamine parameter to zero does not produce oscillations in the vast majority of cases (see Figure 6.6C). It does however markedly increase the overall firing rate of the GPi, severely impairing the ability of the network to select between inputs (see Figure 6.6B). This indicates that it is more likely that it is the network adaptations to the loss of dopamine that cause the beta oscillations of PD rather than the loss of dopamine itself.

Changes in network weights are likely to occur due to homeostatic plasticity mechanisms of neurons, whereby a neuron whose input becomes consistently lower or higher than usual can up or down-regulate the number and efficacy of glutamatergic or GABAergic receptors to bring the neuron's average firing rate back into its optimal range [205]–[208]. There is evidence that changes in the strengths of connections occur in the BG following chronic loss of dopamine. In [209] average firing rates in the rat striatum were shown to increase following 6-OHDA hydrobromide lesion of dopaminergic neurons. Mean firing rates moved from less than 1 spikes/second pre-lesion to around 3.5 spikes/second 15-20 days after lesion. Since the firing rates of the D1 and D2 MSN populations are

differentiated by the presence of dopamine, in its absence the two populations will theoretically fire at the same rate. It is assumed that this is the case. Therefore the effective connection strength from cortex to both striatal populations appears to increase as the MSNs adapt to the complete loss of all dopaminergic innervation. Using the same rationale that was used in the healthy case it can be shown that the effective connection strength of the cortico-striatal connection is around 10, roughly double that in the healthy condition. Similar evidence for this change can be found in [210], [211].

Evidence from [212] indicates that the connection strength between cortex and STN is also increased in PD (though it remains unclear by what mechanism this change occurs). Comparing cortically induced STN neuronal activity in diseased and healthy states showed that STN firing rate in the diseased state is more than double the firing rate in the healthy state. A combined experimental and modelling study [213] confirms that the cortex to STN connection is significantly increased in PD. Shen and Johnson [214] have showed that, in PD, GABA agonists give rise to greater GABAergic PSCs in STN neurons than in the healthy state, indicating that the connection strength between GPe and STN is increased in the diseased state. As well as striatum, STN neurons are also innervated by dopaminergic neurons (not included in this model). STN expresses mostly D2-type dopamine receptors indicating that dopamine loss should increase STN activity. The increase in the connection strength between the GPe and the STN seen in the Shen and

Johnson study may arise as the STN up-regulates GABA receptors in an attempt to bring its firing rate back to normal.

Shown in Figure 6.5C is the effect of multiplying the cortex-STN and cortex-striatum connection strengths by 2 and the GPe-STN strength by 1.5 in the zero dopamine condition. These results indicate that the parameter changes that are seen in PD serve to maintain selection functionality in the absence of dopamine. As is the case in real PD, the model exhibits resting state oscillations that cease when actions are undertaken. However, it should be noted that in real PD, resting state oscillations exist alongside impaired selection capabilities. It may well be the case that this behaviour exists in the model if parameter values are tuned accordingly. To fully analyse the transition to the PD state a bifurcation analysis should be conducted. This is beyond the scope of the current work and is left for a future study.

The mechanism whereby the oscillations are extinguished in our model is the saturation of STN firing rate at its maximum or minimum values. Channels that receive a cortical input that is above background-level cause the active STN populations to fire at their maximum rate. Channels with only background level input cause the STN population of their associated channel to cease firing altogether. Under these conditions the information transfer through STN is rendered binary. The diffuse excitation given to GPi from the STN therefore lacks any of the differences between active channels that are present in the healthy condition (see Figure 6.3). However, selection

function is maintained by the focused inhibition coming directly to the GPi from the D1 striatal population, the *direct pathway* [215]

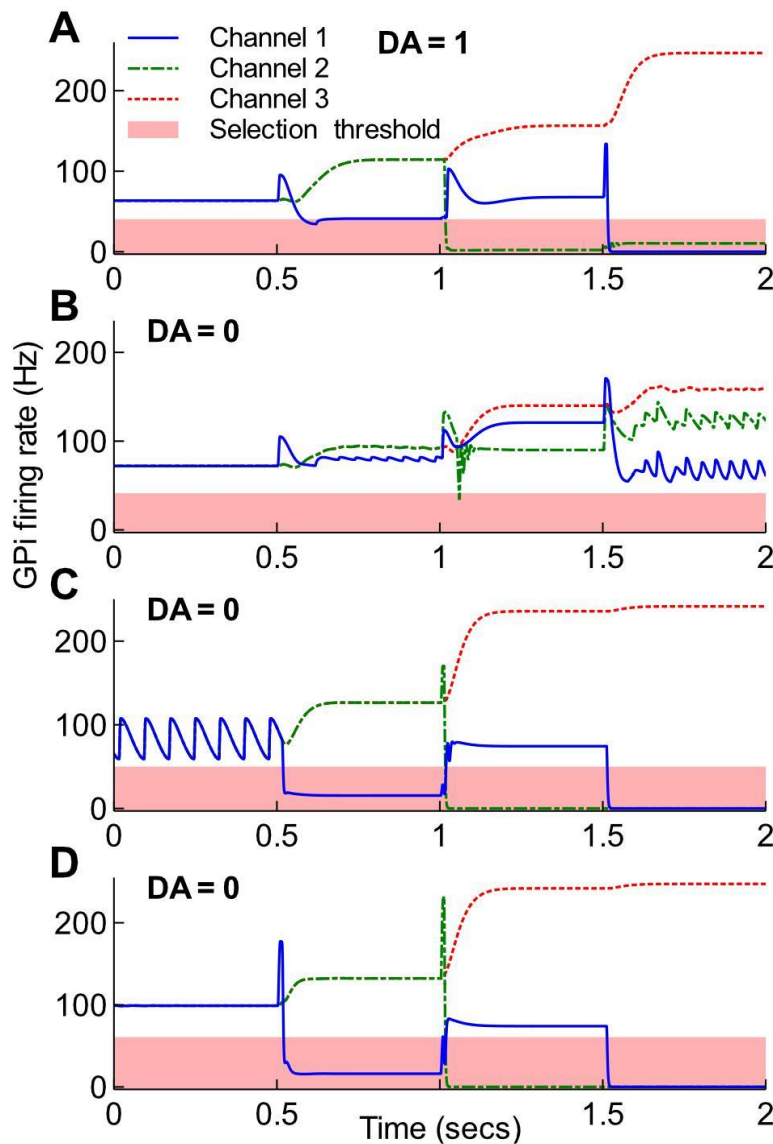


Figure 6.5. Network changes in PD attempt to restore BG functionality. Model BG response to the same 3-channel inputs as Figure 6.3 in three conditions. In A and B model parameters (that were found by SMC-ABC) are as in Figure 5.11. **A)** DA = 1. Healthy response when dopamine level is high. Tonic firing rate when all channels have background level cortical input in the interval $t=0-0.5s$. Single channel selection at moderate inputs and the selection of two channels when both inputs are high. **B)** DA = 0. Immediately after DA loss. When

dopamine is completely absent no channels are selected at all, even when inputs are high. **C)** Connection strength parameters are changed to reflect the major changes that are seen in advanced PD. Connection strengths as above except $W_{ctx-str}$ and $W_{ctx-STN}$ are both twice their healthy values and $W_{GPe-STN}$ is 1.5 times its value in the healthy state. Selection capability is restored. However, when the BG network's inputs are at cortical background level, significant beta oscillations exist. Functionality is restored but at the cost of a resting state oscillation of 14Hz. **D)** Possible remedy. The oscillation can be removed while maintaining functionality by decreasing the connection strength between STN and GPe. All parameters are identical to those in C except $W_{STN-GPe}$, which is 40% of its value in C.

6.5: Targeted GPe GABA antagonists as a possible treatment of PD symptoms

Decreasing the STN-GPe strength halts the resting state oscillation while maintaining selection, even in the absence of dopamine (see Figure 6.5D and Figure 6.6B,C). In our model all 100 model variants cease oscillating when the STN-GPe strength is down to 40% of its original value. Immediately following dopamine loss the increased inhibition of GPe from the striatum leads to a diminished inhibition of the STN by GPe. However, since cells have intrinsic mechanisms with which to maintain an average firing rate [205]–[208], the reduced firing rate of the GPe may be compensated for by increasing the synaptic strength of STN afferents: the exact opposite change to that which would be required to remedy the oscillations. This homeostatic mechanism of individual neurons may stop the network as a whole making the necessary connection strength adjustments that would otherwise allow selection to be maintained and free from oscillations, even in the zero dopamine condition. This suggests a possible therapeutic intervention. If the STN-GPe connection could be artificially weakened then the BG's natural network changes could be allowed to correct for the reduced dopamine levels without the induction of the resting state oscillations. Indeed, it may be the reduction in the strength of this pathway that is responsible for the efficacy of the NMDA antagonist drug *amantadine* (l-adamantanamine hydrochloride) or the benefits of pallidotomies.

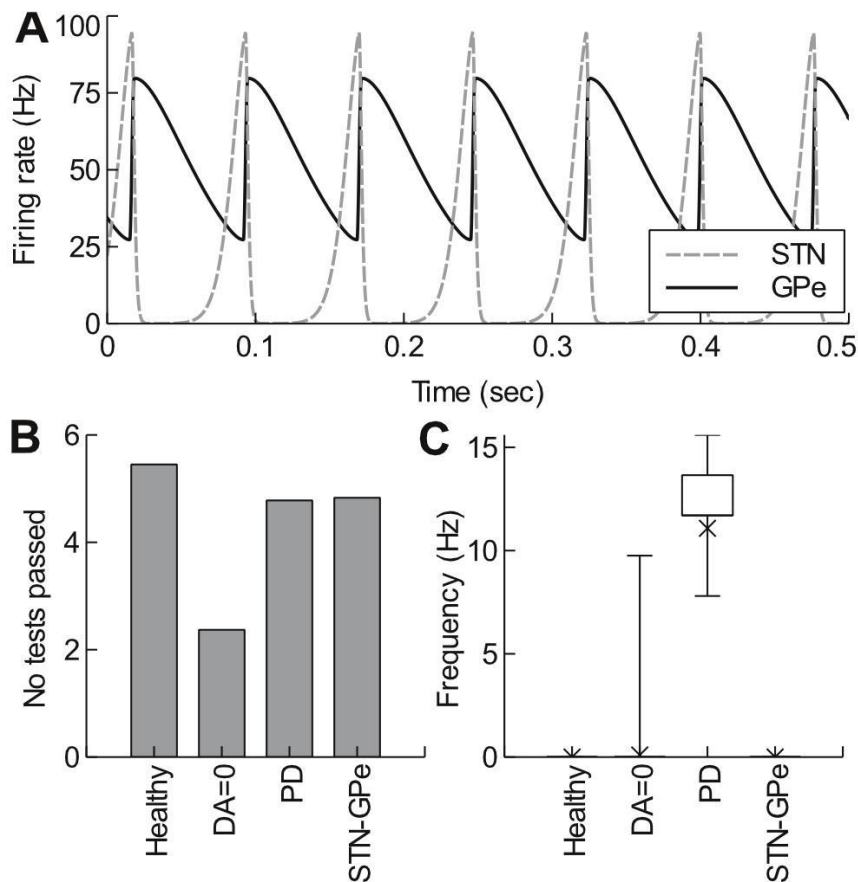


Figure 6.6. Change in selection functionality as DA and connection strengths change.

A) STN and GPe feedback loop oscillating in the beta frequency range. Time series produced using the same parameters as in $t < 0.5$ s in Figure 6.5c. **B** and **C)** Each of the 100 parameter sets in the final iteration of SMC-ABC are compared under 4 conditions. 1) Healthy condition i.e. parameters left unchanged. 2) DA=0. Dopamine is set to zero but all connection strength parameters left unchanged. 3) PD. Dopamine is left at zero but the weights are changed to reflect the changes seen in advanced PD. $W_{\text{ctx-stn}}$ and $W_{\text{ctx-str}}$ are doubled. $W_{\text{GPe-STN}}$ is multiplied by 1.5. 4) STN-GPe. Parameters and dopamine level are as in the PD condition except $W_{\text{STN-GPe}}$ is multiplied by 0.4. **B)** Average number of selection tests passed out of a maximum of 6. The loss of dopamine causes a dramatic fall in the ability of the network to select. The weight changes that occur in PD cause selection ability to be regained. **C)** Frequency of GPi oscillations in each condition. No oscillations in healthy condition. Setting DA=0 causes low frequency oscillations in a very small proportion of cases. The changes in connection strengths in PD cause the network to oscillate in 100% of cases. Multiplying the STN-GPe strength by 0.4 causes all 100 models to cease oscillating.

6.6: Discussion

A new methodology is put forward for the testing of a computational hypothesis. Rather than seeking model parameters that enable the system to function in the hypothesised way, the distribution of parameter values is sought that are in agreement with known experimental data. These parameter sets are then tested for the hypothesised function. Using this methodology the current work shows that the basal ganglia are well suited to the task of selecting between multiple inputs of varying strengths. The model correctly predicts that dopamine loss leads, in the first instance, to the akinesia associated with the Parkinsonian condition. When the changes that are seen in advanced PD are made to the network it also predicts that the network will produce beta oscillations when at rest that cease when actions are undertaken. Our model supports the hypothesis that the beta oscillations recorded from the BG of PD sufferers arise as a result of the changes in the network that are a response to the loss of dopaminergic input, rather than the loss of dopamine itself. A novel result from this work is that the model also illuminates the possible mechanisms of action of some treatments already in use; glutamate antagonists and pallidotomy.

A number of other models have addressed the BG's ability to select between inputs [54], [55], [200], [201]. And many models have addressed the question of the transition to oscillations in the STN-GPe feedback loop [46], [49], [50], or the whole BG-thalamocortical system [213]. However, only Humphries et al. have modelled action selection and oscillatory phenomena

in the same study. Their model was written at a detailed level of description, composed of populations of leaky-integrate-and-fire neurons. While this approach has proved extremely useful, the model is far too detailed to allow numerical or analytic analysis. The work of Gillies [46] showed that increasing the strength of the cortex-STN connection increases oscillations. However, many of their other conclusions rely on the assumption of significant self excitation in the STN. The evidence for such a connection is not thought to be strong enough to play a significant role in either the selection of actions or the generation of oscillations [47], [48].

Nevado Holgado [50] showed, using a simple firing rate model of the STN-GPe loop, that this self excitation was not necessary for the generation of beta oscillations and demonstrated the importance of time constants and delays to the presence and frequency of oscillations. In their study a *healthy* and a *diseased* parameter set were found and the transition into advanced PD was modelled as a linear transition of connection strengths from one to the other. While this approach was a useful simplification for the purposes of an analytical treatment our current work shows that there is a multitude of ways that the network can change that give rise to beta oscillations. Thus the linear progression from health to one specific pathological state may be an oversimplification. This may have clinical implications in that the BG network in Parkinson's sufferers may have changed in different ways between patients, but the observable behavioural symptoms would be the same. It may prove fruitful to use what is known of homeostatic plasticity to

attempt to plot the distribution of possible connection strength changes as PD progresses. The changes seen in animal models, in which dopamine loss happens extremely quickly, may be different from the changes that occur in human PD when dopamine loss is much more gradual. It is an idea worth investigation that the efficacy or otherwise of particular treatments may be explainable by the differences in network changes between patients. Our model is well suited to exploring this space of strength changes and this is an area of study that is ongoing.

A significant difference between the current work and the NH study is that in the current analysis a low background-level of cortical input (4Hz) to the striatum and STN is used whereas NH used a value of 27Hz. A low spike rate was used because the monkeys from which the fitting data was recorded were not performing any tasks. The current work shows that this assumption was well founded, since the model correctly predicts beta oscillations only in the resting state, as is the case with the behaviour of PD sufferers.

Our model seeks to combine the benefits of the many BG modelling studies that preceded it. It includes sufficient physiological detail to give an accurate description of how the firing rates of neural populations interact, but it is not so complex that numerical analyses become intractable. The compact framework of the model enables the modelling of multiple channels. This is of particular importance when modelling PD since it is a disorder in which symptoms exist as both a deficit in selection ability and pathological

oscillations. These are intimately connected phenomena. Our model constitutes the first purely mathematical treatment that can address these issues simultaneously.

Observations of model behaviour indicate that the parameter value ranges found by SMC-ABC yield stable solutions under most combinations of inputs and dopamine levels. In instances where the model displays oscillatory behaviour the frequencies of the oscillations fall into two distinct groups: about 10-20Hz and about 60-80Hz. Experimental observations have been made which find that the spectral activity in the BG does indeed have significantly higher activity in these frequency ranges [216]. In the healthy model these oscillations seem to occur in channels in which the cortical input is above baseline but the channel is not selected. To formalise and fully understand the nature of these oscillations it will be necessary to conduct a numerical bifurcation analysis of the model, focusing on input level, dopamine level and a parameter governing the weight changes involved in disease progression. This work is ongoing and is beyond the scope of the current paper.

Since our current work suggests that the resting state oscillatory phenomena emerge as a consequence of connection strength changes, it will be useful to attempt to uncover the gradual network changes that are seen as PD progresses. This could help us to understand the differences between the BG connection strengths of individual PD sufferers, and may enable us to uncover why certain treatments work for some individuals and not others.

6.7: Summary

- A new principled methodology for testing a computational hypothesis is put forward. Firstly build model connectivity and parameters according to what is known of the physiology. Secondly, find the distributions of the unknown parameters using a sampling-based Bayesian estimation technique. Thirdly, test all identified parameter sets for their ability to perform the hypothesised function. A correlation between ability to perform the function and the goodness of fit to the experimental data should be taken as evidence in favour of the hypothesis.
- The hypothesis that the BG performs action selection is tested using the above methodology. It was found that the hypothesis should be accepted.
- Setting the level of dopaminergic innervations of the striatum of the model leads to increased average activity in the BG output nucleus and so a loss of selection capability. However, setting dopaminergic innervations to zero does not directly lead to resting state oscillations.
- When the same changes are made to the network that occurs with the advance of PD, two notable effects are observed. 1) Selection functionality is restored, even in the absence of any dopaminergic innervations. 2) A resting state oscillation in the beta frequency range occurs. As is the case in real PD, the oscillations cease when cortical input increases above baseline.

Chapter 7: Conclusions and Future Work

Detailed discussion of each part is given at the end of each chapter. Here is outlined the main conclusions of the work as a whole and the general directions for future work in this area.

The main and most general conclusion from the work undertaken is that models of mass action of neural activity are an extremely useful method for assessing healthy and pathological neural activity at the systems level. Results from the work in Chapter 3 demonstrate the effectiveness of analysing temporal features of clinical EEG recordings rather than using solely spectral data as is most often the case. Bifurcation analysis of the neural mass model showed that the model was capable of replicating all the classes of waveform profiles that were seen in the EEG recordings from focal onset epilepsy sufferers, and also showed that seizures follow a characteristic evolution over the timescale of each seizure.

Moreover, the statistical analysis showed that different seizures from the same patient followed the same temporal evolution, whereas seizures from different patients follow slightly different evolutions. However, the analysis also exposed some similarities between seizures from different patients. For example all seizures began with a period of pseudo sinusoidal oscillations, moving through a period of apparently chaotic behaviour before ending the seizure with a period of spike and wave activity. The bifurcation analysis

showed that a wide variety of dynamics are possible with only small variations in the values of a small number of parameters. Of particular importance were the parameters governing the gain in the fast and slow inhibitory feedback loops.

From this analysis it can be concluded that the dynamics of epilepsy critically depend on the balance between fast and slow inhibition in hippocampal cortex. These observations could be used to inform future experimental work focusing on seizure prediction and cessation. Future work in this area will focus on precisely fitting the parameters of the model to the clinical data in order to plot the characteristic path that each patient's seizures take through the low dimensional phase space. This kind of patient specific modelling is becoming increasingly possible and has already been implemented in models absence epilepsy [92]. Its extension to the far more technically challenging problem of focal onset seizures will be able to enable these insights to benefit a far greater number of epilepsy sufferers.

In chapter 4 a Bayesian parameter estimation technique called approximate Bayesian computation (SMC-ABC) is described. Since this technique has not previously been used in neural modelling its use was validated by replicating the results of a previous study. Since the results are consistent with those from the previous study, it was concluded that SMC-ABC is a suitable tool for finding the parameters of neural models.

The most significant conclusion from the work contained in Chapter 5 is that firing rate models can be constructed such that they better represent the

richness of dynamics that are displayed in real neurons without the need to model unknown intracellular processes. By parsimoniously modelling only the input/output relationships between nuclei and their afferents using a second order formulation and variable time constants there is sufficient detail to permit the models to be accurately parametrised using dynamical time series data. It has been shown that approximate Bayesian computation is a suitable tool for finding the parameters of neural models for a number of reasons. Neural models are invariably highly complex and nonlinear and so the likelihood function is often difficult to compute. ABC functions best when low dimensional but highly informative data is used to constrain the search and this is exactly the kind of information that is common in the experimental neuroscience literature. The new methodology defined in this thesis will generalise well to other neural modelling problems.

Conclusions from Chapter 6 are related to the functionality and pathology of the basal ganglia. In the first instance, evidence was found that the basal ganglia are tuned to select between competing cortical inputs. Finding the parameters of the network according to firing rate data yields networks that disinhibit channels for which the inputs are higher than competing channels, as would be required from a selection mechanism. While the hypothesis that the basal ganglia is a selection mechanism has gained significant support over the last decade, support for the idea is not universal [201], so independent theoretical evidence is an important step forward.

The simulation of the development of Parkinson's disease in the model, by setting the dopamine parameter to zero and increasing the connection strengths between certain experimentally identified nuclei, leads to the conclusion that the pathological increase in beta band oscillations is caused not by the decrease in dopamine directly, but rather by the network changes that arise as the network adapts to the reduced dopamine. The simultaneous analysis of both oscillations and basal ganglia functionality has demonstrated how these two phenomena interact. The network connection strength changes that are seen in Parkinson's disease seem to serve to restore the selection functionality of the network, even in the absence of dopamine. However, as the network continues this adaptation, a point is reached whereby the stability of the network cannot be maintained in the resting state. At this point the network oscillates in the beta frequency range, as is seen in Parkinson's sufferers.

Future work will focus on conducting a rigorous bifurcation analysis of the model in order to illuminate this transition to an oscillatory stable state. Parameters of particular importance to this analysis are the level of input from the cortex, the level of tonic dopamine and a parameter governing the change of the network connection strengths between the healthy state and the advanced disease state.

This modelling framework could be used to produce patient specific models of Parkinson's sufferers. Experiments could be conducted on PD sufferers to assess their motor deficits and selection function and the data will be used to

find the parameters of models of their BG. Until the work contained in this thesis was completed, the only models that were capable of quantitatively describing both the selection functionality and the pathological oscillatory phenomena were models that used many spiking neurons and contained a great deal of physiological detail with a large number of parameters. It is likely that the high number of parameters in these models will mean that there is too many degrees of freedom in the models, leading to overfitting and poorly constrained parameter value ranges. The low dimensionality of the model described in this thesis, combined with its direct quantification of connection strengths between nuclei, make this model ideally suited to this patient specific modelling of network changes.

Bibliography

Bibliography

- [1] F. A. C. Azevedo, L. R. B. Carvalho, L. T. Grinberg, J. M. Farfel, R. E. L. Ferretti, R. E. P. Leite, W. Jacob Filho, R. Lent, and S. Herculano-Houzel, "Equal numbers of neuronal and nonneuronal cells make the human brain an isometrically scaled-up primate brain.," *J. Comp. Neurol.*, vol. 513, no. 5, pp. 532–41, Apr. 2009.
- [2] R. I. Goldman, J. M. Stern, J. Engel, and M. S. Cohen, "Simultaneous EEG and fMRI of the alpha rhythm.," *Neuroreport*, vol. 13, no. 18, pp. 2487–92, Dec. 2002.
- [3] A. T. Berg and S. Shinnar, "The risk of seizure recurrence following a first unprovoked seizure," *Neurology*, vol. 41, no. 7, p. 965, 1991.
- [4] E. H. Reynolds, "The early treatment and prognosis of epilepsy.," *Jpn. J. Psychiatry Neurol.*, vol. 42, no. 3, pp. 429–35, Sep. 1988.
- [5] G. V. Goddard, D. C. McIntyre, and C. K. Leech, "A permanent change in brain function resulting from daily electrical stimulation," *Exp. Neurol.*, vol. 25, no. 3, pp. 295–330, 1969.
- [6] a Marson, a Jacoby, a Johnson, L. Kim, C. Gamble, and D. Chadwick, "Immediate versus deferred antiepileptic drug treatment for early epilepsy and single seizures: a randomised controlled trial.," *Lancet*, vol. 365, no. 9476, pp. 2007–13, 2007.
- [7] J. F. Téllez-Zenteno, R. Dhar, and S. Wiebe, "Long-term seizure outcomes following epilepsy surgery: a systematic review and meta-analysis.," *Brain*, vol. 128, no. Pt 5, pp. 1188–98, May 2005.
- [8] M. Avoli, M. a Rogawski, and G. Avanzini, "Generalized epileptic disorders: an update.," *Epilepsia*, vol. 42, no. 4, pp. 445–57, Apr. 2001.
- [9] D. A. McCormick and D. Contreras, "On the cellular and network bases of epileptic seizures," *Annu. Rev. Physiol.*, vol. 63, pp. 815–846, 2001.
- [10] V. Crunelli and N. Leresche, "Childhood absence epilepsy: genes, channels, neurons and networks.," *Nat. Rev. Neurosci.*, vol. 3, no. 5, pp. 371–82, May 2002.
- [11] L. Danober, C. Deransart, a Depaulis, M. Vergnes, and C. Marescaux, "Pathophysiological mechanisms of genetic absence epilepsy in the rat.," *Prog. Neurobiol.*, vol. 55, no. 1, pp. 27–57, May 1998.
- [12] M. Avoli and P. Gloor, "Interaction of cortex and thalamus in spike and wave discharges of feline generalized penicillin epilepsy," *Exp. Neurol.*, vol. 76, no. 1, pp. 196–217, 1982.
- [13] M. Avoli and P. Gloor, "Role of the thalamus in generalized penicillin epilepsy: Observations on decorticated cats," *Exp. Neurol.*, vol. 77, no. 2, pp. 386–402, 1982.

- [14] N. E. Anden, A. Dahlstroem, K. Fuxe, and K. Larsson, "Further evidence for the presence of nigro-striatal dopamine neurons in the rat," *Am. J. Anat.*, vol. 116, pp. 329–33, Jan. 1965.
- [15] M. Shiba, J. H. Bower, D. M. Maraganore, S. K. McDonnell, B. J. Peterson, J. E. Ahlskog, D. J. Schaid, and W. A. Rocca, "Anxiety disorders and depressive disorders preceding Parkinson's disease: A case-control study," *Mov. Disord.*, vol. 15, no. 4, pp. 669–677, Jul. 2000.
- [16] W. C. Koller, "Sensory symptoms in Parkinson's disease," *Neurology*, vol. 34, no. 7, pp. 957–957, Jul. 1984.
- [17] K. R. Chaudhuri, D. G. Healy, and A. H. Schapira, "Non-motor symptoms of Parkinson's disease: diagnosis and management," *Lancet Neurol.*, vol. 5, no. 3, pp. 235–245, 2006.
- [18] W. Weiner, L. Shulman, and A. Lang, *Parkinson's disease: A complete guide for patients and families*. 2001.
- [19] C. C. McIntyre, M. Savasta, L. Kerkerian-Le Goff, and J. L. Vitek, "Uncovering the mechanism(s) of action of deep brain stimulation: activation, inhibition, or both," *Clin. Neurophysiol.*, vol. 115, no. 6, pp. 1239–1248, 2004.
- [20] C. Beurrier, B. Bioulac, J. Audin, and C. Hammond, "High-Frequency Stimulation Produces a Transient Blockade of Voltage-Gated Currents in Subthalamic Neurons," *J Neurophysiol.*, vol. 85, no. 4, pp. 1351–1356, Apr. 2001.
- [21] F. Urbano, E. Leznik, and R. Llinás, "Cortical activation patterns evoked by afferent axons stimuli at different frequencies: an in vitro voltage-sensitive dye imaging study," *Thalamus Relat. Syst.*, vol. 1, no. 04, p. 371, Apr. 2006.
- [22] J. O. Dostrovsky and A. M. Lozano, "Mechanisms of deep brain stimulation," *Mov. Disord.*, vol. 17 Suppl 3, pp. S63–8, Jan. 2002.
- [23] E. B. Montgomery and K. B. Baker, "Mechanisms of deep brain stimulation and future technical developments," *Neurol. Res.*, vol. 22, no. 3, pp. 259–66, Apr. 2000.
- [24] D. J. Amit, *Modeling Brain Function: The World of Attractor Neural Networks*. Cambridge University Press, 1992, p. 504.
- [25] J. Dobbing, "Undernutrition and the Developing Brain: The Relevance of Animal Models to the Human Problem," *Nutr. Dieta*, 1972.
- [26] C. Kornetsky, "Animal models: promises and problems," *Anim. Model. Depress.*, 1989.
- [27] A. Destexhe and D. Contreras, "Spike-and-wave oscillations based on the properties of GABA_B receptors," *J. Neurosci.*, vol. 18, pp. 9099–9111, 1998.

Bibliography

- [28] a Destexhe, D. Contreras, and M. Steriade, "Mechanisms underlying the synchronizing action of corticothalamic feedback through inhibition of thalamic relay cells.," *J. Neurophysiol.*, vol. 79, no. 2, pp. 999–1016, Feb. 1998.
- [29] M. Breakspear, J. A. Roberts, J. R. Terry, S. Rodrigues, N. Mahant, and P. A. Robinson, "A unifying explanation of primary generalized seizures through nonlinear brain modeling and bifurcation analysis.," *Cereb. Cortex*, vol. 16, no. 9, pp. 1296–313, Sep. 2006.
- [30] F. Marten, "Analysis of seizure evolution through neural mass modelling," *Philosophy*, no. January, 2011.
- [31] M. Brons, M. Krupa, and M. Wechselberger, "Mixed mode oscillations due to the generalised canard phenomena," *Fields Inst. Commun.*, vol. 49, pp. 39–64, 2006.
- [32] R. D. Traub, M. A. Whittington, E. H. Buhl, F. E. N. LeBeau, A. Bibbig, S. Boyd, H. Cross, and T. Baldeweg, "A Possible Role for Gap Junctions in Generation of Very Fast EEG Oscillations Preceding the Onset of, and Perhaps Initiating, Seizures," *Epilepsia*, vol. 42, no. 2, pp. 153–170, Jul. 2008.
- [33] A. van Rotterdam, F. H. Lopes da Silva, J. van den Ende, M. A. Viergever, and A. J. Hermans, "A model of the spatial-temporal characteristics of the alpha rhythm," *Bull. Math. Biol.*, vol. 44, no. 2, pp. 283–305, 1982.
- [34] B. H. Jansen and V. G. Rit, "Electroencephalogram and visual evoked potential generation in a mathematical model of coupled cortical columns," *Biol. Cybern.*, vol. 73, no. 4, pp. 357–366, Sep. 1995.
- [35] P. Brown, A. Oliviero, P. Mazzone, A. Insola, P. Tonali, and V. Di Lazzaro, "Dopamine Dependency of Oscillations between Subthalamic Nucleus and Pallidum in Parkinson's Disease," *J. Neurosci.*, vol. 21, no. 3, pp. 1033–1038, Feb. 2001.
- [36] M. Cassidy, "Movement-related changes in synchronization in the human basal ganglia," *Brain*, vol. 125, no. 6, pp. 1235–1246, Jun. 2002.
- [37] A. A. Kühn, D. Williams, A. Kupsch, P. Limousin, M. Hariz, G.-H. Schneider, K. Yarrow, and P. Brown, "Event-related beta desynchronization in human subthalamic nucleus correlates with motor performance.," *Brain*, vol. 127, no. Pt 4, pp. 735–46, Apr. 2004.
- [38] R. Levy, "Dependence of subthalamic nucleus oscillations on movement and dopamine in Parkinson's disease," *Brain*, vol. 125, no. 6, pp. 1196–1209, Jun. 2002.
- [39] L. W. Swanson, A. Björklund, T. Hökfelt, C. R. Gerfen, and C. J. Wilson, "Chapter II The basal ganglia," *Handb. Chem. Neuroanat.*, vol. 12, pp. 371–468, 1996.
- [40] G. Glynn and S. O. Ahmad, "Three-dimensional electrophysiological topography of the rat corticostriatal system.," *J. Comp. Physiol. A. Neuroethol. Sens. Neural. Behav. Physiol.*, vol. 188, no. 9, pp. 695–703, Oct. 2002.

- [41] G. Alexander, "Parallel organization of functionally segregated circuits linking basal ganglia and cortex," *Annu. Rev. ...*, 1986.
- [42] R. L. Albin, A. B. Young, and J. B. Penney, "The functional anatomy of basal ganglia disorders," *Trends Neurosci.*, vol. 12, no. 10, pp. 366–375, 1989.
- [43] A. Nambu, H. Tokuno, and M. Takada, "Functional significance of the cortico-subthalamo-pallidal 'hyperdirect' pathway.," *Neurosci. Res.*, vol. 43, no. 2, pp. 111–7, Jun. 2002.
- [44] Y. Temel, A. Blokland, H. W. M. Steinbusch, and V. Visser-Vandewalle, "The functional role of the subthalamic nucleus in cognitive and limbic circuits.," *Prog. Neurobiol.*, vol. 76, no. 6, pp. 393–413, Aug. 2005.
- [45] Y. Smith, M. D. Bevan, E. Shink, and J. P. Bolam, "Microcircuitry of the direct and indirect pathways of the basal ganglia," *Neuroscience*, vol. 86, no. 2, pp. 353–387, 1998.
- [46] A. Gillies, D. Willshaw, and Z. Li, "Subthalamic-pallidal interactions are critical in determining normal and abnormal functioning of the basal ganglia.," *Proc. Biol. Sci.*, vol. 269, no. 1491, pp. 545–51, Mar. 2002.
- [47] C. Hammond and J. Yelnik, "Intracellular labelling of rat subthalamic neurones with horseradish peroxidase: Computer analysis of dendrites and characterization of axon arborization," *Neuroscience*, vol. 8, no. 4, pp. 781–790, 1983.
- [48] F. Sato, M. Parent, M. Levesque, and A. Parent, "Axonal branching pattern of neurons of the subthalamic nucleus in primates.," *J. Comp. Neurol.*, vol. 424, no. 1, pp. 142–52, Aug. 2000.
- [49] D. Terman, J. E. Rubin, a C. Yew, and C. J. Wilson, "Activity patterns in a model for the subthalamopallidal network of the basal ganglia.," *J. Neurosci.*, vol. 22, no. 7, pp. 2963–76, Apr. 2002.
- [50] A. J. Nevado Holgado, J. R. Terry, and R. Bogacz, "Conditions for the generation of beta oscillations in the subthalamic nucleus-globus pallidus network.," *J. Neurosci.*, vol. 30, no. 37, pp. 12340–52, Sep. 2010.
- [51] A. C. Marreiros, H. Cagnan, R. J. Moran, K. J. Friston, and P. Brown, "Basal ganglia–cortical interactions in Parkinsonian patients," *Neuroimage*, vol. 66, pp. 301–310, 2013.
- [52] P. Redgrave, T. J. Prescott, and K. Gurney, "The basal ganglia: a vertebrate solution to the selection problem?," *Neuroscience*, vol. 89, no. 4, pp. 1009–1023, 1999.
- [53] K. Gurney, T. J. Prescott, and P. Redgrave, "A computational model of action selection in the basal ganglia. I. A new functional anatomy.," *Biol. Cybern.*, vol. 84, no. 6, pp. 401–10, Jun. 2001.

Bibliography

- [54] K. Gurney, T. J. Prescott, and P. Redgrave, "A computational model of action selection in the basal ganglia. II. Analysis and simulation of behaviour.," *Biol. Cybern.*, vol. 84, no. 6, pp. 411–23, Jun. 2001.
- [55] M. D. Humphries, R. D. Stewart, and K. N. Gurney, "A physiologically plausible model of action selection and oscillatory activity in the basal ganglia.," *J. Neurosci.*, vol. 26, no. 50, pp. 12921–42, Dec. 2006.
- [56] O. Hikosaka, Y. Takikawa, and R. Kawagoe, "Role of the Basal Ganglia in the Control of Purposeful Saccadic Eye Movements," *Physiol Rev*, vol. 80, no. 3, pp. 953–978, Jul. 2000.
- [57] G. S. Berns and T. J. Sejnowski, "A computational model of how the basal ganglia produce sequences.," *J. Cogn. Neurosci.*, vol. 10, no. 1, pp. 108–21, Jan. 1998.
- [58] M. J. Frank, B. Loughry, and R. C. O'Reilly, "Interactions between frontal cortex and basal ganglia in working memory: a computational model.," *Cogn. Affect. Behav. Neurosci.*, vol. 1, no. 2, pp. 137–60, Jun. 2001.
- [59] R. C. O'Reilly and M. J. Frank, "Making working memory work: a computational model of learning in the prefrontal cortex and basal ganglia.," *Neural Comput.*, vol. 18, no. 2, pp. 283–328, Feb. 2006.
- [60] L. Segel and M. Slemrod, "The quasi-steady-state assumption: a case study in perturbation," *SIAM Rev.*, 1989.
- [61] I. Fodor, "A survey of dimension reduction techniques," 2002.
- [62] H. R. Wilson and J. D. Cowan, "Excitatory and inhibitory interactions in localized populations of model neurons.," *Biophys. J.*, vol. 12, no. 1, pp. 1–24, Jan. 1972.
- [63] F. H. Lopes da Silva, A. Hoeks, H. Smits, and L. H. Zetterberg, "Model of brain rhythmic activity," *Kybernetik*, vol. 15, no. 1, pp. 27–37, 1974.
- [64] P. L. Nunez, "The Brain Wave Equation: A Model for the EEG.," *Math. Biosci.*, vol. 21, pp. 279–297, 1974.
- [65] S. Coombes, "Waves, bumps, and patterns in neural field theories.," *Biol. Cybern.*, vol. 93, no. 2, pp. 91–108, Aug. 2005.
- [66] S. Amari, "Dynamics of pattern formation in lateral-inhibition type neural fields.," *Biol. Cybern.*, vol. 27, pp. 77–87, 1977.
- [67] S. Coombes, "Large-scale neural dynamics: simple and complex.," *Neuroimage*, vol. 52, no. 3, pp. 731–9, Sep. 2010.
- [68] D. Liley and I. Bojak, "Understanding the transition to seizure by modeling the epileptiform activity of general anesthetic agents," *J. Clin. Neurophysiol.*, 2005.

- [69] P. N. Taylor and G. Baier, "A spatially extended model for macroscopic spike-wave discharges," *J. Comput. Neurosci.*, May 2011.
- [70] S. Amari, "Learning Patterns of Sequences by Self-Organizing Nets of Threshold Elements," *IEEE Trans. Comput.*, vol. c-21, no. 11, pp. 1197–1206, 1972.
- [71] F. Marten, S. Rodrigues, O. Benjamin, M. P. Richardson, and J. R. Terry, "Onset of polyspike complexes in a mean-field model of human electroencephalography and its application to absence epilepsy," *Philos. Trans. A. Math. Phys. Eng. Sci.*, vol. 367, no. 1891, pp. 1145–61, Mar. 2009.
- [72] F. Wendling, J. Bellanger, F. Bartolomei, and P. Chauvel, "Relevance of nonlinear lumped-parameter models in the analysis of depth-EEG epileptic signals," *Biol. Cybern.*, vol. 83, no. 4, pp. 367–378, Sep. 2000.
- [73] D. T. J. Liley, P. J. Cadusch, and M. P. Dafilis, "A spatially continuous mean field theory of electrocortical activity," Aug. 2002.
- [74] F. H. Lopez da Silva, A. Hoeks, H. Smits, and L. H. Zetterberg, "Model of Brain Rhythmic Activity: The Alpha-Rhythm of the Thalamus," *Kybernetik*, vol. 15, pp. 27–37, 1974.
- [75] F. Wendling, J. J. Bellanger, F. Bartolomei, and P. Chauvel, "Relevance of nonlinear lumped-parameter models in the analysis of depth-EEG epileptic signals," *Biol. Cybern.*, vol. 83, no. 4, pp. 367–78, Oct. 2000.
- [76] F. Wendling, A. Hernandez, J.-J. Bellanger, P. Chauvel, and F. Bartolomei, "Interictal to ictal transition in human temporal lobe epilepsy: insights from a computational model of intracerebral EEG," *J. Clin. Neurophysiol.*, vol. 22, no. 5, pp. 343–56, Oct. 2005.
- [77] A. Blenkinsop, A. Valentin, M. P. Richardson, and J. R. Terry, "The dynamic evolution of focal-onset epilepsies - combining theoretical and clinical observations," *Eur. J. Neurosci.*, vol. 36, no. 2, pp. 2188–200, Jul. 2012.
- [78] O. David and K. J. Friston, "A neural mass model for MEG/EEG," *Neuroimage*, vol. 20, no. 3, pp. 1743–1755, 2003.
- [79] P. Suffczynski, S. Kalitzin, G. Pfurtscheller, and F. . Lopes da Silva, "Computational model of thalamo-cortical networks: dynamical control of alpha rhythms in relation to focal attention," *Int. J. Psychophysiol.*, vol. 43, no. 1, pp. 25–40, 2001.
- [80] A. Hedström and I. Olsson, "Epidemiology of absence epilepsy: EEG findings and their predictive value," *Pediatr. Neurol.*, vol. 7, no. 2, pp. 100–104, 1991.
- [81] S. Rodrigues, D. Barton, F. Marten, M. Kibuuka, G. Alarcon, M. P. Richardson, and J. R. Terry, "A method for detecting false bifurcations in dynamical systems: application to neural-field models," *Biol. Cybern.*, vol. 102, no. 2, pp. 145–54, Feb. 2010.

Bibliography

- [82] C. Koch, M. Rapp, and I. Segev, "A brief history of time (constants).," *Cereb. Cortex*, vol. 6, no. 2, pp. 93–101, 1996.
- [83] O. Bernander, R. J. Douglas, K. A. Martin, and C. Koch, "Synaptic background activity influences spatiotemporal integration in single pyramidal cells.," *Proc. Natl. Acad. Sci.*, vol. 88, no. 24, pp. 11569–11573, Dec. 1991.
- [84] Y. Tachibana, H. Kita, S. Chiken, M. Takada, and A. Nambu, "Motor cortical control of internal pallidal activity through glutamatergic and GABAergic inputs in awake monkeys.," *Eur. J. Neurosci.*, vol. 27, no. 1, pp. 238–53, Jan. 2008.
- [85] G. Ermentrout and D. Terman, "Firing rate models," *Math. Found. Neurosci.*, 2010.
- [86] P. Dayan, L. Abbott, and L. Abbott, "Theoretical neuroscience: Computational and mathematical modeling of neural systems," 2001.
- [87] T. Vogels, K. Rajan, and L. Abbott, "Neural network dynamics," *Annu. Rev. Neurosci.*, 2005.
- [88] B. H. Jansen, G. Zouridakis, and M. E. Brandt, "Biological Cybernetics of flash visual evoked potentials," *Electr. Eng.*, vol. 283, pp. 275–283, 1993.
- [89] P. a Robinson, C. J. Rennie, D. L. Rowe, and S. C. O'Connor, "Estimation of multiscale neurophysiologic parameters by electroencephalographic means.," *Hum. Brain Mapp.*, vol. 23, no. 1, pp. 53–72, Sep. 2004.
- [90] I. Bojak and D. Liley, "Modeling the effects of anesthesia on the electroencephalogram," *Phys. Rev. E*, vol. 71, no. 4, pp. 1–22, Apr. 2005.
- [91] F. Wendling, F. Bartolomei, J. Bellanger, and P. Chauvel, "Epileptic fast activity can be explained by a model of impaired GABAergic dendritic inhibition," *Eur. J. Neurosci.*, vol. 15, no. 9, pp. 1499–1508, May 2002.
- [92] A. J. Nevado Holgado, F. Marten, M. Richardson, and J. R. Terry, "Characterising the dynamics of EEG waveforms as the path through parameter space of a neural mass model: Application to epilepsy seizure evolution.," *Neuroimage*, vol. 59, no. 3, pp. 2374–2392, 2011.
- [93] K. J. Friston, L. Harrison, and W. Penny, "Dynamic causal modelling," *Neuroimage*, vol. 19, no. 4, pp. 1273–1302, 2003.
- [94] G. Lohmann, K. Erfurth, K. Müller, and R. Turner, "Critical comments on dynamic causal modelling," *NeuroImage*, vol. 59, no. 3, pp. 2322–2329, 2012.
- [95] D. Rubin, "Bayesianly justifiable and relevant frequency calculations for the applied statistician," *Ann. Stat.*, vol. 12, no. 4, pp. 1151–1172, 1984.
- [96] D. Ruppert and M. Wand, "Multivariate locally weighted least squares regression," *Ann. Stat.*, vol. 22, no. 3, pp. 1346–1370, 1994.

- [97] M. G. B. Blum and O. François, "Non-linear regression models for Approximate Bayesian Computation," *Stat. Comput.*, vol. 20, no. 1, pp. 63–73, Mar. 2009.
- [98] P. Marjoram, J. Molitor, V. Plagnol, and S. Tavaré, "Markov chain Monte Carlo without likelihoods," *Proc. Natl. Acad. Sci. U. S. A.*, vol. 100, no. 26, pp. 15324–8, Dec. 2003.
- [99] T. Toni, D. Welch, N. Strelkowa, A. Ipsen, and M. P. H. Stumpf, "Approximate Bayesian computation scheme for parameter inference and model selection in dynamical systems," *J. R. Soc. Interface*, vol. 6, no. 31, pp. 187–202, Feb. 2009.
- [100] S. A. Sisson, Y. Fan, and M. M. Tanaka, "Sequential Monte Carlo without likelihoods," *Proc. Natl. Acad. Sci. U. S. A.*, vol. 104, no. 6, pp. 1760–5, Feb. 2007.
- [101] M. Beaumont, W. Zhang, and D. J. Balding, "Approximate Bayesian Computation in Population Genetics," *Genetics*, vol. 162, no. 4, pp. 2025–2035, Dec. 2002.
- [102] M. Beaumont, "Approximate Bayesian Computation in Evolution and Ecology," *Annu. Rev. Ecol. Evol. Syst.*, vol. 41, no. 1, pp. 379–406, Dec. 2010.
- [103] F. Grimbert and O. Faugeras, "Bifurcation analysis of Jansen's neural mass model," *Neural Comput.*, vol. 18, pp. 3052–3068, 2006.
- [104] A. Spiegler, T. R. Knösche, J. Haueisen, and F. M. Atay, "Complex behavior in a modified Jansen and Rit neural mass model," *BMC Neurosci.*, vol. 12, no. Suppl 1, p. P5, 2011.
- [105] J. Touboul, F. Wendling, P. Chauvel, and O. Faugeras, "Neural mass activity, bifurcations, and epilepsy," *Neural Comput.*, vol. 23, no. 12, pp. 3232–86, Dec. 2011.
- [106] J. Touboul, F. Wendling, P. Chauvel, and O. Faugeras, "Neural mass activity, bifurcations, and epilepsy," *Neural Comput.*, vol. 23, no. 12, pp. 3232–86, Dec. 2011.
- [107] H. K. M. Meeren, J. P. M. Pijn, E. L. J. M. Van Luijtelaar, A. M. L. Coenen, and F. H. Lopes da Silva, "Cortical focus drives widespread corticothalamic networks during spontaneous absence seizures in rats," *J. Neurosci.*, vol. 22, no. 4, pp. 1480–95, Feb. 2002.
- [108] C. J. Stam, "Nonlinear dynamical analysis of EEG and MEG: Review of an emerging field," *Clin. Neurophysiol.*, vol. 116, no. 10, pp. 2266–2301, 2005.
- [109] A. J. Nevado-Holgado, F. Marten, M. P. Richardson, and J. R. Terry, "Characterising the dynamics of EEG waveforms as the path through parameter space of a neural mass model: Application to epilepsy seizure evolution," *Neuroimage*, vol. 59, no. 3, pp. 2374–2392, 2012.
- [110] F. Wendling, "Computational models of epileptic activity: a bridge between observation and pathophysiological interpretation," 2008.

Bibliography

- [111] M. Breakspear, V. Jirsa, G. Deco, A. Spiegler, S. J. Kiebel, F. M. Atay, and T. R. Knösche, "Bifurcation analysis of neural mass models: Impact of extrinsic inputs and dendritic time constants," *Neuroimage*, vol. 52, no. 3, pp. 1041–1058, 2010.
- [112] J. Touboul, "Codimension Two Bifurcations and Rhythms in Neural Mass Models," pp. 1–50, 2009.
- [113] P. D. Williamson, V. M. Thadani, J. A. French, T. M. Darcey, R. H. Mattson, S. S. Spencer, and D. D. Spencer+, "Medial Temporal Objective Lobe Epilepsy: Videotape Analysis of Clinical Seizure Characteristics," *Epilepsia*, vol. 39, no. 11, pp. 1182–1188, Nov. 1998.
- [114] M. Catani, D. Stuss, J. O'Muircheartaigh, and M. P. Richardson, "Epilepsy and the frontal lobes," *Cortex*, vol. 48, no. 2, pp. 144–155, 2012.
- [115] D. Bosnyakova, A. Gabova, A. Zharikova, V. Gnezditski, G. Kuznetsova, and G. van Luijtelaar, "Some peculiarities of time–frequency dynamics of spike–wave discharges in humans and rats," *Clin. Neurophysiol.*, vol. 118, no. 8, pp. 1736–1743, 2007.
- [116] M. Breakspear, J. Roberts, J. R. Terry, S. Rodrigues, N. Mahant, and P. Robinson, "A unifying explanation of primary generalized seizures through nonlinear brain modeling and bifurcation analysis.," *Cereb. Cortex*, vol. 16, no. 9, pp. 1296–313, Sep. 2006.
- [117] D. W. Cope, G. Di Giovanni, S. J. Fyson, G. Orbán, A. C. Errington, M. L. Lorincz, T. M. Gould, D. a Carter, and V. Crunelli, "Enhanced tonic GABAA inhibition in typical absence epilepsy.," *Nat. Med.*, vol. 15, no. 12, pp. 1392–8, Dec. 2009.
- [118] F. Marten, S. Rodrigues, P. Suffczynski, M. Richardson, and J. Terry, "Derivation and analysis of an ordinary differential equation mean-field model for studying clinically recorded epilepsy dynamics," *Phys. Rev. E*, vol. 79, no. 2, pp. 1–7, Feb. 2009.
- [119] S. Rodrigues, D. Barton, R. Szalai, O. Benjamin, M. P. Richardson, and J. R. Terry, "Transitions to spike-wave oscillations and epileptic dynamics in a human cortico-thalamic mean-field model," *J. Comput. Neurosci.*, pp. 507–526, 2009.
- [120] M. Steriade, *Neuronal Substrates of Sleep and Epilepsy*. Cambridge University Press, 2003, p. 522.
- [121] P. Suffczynski, F. Lopes da Silva, J. Parra, D. Velis, and S. Kalitzin, "Epileptic transitions: model predictions and experimental validation.," *J. Clin. Neurophysiol.*, vol. 22, no. 5, pp. 288–99, Oct. 2005.
- [122] P. D. Williamson, J. A. French, V. M. Thadani, J. H. Kim, R. A. Novelly, S. S. Spencer, D. D. Spencer, and R. H. Mattson, "Characteristics of medial temporal lobe epilepsy: II. Interictal and ictal scalp electroencephalography, neuropsychological testing, neuroimaging, surgical results, and pathology.," *Ann. Neurol.*, vol. 34, no. 6, pp. 781–7, Dec. 1993.

- [123] J. S. Ebersole and S. V. Pacia, "Localization of Temporal Lobe Foci by Ictal EEG Patterns," *Epilepsia*, vol. 37, no. 4, pp. 386–399, Apr. 1996.
- [124] S. V. Pacia and J. S. Ebersole, "Intracranial EEG Substrates of Scalp Ictal Patterns from Temporal Lobe Foci," *Epilepsia*, vol. 38, no. 6, pp. 642–654, Jun. 1997.
- [125] S.-A. Lee, D. D. Spencer, and S. S. Spencer, "Intracranial EEG Seizure-Onset Patterns in Neocortical Epilepsy," *Epilepsia*, vol. 41, no. 3, pp. 297–307, Mar. 2000.
- [126] J. Margerison and J. Corsellis, "A neuropathological study of the brain in epilepsy, with particular reference to the temporal lobes," *Brain*, vol. 89, no. 3, pp. 499–530, 1966.
- [127] R. S. Sloviter, C. A. Zappone, A. V. Bumanglag, B. A. Norwood, and H. Kudrimoti, "On the relevance of prolonged convulsive status epilepticus in animals to the etiology and neurobiology of human temporal lobe epilepsy," *Epilepsia*, vol. 48, no. s8, pp. 6–10, Nov. 2007.
- [128] D. C. McIntyre and K. L. Gilby, "Mapping seizure pathways in the temporal lobe," *Epilepsia*, vol. 49 Suppl 3, pp. 23–30, Jan. 2008.
- [129] O. David, T. Blauwblomme, A.-S. Job, S. Chabardès, D. Hoffmann, L. Minotti, and P. Kahane, "Imaging the seizure onset zone with stereo-electroencephalography," *Brain*, vol. 134, no. Pt 10, pp. 2898–911, Oct. 2011.
- [130] C. Kennedy, "Metabolic Mapping of the Primary Visual System of the Monkey by means of the Autoradiographic [¹⁴C]deoxyglucose Technique," *Proc. Natl. Acad. Sci.*, vol. 73, no. 11, pp. 4230–4234, Nov. 1976.
- [131] J. Engel, L. Wolfson, and L. Brown, "Anatomical correlates of electrical and behavioral events related to amygdaloid kindling," *Ann. Neurol.*, vol. 3, no. 6, pp. 538–44, Jun. 1978.
- [132] H. G. Niessen, F. Angenstein, S. Vielhaber, C. Frisch, A. Kudin, C. E. Elger, H.-J. Heinze, H. Scheich, and W. S. Kunz, "Volumetric magnetic resonance imaging of functionally relevant structural alterations in chronic epilepsy after pilocarpine-induced status epilepticus in rats," *Epilepsia*, vol. 46, no. 7, pp. 1021–6, Jul. 2005.
- [133] M. R. Newton, S. F. Berkovic, M. C. Austin, C. C. Rowe, W. J. McKay, and P. F. Bladin, "SPECT in the localisation of extratemporal and temporal seizure foci," *J. Neurol. Neurosurg. Psychiatry*, vol. 59, no. 1, pp. 26–30, Jul. 1995.
- [134] K. Goffin, W. Van Paesschen, P. Dupont, and K. Van Laere, "Longitudinal microPET imaging of brain glucose metabolism in rat lithium-pilocarpine model of epilepsy," *Exp. Neurol.*, vol. 217, no. 1, pp. 205–209, 2009.
- [135] P. L. Nunez and R. Srinivasan, *Electric Fields of the Brain: The Neurophysics of EEG*, vol. 4. Oxford University Press, 2006, p. 611.

Bibliography

- [136] E. M. Izhikevich and G. M. Edelman, "Large-scale model of mammalian thalamocortical systems," *Proc. Natl. Acad. Sci. U. S. A.*, vol. 105, no. 9, pp. 3593–8, Mar. 2008.
- [137] W. J. Freeman, *Mass Action in the Nervous System - Examination of the Neurophysiological Basis of Adaptive Behavior through the EEG*. Academic Press - Harcourt Brace Jovanovich Publishers, 1975.
- [138] B. H. Jansen and V. G. Rit, "Electroencephalogram and visual evoked potential generation in a mathematical model of coupled cortical columns," *Biol. Cybern.*, vol. 73, pp. 357–366, 1995.
- [139] G. Deco, V. K. Jirsa, P. A. Robinson, M. Breakspear, and K. Friston, "The dynamic brain: From spiking neurons to neural masses and cortical fields," *PLoS Comput. Biol.*, vol. 4(8), pp. 1–35, 2008.
- [140] a M. Thomson and D. C. West, "Fluctuations in pyramid-pyramid excitatory postsynaptic potentials modified by presynaptic firing pattern and postsynaptic membrane potential using paired intracellular recordings in rat neocortex," *Neuroscience*, vol. 54, no. 2, pp. 329–46, May 1993.
- [141] I. A. Kuznetsov, *Elements of Applied Bifurcation Theory (Google eBook)*, vol. 1. Springer, 1998, p. 591.
- [142] B. Peng, V. Gaspar, and K. Showalter, "False Bifurcations in Chemical Systems: Canards," *Philos. Trans. R. Soc. A Math. Phys. Eng. Sci.*, vol. 337, no. 1646, pp. 275–289, Nov. 1991.
- [143] F. Marten, S. Rodrigues, O. Benjamin, M. P. Richardson, and J. R. Terry, "Onset of polyspike complexes in a mean-field model of human electroencephalography and its application to absence epilepsy," *Philos. Trans. A. Math. Phys. Eng. Sci.*, vol. 367, no. 1891, pp. 1145–61, Mar. 2009.
- [144] B. Krauskopf, H. M. Osinga, and J. Galán-Vioque, Eds., *Numerical Continuation Methods for Dynamical Systems*. Dordrecht: Springer Netherlands, 2007.
- [145] B. Ermentrout, *Simulating, Analyzing, and Animating Dynamical Systems: A Guide to XPPAUT for Researchers and Students (Google eBook)*. SIAM, 2002, p. 290.
- [146] K. Engelborghs, *DDE-BIFTOOL: a Matlab package for bifurcation analysis of delay differential equations*, no. March. Katholieke Universiteit Leuven Department of Computer Science, 2000, pp. 1–36.
- [147] F. Grimbert and O. Faugeras, "Bifurcation analysis of Jansen's neural mass model," *Neural Comput.*, vol. 18, no. 12, pp. 3052–68, Dec. 2006.
- [148] J. Pijn, "Quantitative evaluation of EEG signals in epilepsy: nonlinear associations, time delays and nonlinear dynamics," 1990.

- [149] J. Theiler, S. Eubank, A. Longtin, B. Galdrikian, and J. Doyne Farmer, "Testing for nonlinearity in time series: the method of surrogate data," *Phys. D Nonlinear Phenom.*, vol. 58, no. 1, pp. 77–94, 1992.
- [150] L. van Veen and D. Liley, "Chaos via Shilnikov's Saddle-Node Bifurcation in a Theory of the Electroencephalogram," *Phys. Rev. Lett.*, vol. 97, no. 20, p. 208101, Nov. 2006.
- [151] I. Pavlov, N. Huusko, M. Drexel, E. Kirchmair, G. Sperk, A. Pitkänen, and M. C. Walker, "Progressive loss of phasic, but not tonic, GABAA receptor-mediated inhibition in dentate granule cells in a model of post-traumatic epilepsy in rats," *Neuroscience*, vol. 194, pp. 208–219, 2011.
- [152] R.-Z. Zhan and J. V. Nadler, "Enhanced tonic GABA current in normotopic and hilar ectopic dentate granule cells after pilocarpine-induced status epilepticus," *J. Neurophysiol.*, vol. 102, no. 2, pp. 670–81, Aug. 2009.
- [153] D. B. Rubin, "Bayesianly Justifiable and Relevant Frequency Calculations for the Applies Statistician," *Ann. Stat.*, vol. 12, no. 4, pp. 1151–1172, Dec. 1984.
- [154] S. Tavaré, D. J. Balding, R. C. Griffiths, and P. Donnelly, "Inferring Coalescence Times From DNA Sequence Data," *Genetics*, vol. 145, no. 2, pp. 505–518, Feb. 1997.
- [155] M. Beaumont, J. Cornuet, J. Marin, and C. Robert, "Adaptive approximate Bayesian computation," *Biometrika*, vol. 96, no. 4, pp. 983–990, Oct. 2009.
- [156] M. Sunnåker, A. G. Busetto, E. Numminen, J. Corander, M. Foll, and C. Dessimoz, "Approximate Bayesian computation," *PLoS Comput. Biol.*, vol. 9, no. 1, p. e1002803, Jan. 2013.
- [157] H. Robbins and S. Monro, "A stochastic approximation method," *Ann. Math. Stat.*, 1951.
- [158] J. Kiefer and J. Wolfowitz, "Stochastic estimation of the maximum of a regression function," *Ann. Math. Stat.*, 1952.
- [159] D. Goldberg and J. Holland, "Genetic algorithms and machine learning," *Mach. Learn.*, 1988.
- [160] S. Russell, P. Norvig, and A. Intelligence, "A modern approach," *Artif. Intell. Prentice-Hall, ...*, 1995.
- [161] R. Eberhart and J. Kennedy, "A new optimizer using particle swarm theory," ... *sixth Int. Symp. ...*, 1995.
- [162] K. Gurney, M. Humphries, R. Wood, T. Prescott, and P. Redgrave, "Testing computational hypotheses of brain systems function: a case study with the basal ganglia," *Netw. Comput. Neural Syst.*, vol. 15, no. 4, pp. 263–290, Nov. 2004.

Bibliography

- [163] J. W. Mink, "The basal ganglia: focused selection and inhibition of competing motor programs.," *Prog. Neurobiol.*, vol. 50, no. 4, pp. 381–425, 1996.
- [164] J. M. Tepper and J. P. Bolam, "Functional diversity and specificity of neostriatal interneurons," *Curr. Opin. Neurobiol.*, vol. 14, no. 6, pp. 685–692, 2004.
- [165] J. Bolam and J. Hanley, "Synaptic organisation of the basal ganglia," *J. Anat.*, 2000.
- [166] D. Akkal, P. Burbaud, J. Audin, and B. Bioulac, "Responses of substantia nigra pars reticulata neurons to intrastriatal D1 and D2 dopaminergic agonist injections in the rat," *Neurosci. Lett.*, vol. 213, no. 1, pp. 66–70, 1996.
- [167] C. Gerfen, T. Engber, L. Mahan, Z. Susel, T. Chase, F. Monsma, and D. Sibley, "D1 and D2 dopamine receptor-regulated gene expression of striatonigral and striatopallidal neurons," *Science (80-.)*, vol. 250, no. 4986, pp. 1429–1432, Dec. 1990.
- [168] Y. Kawaguchi, "Projection subtypes of rat neostriatal matrix cells revealed by intracellular injection of biocytin," *J. ...*, 1990.
- [169] A. Parent and L.-N. Hazrati, "Functional anatomy of the basal ganglia. II. The place of subthalamic nucleus and external pallidum in basal ganglia circuitry," *Brain Res. Rev.*, vol. 20, no. 1, pp. 128–154, 1995.
- [170] Y. Wu, S. Richard, and A. Parent, "The organization of the striatal output system: a single-cell juxtacellular labeling study in the rat," *Neurosci. Res.*, vol. 38, no. 1, pp. 49–62, 2000.
- [171] L.-N. Hazrati, A. Parent, S. Mitchell, and S. N. Haber, "Evidence for interconnections between the two segments of the globus pallidus in primates: a PHA-L anterograde tracing study," 1990.
- [172] L. J. Ryan and K. B. Clark, "The role of the subthalamic nucleus in the response of globus pallidus neurons to stimulation of the prelimbic and agranular frontal cortices in rats," *Exp. Brain Res.*, vol. 86, no. 3, Sep. 1991.
- [173] H. Kita, "Responses of globus pallidus neurons to cortical stimulation: intracellular study in the rat," *Brain Res.*, vol. 589, no. 1, pp. 84–90, 1992.
- [174] H. Kita, "Parvalbumin-immunopositive neurons in rat globus pallidus: a light and electron microscopic study," 1994.
- [175] H. Kita and S. T. Kita, "The morphology of globus pallidus projection neurons in the rat: an intracellular staining study," 1994.
- [176] P. Mailly, S. Charpier, A. Menetrey, and J.-M. Deniau, "Three-Dimensional Organization of the Recurrent Axon Collateral Network of the Substantia Nigra Pars Reticulata Neurons in the Rat," *J. Neurosci.*, vol. 23, no. 12, pp. 5247–5257, Jun. 2003.

- [177] T. Moriizumi, Y. Nakamura, S. Okoyama, and Y. Kitao, "Synaptic organization of the cat entopeduncular nucleus with special reference to the relationship between the afferents to entopedunculothalamic projection neurons: An electron microscope study by a combined degeneration and horseradish peroxidase tracin," *Neuroscience*, vol. 20, no. 3, pp. 797–816, 1987.
- [178] A. Nambu, H. Tokuno, I. Hamada, H. Kita, M. Imanishi, T. Akazawa, Y. Ikeuchi, and N. Hasegawa, "Excitatory Cortical Inputs to Pallidal Neurons Via the Subthalamic Nucleus in the Monkey Excitatory Cortical Inputs to Pallidal Neurons Via the Subthalamic Nucleus in the Monkey," vol. 84, pp. 289–300, 2000.
- [179] O. Bernander, R. J. Douglas, K. a Martin, and C. Koch, "Synaptic background activity influences spatiotemporal integration in single pyramidal cells.," *Proc. Natl. Acad. Sci. U. S. A.*, vol. 88, no. 24, pp. 11569–73, Dec. 1991.
- [180] M. C. Bellingham and B. Walmsley, "A novel presynaptic inhibitory mechanism underlies paired pulse depression at a fast central synapse.," *Neuron*, vol. 23, no. 1, pp. 159–70, May 1999.
- [181] H. Kitano, I. Tanibuchi, and K. Jinnai, "The distribution of neurons in the substantia nigra pars reticulata with input from the motor, premotor and prefrontal areas of the cerebral cortex in monkeys," *Brain Res.*, vol. 784, no. 1, pp. 228–238, 1998.
- [182] T. S. Gertler, C. S. Chan, and D. J. Surmeier, "Dichotomous anatomical properties of adult striatal medium spiny neurons.," *J. Neurosci.*, vol. 28, no. 43, pp. 10814–24, Oct. 2008.
- [183] M. a Farries, H. Kita, and C. J. Wilson, "Dynamic spike threshold and zero membrane slope conductance shape the response of subthalamic neurons to cortical input.," *J. Neurosci.*, vol. 30, no. 39, pp. 13180–91, Sep. 2010.
- [184] a J. Cooper and I. M. Stanford, "Electrophysiological and morphological characteristics of three subtypes of rat globus pallidus neurone in vitro.," *J. Physiol.*, vol. 527 Pt 2, pp. 291–304, Sep. 2000.
- [185] E. Bauswein, C. Fromm, and a Preuss, "Corticostriatal cells in comparison with pyramidal tract neurons: contrasting properties in the behaving monkey.," *Brain Res.*, vol. 493, no. 1, pp. 198–203, Jul. 1989.
- [186] D. Plenz and S. T. Kitai, "Up and down states in striatal medium spiny neurons simultaneously recorded with spontaneous activity in fast-spiking interneurons studied in cortex-striatum-substantia nigra organotypic cultures.," *J. Neurosci.*, vol. 18, no. 1, pp. 266–83, Jan. 1998.
- [187] D. Jaeger and H. Kita, "Functional connectivity and integrative properties of globus pallidus neurons.," *Neuroscience*, vol. 198, pp. 44–53, Dec. 2011.

Bibliography

- [188] H. Kita, S. Chiken, Y. Tachibana, and A. Nambu, "Origins of GABA(A) and GABA(B) receptor-mediated responses of globus pallidus induced after stimulation of the putamen in the monkey.," *J. Neurosci.*, vol. 26, no. 24, pp. 6554–62, Jun. 2006.
- [189] A. H. Gittis, A. B. Nelson, M. T. Thwin, J. J. Palop, and A. C. Kreitzer, "Distinct roles of GABAergic interneurons in the regulation of striatal output pathways.," *J. Neurosci.*, vol. 30, no. 6, pp. 2223–34, Feb. 2010.
- [190] A. Adler, I. Finkes, S. Katabi, Y. Prut, and H. Bergman, "Encoding by synchronization in the primate striatum.," *J. Neurosci.*, vol. 33, no. 11, pp. 4854–66, Mar. 2013.
- [191] H. Kita, S. Chiken, Y. Tachibana, and A. Nambu, "Origins of GABA(A) and GABA(B) receptor-mediated responses of globus pallidus induced after stimulation of the putamen in the monkey.," *J. Neurosci.*, vol. 26, no. 24, pp. 6554–62, Jun. 2006.
- [192] H. Kita, "Globus pallidus external segment.," *Prog. Brain Res.*, vol. 160, no. 06, pp. 111–33, Jan. 2007.
- [193] F. Sato, P. Lavallée, M. Lévesque, and a Parent, "Single-axon tracing study of neurons of the external segment of the globus pallidus in primate.," *J. Comp. Neurol.*, vol. 417, no. 1, pp. 17–31, Jan. 2000.
- [194] H. Kita, a Nambu, K. Kaneda, Y. Tachibana, and M. Takada, "Role of ionotropic glutamatergic and GABAergic inputs on the firing activity of neurons in the external pallidum in awake monkeys.," *J. Neurophysiol.*, vol. 92, no. 5, pp. 3069–84, Nov. 2004.
- [195] D. Jaeger and H. Kita, "Functional connectivity and integrative properties of globus pallidus neurons.," *Neuroscience*, vol. 198, pp. 44–53, Dec. 2011.
- [196] G. Chevalier and J. M. Deniau, "Disinhibition as a basic process in the expression of striatal functions," *Trends Neurosci.*, vol. 13, no. 7, pp. 277–280, 1990.
- [197] J. W. Mink and W. T. Thach, "Basal ganglia intrinsic circuits and their role in behavior," *Curr. Opin. Neurobiol.*, vol. 3, no. 6, pp. 950–957, 1993.
- [198] T. J. Prescott, P. Redgrave, and K. Gurney, "Layered Control Architectures in Robots and Vertebrates," *Adapt. Behav.*, vol. 7, no. 1, pp. 99–127, Jan. 1999.
- [199] M. D. Humphries and K. N. Gurney, "The role of intra-thalamic and thalamocortical circuits in action selection," Aug. 2002.
- [200] D. G. Beiser and J. C. Houk, "Model of Cortical-Basal Ganglionic Processing: Encoding the Serial Order of Sensory Events," *J Neurophysiol*, vol. 79, no. 6, pp. 3168–3188, Jun. 1998.
- [201] M. J. Frank, "Dynamic dopamine modulation in the basal ganglia: a neurocomputational account of cognitive deficits in medicated and nonmedicated Parkinsonism.," *J. Cogn. Neurosci.*, vol. 17, no. 1, pp. 51–72, Jan. 2005.

- [202] D. Purves, *Neuroscience, Fourth Edition*. Sinauer Associates, Inc., 2007, p. 857.
- [203] M. R. DeLong and T. Wichmann, "Circuits and circuit disorders of the basal ganglia," *Arch. Neurol.*, vol. 64, no. 1, pp. 20–4, Jan. 2007.
- [204] P. Brown and C. Marsden, "What do the basal ganglia do?," *The Lancet*, vol. 351, no. 9118, pp. 1801–1804, 1998.
- [205] G. G. Turrigiano and S. B. Nelson, "Homeostatic plasticity in the developing nervous system," *Nat. Rev. Neurosci.*, vol. 5, no. 2, pp. 97–107, Feb. 2004.
- [206] A. J. Watt, M. C. van Rossum, K. M. MacLeod, S. B. Nelson, and G. G. Turrigiano, "Activity Coregulates Quantal AMPA and NMDA Currents at Neocortical Synapses," *Neuron*, vol. 26, no. 3, pp. 659–670, 2000.
- [207] D. V. Lissin, "Activity differentially regulates the surface expression of synaptic AMPA and NMDA glutamate receptors," *Proc. Natl. Acad. Sci.*, vol. 95, no. 12, pp. 7097–7102, Jun. 1998.
- [208] R. J. O'Brien, S. Kamboj, M. D. Ehlers, K. R. Rosen, G. D. Fischbach, and R. L. Huganir, "Activity-Dependent Modulation of Synaptic AMPA Receptor Accumulation," *Neuron*, vol. 21, no. 5, pp. 1067–1078, 1998.
- [209] K. Y. Tseng, F. Kasanetz, L. Kargieman, L. a Riquelme, and M. G. Murer, "Cortical slow oscillatory activity is reflected in the membrane potential and spike trains of striatal neurons in rats with chronic nigrostriatal lesions," *J. Neurosci.*, vol. 21, no. 16, pp. 6430–9, Aug. 2001.
- [210] L. J. Kish, M. R. Palmer, and G. A. Gerhardt, "Multiple single-unit recordings in the striatum of freely moving animals: effects of apomorphine and d-amphetamine in normal and unilateral 6-hydroxydopamine-lesioned rats," *Brain Res.*, vol. 833, no. 1, pp. 58–70, 1999.
- [211] P. O'Donnell, "Dopamine gating of forebrain neural ensembles," *Eur. J. Neurosci.*, vol. 17, no. 3, pp. 429–435, Feb. 2003.
- [212] P. J. Magill, J. P. Bolam, and M. D. Bevan, "Dopamine regulates the impact of the cerebral cortex on the subthalamic nucleus-globus pallidus network," *Neuroscience*, vol. 106, no. 2, pp. 313–30, Jan. 2001.
- [213] R. J. Moran, N. Mallet, V. Litvak, R. J. Dolan, P. J. Magill, K. J. Friston, and P. Brown, "Alterations in brain connectivity underlying beta oscillations in Parkinsonism," *PLoS Comput. Biol.*, vol. 7, no. 8, p. e1002124, Aug. 2011.
- [214] K. Shen and S. Johnson, "Dopamine depletion alters responses to glutamate and GABA in the rat subthalamic nucleus," *Neuroreport*, 2005.
- [215] R. L. Albin, A. B. Young, and J. B. Penney, "The functional anatomy of basal ganglia disorders," *Mov. Disord.*, vol. 12, no. 10, pp. 366–375, 1989.

Bibliography

- [216] P. Brown, "Oscillatory nature of human basal ganglia activity: relationship to the pathophysiology of Parkinson's disease.," *Mov. Disord.*, vol. 18, no. 4, pp. 357-63, Apr. 2003.